Ferdowsi University of Mashhad

Print ISSN 2008-9147
Online ISSN 2717-3364
Numbers: 25

JCMR

Journal of Cell and Molecular Research

Volume 13, Number 1, Summer, 2021

بسم الله الرحمن الرحیم

Issuance License No. 124/902-27.05.2008 from Ministry of Culture and Islamic Guidance
Scientific Research Issuance License No. 161675 from the Ministry of Science, Research and Technology, Iran

Journal of Cell and Molecular Research (JCMR)

Volume 13, Number 1, Summer, 2021

JCMR Office: Department of Biology, Faculty of Sciences, Ferdowsi University of Mashhad, Mashhad, Iran.
Postal Code: 9177948953
P.O. Box: 917751436
Tel: +98-513-8804063/+98-9156996326
Fax: +98-513-8795162
E-mail: jcmr@um.ac.ir
Online Submission: http://jcmr.um.ac.ir

Table of Contents

Journal of Cell and Molecular Research (2021) 13 (1), 1-9 DOI: 10.22067/JCMR.2021.71604.1015

Research Article

A Multi-faceted Approach for Prediction of Genome Safe Harbor Loci in the Chicken Genome

Nima Dehdilani [1,2], Mohsen Fathi Najafi [3], Hesam Dehghani [1,2,4,*]

[1] *Division of Biotechnology, Faculty of Veterinary Medicine, Ferdowsi University of Mashhad, Mashhad, Iran*
[2] *Stem Cell Biology and Regenerative Medicine Research Group, Research Institute of Biotechnology, Ferdowsi University of Mashhad, Mashhad, Iran*
[3] *Education and Extension Organization (AREEO), Agricultural Research, Razi Vaccine and Serum Research Institute, Mashhad, Branch, Mashhad, Iran*
[4] *Department of Basic Sciences, Faculty of Veterinary Medicine, Ferdowsi University of Mashhad, Mashhad, Iran*

Received 23 July 20201 Accepted 23 August 2021

Abstract

To achieve a reliable and persistent expression, the transgene should be precisely integrated into the genome safe harbor (GSH) loci. Little attention has been paid to find the safe harbor loci of the chicken (*Gallus gallus domesticus*) genome. Identification and characterization of GSH loci that allow the persistent and reliable expression of knock-in genes could be a major area of interest within the field of transgenic technology and is central to the development of transgenic livestock. Randomly integrated transgenes might encounter position effects and epigenetic silencing, so unstable phenotypes, as well as unreliable and unpredictable expression of the knock-in transgene could occur. In contrast to random gene insertion, site-specific gene targeting provides a superior strategy that exploits homologous recombination to insert a transgene of interest into a pre-determined locus. In this study, based on bioinformatics, gene expression atlas, and Hi-C analyses, the GSH region was predicted in the chicken genome between *DRG1* and *EIF4ENIF1* genes. To do so, we introduce a fast and easy-to-use pipeline that allows the prediction of orthologue GSH loci in all organisms, especially chickens. In addition, the procedure to design Cas9/gRNA expression and targeting vectors for targeting these predicted GSH regions is described in detail.

***Keywords*:** Genome safe harbor loci, Genetically engineered birds, Transgenic chicken, CRISPR/Cas9, Gene expression atlas, Hi-C map.

Introduction

It has become increasingly important to determine regions that support the integration and long-term expression of a transgene in the genome. Considerable efforts have been underway to elucidate genomic safe harbor (GSH) loci that could potentially support long-term expressions within the field of transgenesis and recombinant protein production (Sadelain et al., 2011). The discovery of a GSH locus that allows reliable and consistent expression of a knock-in gene without triggering the functional disruption of internal genes is of utmost importance to develop bioreactors (Papapetrou et al., 2011; Ruan et al., 2015).

There is a growing number of strategies to screen and identify GSH loci. Traditional strategies are expensive, cumbersome, and time-consuming. For example, to identify and explore potential GSH loci, the "gene trapping" method has been used that relies on random integration of a promoterless reporter construct across the genome to indicate the expression of an endogenous gene (Stanford et al., 2001). Then, the integration sites are evaluated to find the regions with the highest expressions (Papapetrou et al., 2011). Such a reverse screening strategy is very laborious, as numerous sites which are subjected to reporter insertion should be analyzed. Another method to find the potential GSH loci is based on whole transcriptome sequencing, which could be expensive and needs specialized analyses (Ma et al., 2018). The *in vivo* imaging (Rizzi et al., 2017) of reporter animals which could be performed to find suitable loci for transgene integration, is also time-consuming and uneconomical. More recently, a systematic approach that combines the RNA-seq data with the High-throughput Chromosome Conformation Capture (Hi-C) data was proposed to predict the GSH regions (Hilliard and Lee, 2021). This approach is more informative and applicable, but the high cost is the main constraint against its universal use. However, it is helpful and cost-effective to do data-mining and similarity-finding

*Corresponding author's e-mail address: *dehghani@um.ac.ir*

experiments on the data adopted from validated GSH loci databases to identify potential orthologous GSH regions. Hence, it would be easy to predict actively transcribed regions, transcriptionally permissive topologically associating domains (TADs), and nucleosome-poor regions (Fishman et al., 2019; Hilliard and Lee, 2021; Zhao et al., 2019). A comparative genomics approach could also be applied to screen and detect similar sites/homologous sequences among different species (Irion et al., 2007; Li et al., 2014; Wu et al., 2016; Yang et al., 2016b).

Here, we introduce a novel, cost-effective, and easy-to-use pipeline to predict the potential GSH loci in the eukaryotic genome. We applied this pipeline to analyze the gene expression atlas, and Hi-C data to identify a potential GSH locus in the chicken genome. Then, we describe the procedure for designing CRISPR-based targeting and Cas9/gRNA expression vectors that are applicable for targeting these predicted GSH regions.

Materials and Methods

Pipeline for prediction of GSH loci

We used a five-step, fast, and easy-to-use pipeline to predict an orthologous GSH locus in the *Gallus gallus domesticus* genome (Figure 1). In the first step, genes around the validated GSH locus were found based on their sequence similarities in the chicken genome. The validated locus, the intergenic sequence between *DRG1* and *EIF4ENIF1* genes, was previously reported as a potential GSH locus in *Sus scrofa*, *Mus musculus*, and *Homo sapiens*. To this end, gene similarities around the predicted GSH locus were compared to the genes around the validated GSH locus using the NCBI Genome Data Viewer (GDV) browser (https://www.ncbi.nlm.nih.gov/genome/gdv/). In the second step, the intergenic sequence between *DRG1* and *EIF4ENIF1* genes from *Sus scrofa*, *Mus musculus*, and *Homo sapiens* was used as a template to perform a pairwise alignment (EMBOSS Water algorithm) against the similar intergenic sequence of the *Gallus gallus domesticus* (taxid: 9031) genome. In the third step, the predicted GSH locus was evaluated for the presence of possible annotated coding or non-coding genes using the NCBI GDV (*Gallus gallus* genome assembly GRCg6a) and the UCSC Genome Browser (https://genome.ucsc.edu/cgi-bin/hgGateway; chicken assembly GRCg6a/galGal6; Mar. 2018). In the fourth step, benefiting from chicken RNAseq data, the expression levels (transcript per millions; TPM) of the genes flanking the intergenic locus of interest were determined using the Gene Expression Atlas (https://www.ebi.ac.uk/gxa/home). In the fifth step, the chicken Hi-C data were used to predict the coordination of the GSH locus with its adjacent genes using the Hi-C map (Supplementary file 1). For visualizing the Hi-C map, the Juicebox software, version 1.9.0 (https://github.com/aidenlab/Juicebox/wiki/Download) was used to find the location of interest (coordinate system of the map corresponds to the genome version GalGal5). Then, the gene coordinates were compared with the locations of TAD boundaries. The map with the gene tracks is available in the following URL (http://sites.icgbio.ru/ontogen/wp-content/uploads/MolMechDevDepart/GCF_000002315.4_Gallus_gallus-5.0_genomic.gff.genes.bed). Alternatively, defined TAD boundaries were computationally adopted from the following URL (http://sites.icgbio.ru/ontogen/wp-content/uploads/MolMechDevDepart/subTADs-ChEF-all-HindIII-40k.hm.gzipped_matrix.jucebox_domains.annotation).

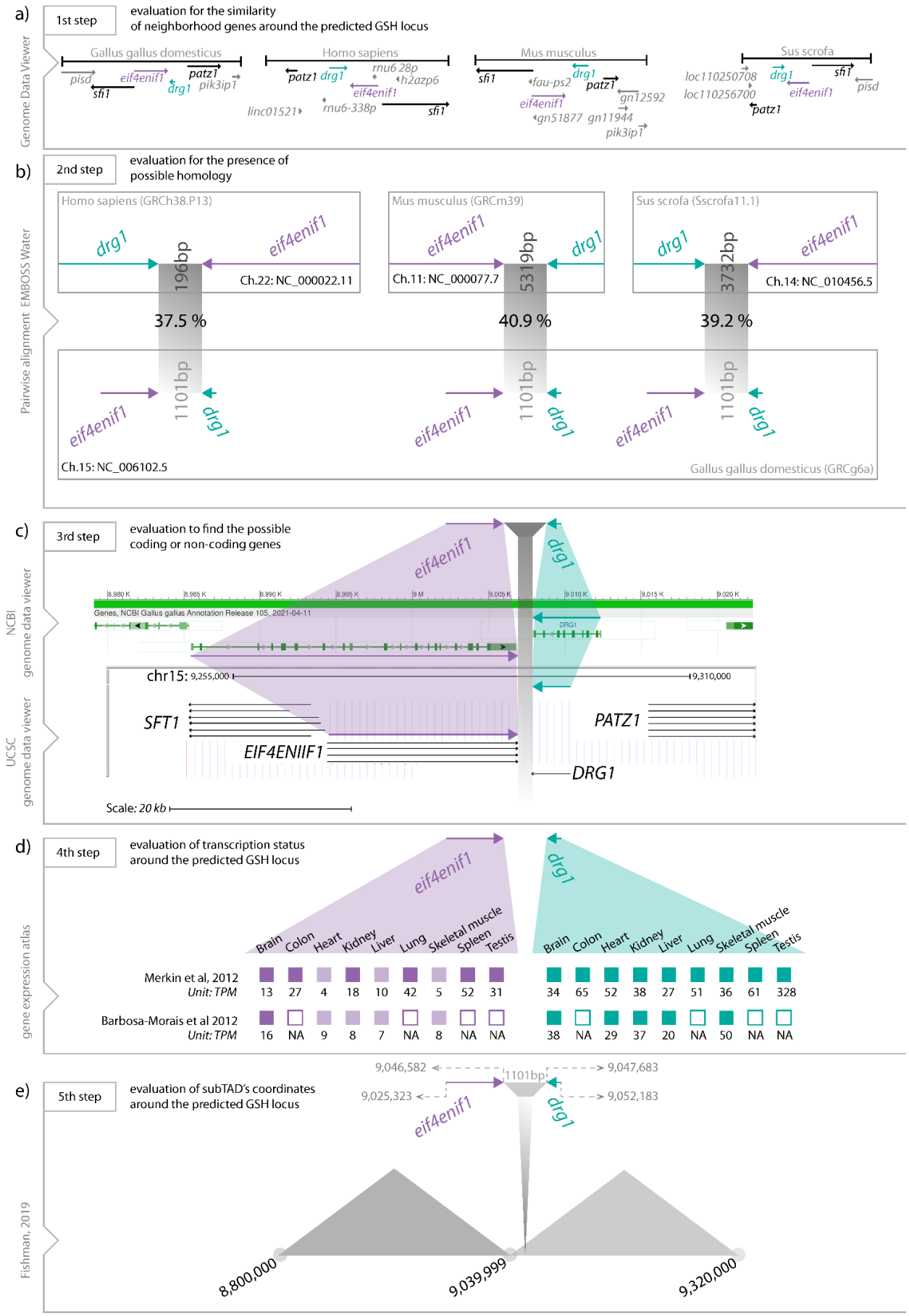
a)
1st step
evaluation for the similarity
of neighborhood genes around the predicted GSH locus
Genome Data Viewer
Gallus gallus domesticus
Homo sapiens
Mus musculus
Sus scrofa
b)
2nd step
evaluation for the presence of
possible homology
Pairwise alignment EMBOSS Water
Homo sapiens (GRCh38.P13)
Mus musculus (GRCm39)
Sus scrofa (Sscrofa11.1)
Ch.22: NC_000022.11
Ch.11: NC_000077.7
Ch.14: NC_010456.5
196bp
5319bp
3732bp
37.5 %
40.9 %
39.2 %
1101bp
Ch.15: NC_006102.5
Gallus gallus domesticus (GRCg6a)
c)
3rd step
evaluation to find the possible
coding or non-coding genes
NCBI genome data viewer
UCSC genome data viewer
Genes, NCBI Gallus gallus Annotation Release 105, 2021-04-11
chr15: 9,255,000
9,310,000
SFT1
EIF4ENIIF1
PATZ1
DRG1
Scale: 20 kb
d)
4th step
evaluation of transcription status
around the predicted GSH locus
gene expression atlas
Brain Colon Heart Kidney Liver Lung Skeletal muscle Spleen Testis
Merkin et al, 2012
Unit: TPM
13 27 4 18 10 42 5 52 31
34 65 52 38 27 51 36 61 328
Barbosa-Morais et al 2012
Unit: TPM
16 NA 9 8 7 NA 8 NA NA
38 NA 29 37 20 NA 50 NA NA
e)
5th step
evaluation of subTAD's coordinates
around the predicted GSH locus
Fishman, 2019
9,046,582
9,025,323
1101bp
9,047,683
9,052,183
8,800,000
9,039,999
9,320,000

Figure 1. A schematic depiction for deciphering a genome safe harbor locus in the chicken genome. a) Comparison of gene distribution around the validated GSH locus in human (*Homo sapiens*), mouse (*Mus musculus*), and pig (*Sus scrofa*) genome with the same region in the chicken genome using NCBI Genome Data Viewer; b) Pairwise alignment of the predicted chicken GSH locus and validated GSH loci in human, mouse, and pig genomes by EMBOSS Water algorithm for calculation of sequence identity; c) Screening for possible coding or non-coding genes in the predicted chicken GSH locus by NCBI and UCSC genome data viewers; d) Expression levels of *DRG1* and *EIF4ENIF1* in several tissues adopted from gene expression atlas; e) Coordinates of chicken subTADs around the predicted chicken GSH locus. Abbreviations: ch/chr, chromosome; bp, base pair; TPM, transcripts per million; NA, not applicable.

Designing Cas9/gRNA expression and CRISPR-based targeting vectors

To design a highly specific gRNA for the predicted chicken GSH locus, the intergenic sequence between *DRG1* and *EIF4ENIF1* genes was subjected to the CHOPCHOP search engine (https://chopchop.cbu.uib.no/). The predicted gRNA expressing sequence with high specificity to the predicted GSH locus was selected and synthesized (Macrogen, South Korea) as 20 bp forward (P1, Table 1) and reverse (P2) oligonucleotides with appropriate overhangs (cacc, for the forward oligonucleotide; and aaac, for the reverse oligonucleotide) to be cloned into the *Bbs*I site in the gRNA expression vector (pSpCas9(BB)-2A-Puro (PX459) V2.0; Plasmid #62988; Addgene, USA). The annealed gRNA oligonucleotide was phosphorylated by T4 polynucleotide kinase (PNK; Thermofischer, EK0031) for 30 min at 37 °C followed by a 30 min inactivation at 70 °C. To calculate the insert: vector molar ratio, the annealed oligonucleotides were run on a 2% agarose gel, and their integrated density index was determined using the ImageJ software (https://imagej.nih.gov/ij/download.html) . The gRNA expression vector was subjected to *Bbs*I enzymatic digestion for 1h, and the subsequent heat-inactivation for 30 min at 70 °C. Then, it was dephosphorylated with fast alkaline phosphatase (Thermofischer, EF0654) for 10 min at 37 °C, and heat-inactivated for 30 min at 70 °C. Using T4 DNA ligase (Thermofischer, EL0011), the phosphorylated gRNA was ligated to the digested and dephosphorylated gRNA expression vector for 3h at 16 °C which was followed by 12h at 4 °C.

To design a CRISPR/Cas9-based targeting vector, a plasmid containing CMV-PAC^r-IRES-EGFP cassette (Figure 2b; constructed in this laboratory) was used. This plasmid contains *Pvu*I-*Xho*I sites upstream of CMV, and *Nhe*I-*Xcm*I sites downstream of EGFP. Left and right homology arms (LHA and RHA, respectively) with approximately 500-bp length were amplified from the chicken genomic DNA by appropriate primers, including *Pvu*I cut site at the 5′-end of LHA (P3), *Xho*I cut site at the 3′-end of LHA (P4), *Nhe*I cut site at the 5′-end of RHA (P5), and *Xcm*I cut site at the 3′-end of RHA (P6). In two steps, arms were cloned into the targeting vector. At the first step, the EGFP plasmid was cut with *Nhe*I-*Xcm*I for 3h at 37 °C, followed by dephosphorylation with fast alkaline phosphatase for 10 min at 37 °C, and heat-inactivation for 30 min at 70 °C. The amplified RHA was cut with *Nhe*I and *Xcm*I for 3h at 37 °C. A 1:3 vector to insert molar ratio was used to ligate the amplified RHA into the EGFP vector by the T4 DNA ligase. The generated vector was called the pre-targeting vector. At the second step, the pre-targeting vector was cut with *Pvu*I and *Xho*I for 3h at 37 °C, followed by dephosphorylation with fast alkaline phosphatase for 10 min at 37 °C, and heat-inactivation for 30 min at 70 °C. The amplified LHA was cut with the *Pvu*I and *Xho*I for 3h at 37 °C. A 1:3 vector to insert molar ratio was used to ligate the amplified LHA into the pre-targeting vector by the T4 ligase. The generated vector was called the CRISPR/Cas9-based targeting vector.

For all cloning procedures, 5µl of the ligation mix was transformed into *E. coli* DH5α followed by overnight incubation at 37 °C. Colony PCR was performed on transformants by vector-specific, and insert-specific primers (Figure 2), and positive clones were grown for plasmid extraction using the Plasmid DNA Isolation Kit (DENAzist Asia, Iran). Cloning verification was performed using restriction enzyme digestion (Figure 2).

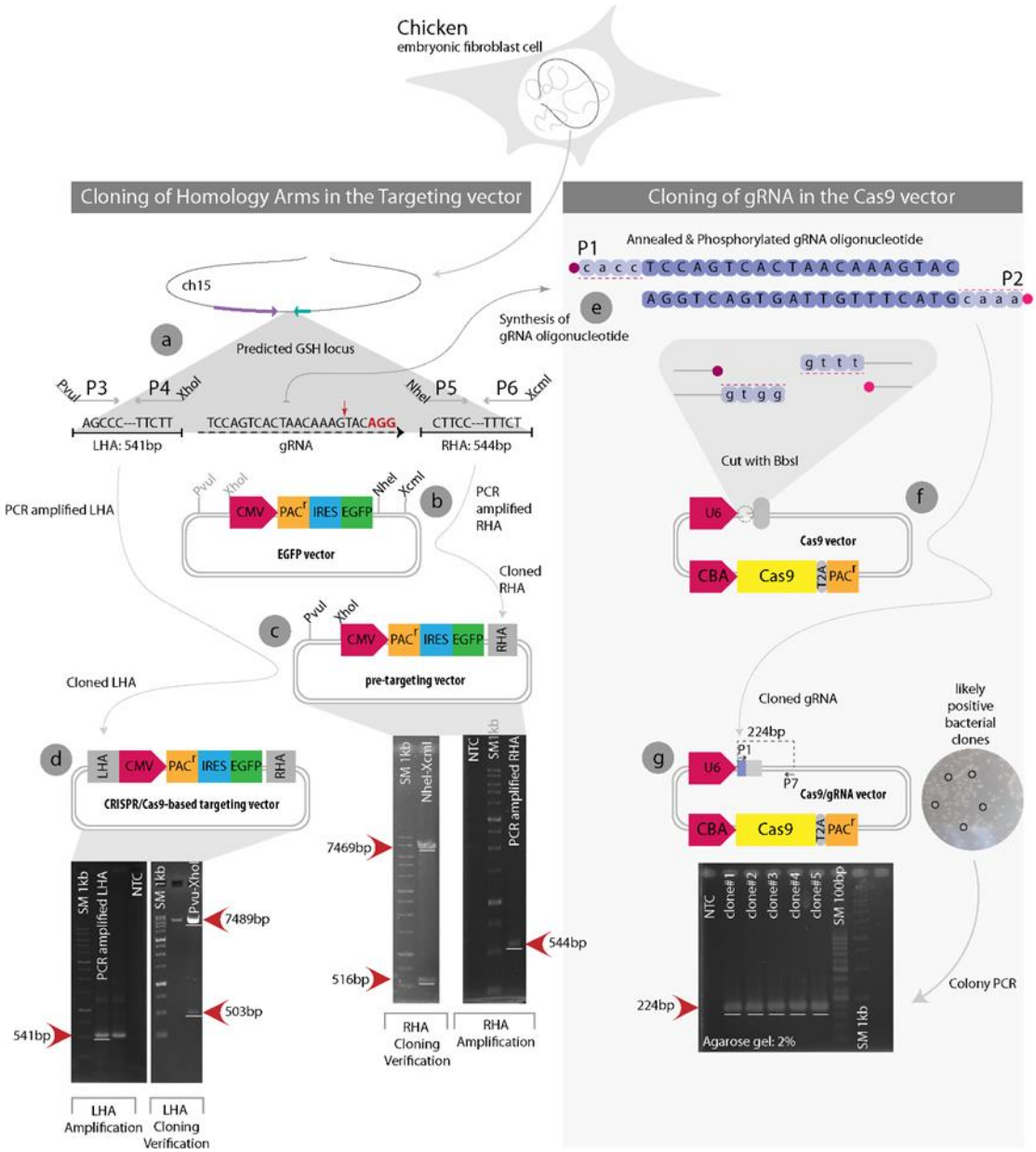

Figure 2. The proposed standard strategy for constructing the GSH targeting vector. a) A specific gRNA sequence in the predicted chicken GSH locus and the corresponding Cas9 cut site (red arrow) are depicted. P3 and P4 primers containing restriction enzyme sites for *Pvu*I and *Xho*I, as well as P5 and P6 primers containing restriction enzyme sites for *Nhe*I and *Xcm*I were designed and synthesized. b) A 544-bp PCR amplified RHA was cut with *Nhe*I/*Xcm*I. Then, the 516-bp RHA was cloned into the EGFP vector (7469-bp) to generate a pre-targeting vector (8012-bp). c) Cloning verification of RHA was performed by *Nhe*I/*Xcm*I digestion. The 516-bp RHA band and 7469-bp vector backbone were detected on the agarose gel. d) A 541-bp PCR amplified LHA was cut with *Pvu*I/*Xho*I. Then, the 503-bp LHA was cloned into the pre-targeting vector (7489-bp) to generate a CRISPR-based targeting vector (7992-bp). Verification of the LHA cloning was performed by *Pvu*I/*Xho*I. The 503-bp LHA band and 7489-bp vector backbone were detected on the agarose gel. e) gRNA oligonucleotides (P1 and P2) containing *Bbs*I overhangs were synthesized, annealed, and phosphorylated. f) gRNA oligonucleotides containing *Bbs*I overhangs were cloned into the *Bbs*I-digested Cas9 vector. g) Colony PCR was performed to verify the cloning of gRNA using P1 and P7 primers, and a 224-bp band was detected on the agarose gel. Abbreviations: LHA, left homology arm; RHA, right homology arm; SM, size marker; NTC, non-template control; bp, base pairs; gRNA, guide RNA; P, primer.

Results

Gene similarities around the validated GSH loci and predicted GSH locus

In mice (Tasic et al., 2011), humans (Zhu et al., 2014), and pigs (Ruan et al., 2015), the region between the *DRG1* and *EIF4ENIF1* genes has been

identified as a validated GSH locus to support the consistent expression of transgenes over time. The regions around the *DRG1* and *EIF4ENIF1* genes in the chicken genome are similar to the organisms mentioned above and include a gene-dense area. In the mouse, human, and pig genomes, the *sfi1* and *patz1* genes are located upstream of *EIF4ENIF1* and *DRG1* genes, respectively. Also, the direction of *EIF4ENIF1* and *DRG1* genes are towards each other in these organisms. These data suggest that the gene organization around the predicted GSH locus in the chicken genome is identical with the validated GSH loci (Figure 1a).

Finding possible similarities using the Water algorithm of pairwise alignment

To designate the orthologous GSH locus in the chicken genome, we first located the *DRG1* and *EIF4ENIF1* genes in the chicken genome. Local pairwise alignment (Water algorithm) describes the most similar region(s) within the sequences to be aligned. It was performed to find the possible similarity of known GSH intergenic locus in the human (GRCh38.P13), mouse (GRCm39), and pig (Sscrofa11.1) genomes with the same locus in chicken. To this end, the following regions, all from the intergenic locus between the *DRG1* and *EIF4ENIF1* genes, were selected and pairwise aligned to an 1100-bp region of the same locus in the chicken genome (NC_052546.1; Ch.15 from 9286985..9286084): a 195-bp region from the human genome (NC_000022.11; Ch.22 from 31434452 to 31434648), a 5318-bp region from the mouse genome (NC_000077.7; Ch.11 from 3194588 to 3199907), and a 3731-bp region from the pig genome (NC_010456.5; Ch.14 from 48153103 to 48156835). The results showed that the intergenic locus between the *DRG1* and *EIF4ENIF1* genes in the chicken genome has similarity scores of 37.5%, 40.9%, and 39.2% with the corresponding regions from the human, mouse, and pig genomes, respectively (Figure 1b).

Searching for possible coding and non-coding genes in the predicted GSH locus

The presence of any annotated coding and non-coding genes in the intergenic region between the chicken *DRG1* and *EIF4ENIF1* genes was evaluated using the UCSC Genome Browser (chicken assembly; Mar. 2018 GRCg6a/galGal6), and the NCBI Genome Data Viewer (GRCg6a). The results showed no coding/non-coding genes at a distance between these two genes (Figure 1c).

Evaluating the transcriptional status of genes adjacent to the predicted GSH locus

It has been demonstrated that the transgene can be expressed reliably in the actively transcribed regions of the genome. The transcriptional status of *DRG1* and *EIF4ENIF1* genes was evaluated using the RNAseq data adopted from the Gene Expression Atlas. RNAseq data showed that the *DRG1* gene is actively transcribed in several tissues. In contrast, the transcription of the *EIF4ENIF1* gene is variable among tissues. Hence, here the insertion site of the transgene of interest was designated near the *DRG1* gene (Figure 1d).

Designating the topological location of the predicted GSH locus using the TAD data

Several studies have confirmed that gene clusters located in a given TAD are regulated similarly (Hilliard and Lee, 2021). Transgenes inserted into a TAD containing actively transcribed genes maintain their transcriptional activity. Benefiting from the Hi-C data of chicken embryonic fibroblasts (Fishman et al., 2019), we located the topological position of the *DRG1* and *EIF4ENIF1* genes related to the adjacent TAD. It was surprising that the transgene insertion site was located in an individual active TAD near the *DRG1* gene (Figure 1e).

Constructing gRNA expression and CRISPR/Cas9-based targeting vectors

Synthetic gRNA oligonucleotides specific to the predicted GSH locus were cloned into the Cas9 expression vector and confirmed with P1 and P7 primers (Table 1). Five clones of transformants were checked with colony PCR. To construct the CRISPR/Cas9-based targeting vector, the isogenic 544-bp right homology arm was amplified using P5 and P6 primers (Table 1). Then, it was cloned into the pre-targeting vector. The pre-targeting vector was cut with *Nhe*I and *Xcm*I, and the 516-bp and 7469-bp bands were detected on the agarose gel. Then, the isogenic 541-bp left homology arm was amplified using P3 and P4 primers (Table 1), confirmed and cloned into the pre-targeting vector. For verification of LHA cloning, a CRISPR-based targeting vector was cut with *Pvu*I and *Xho*I, and 503-bp and 7489-bp bands were detected on the agarose gel.

Table 1. List of primers used in this study.

Primer	Sequence (5′ to 3′)	Length (bp)
P1	CACCTCCAGTCACTAACAAAGTAC	20-mer
P2	AAACGTACTTTGTTAGTGACTGGA	20-mer
P3	CATGCATTAGTTCGCGATCGAGCCCTAGGGGAGGTCCTG	39-mer
P4	TGGCGACCGGTACCCTCGAGAAGAATTTCCTGCTTATTTGACTTCTCC	48-mer
P5	CTTTCTAGGGTTAAGCTAGCCTTCCACTAGTATAAACAATTG	42-mer
P6	TGGTGCCACCTATGTTGTGGAGAAATAAAACTGCTCTCCC	40-mer
P7	CGGGCCATTTACCGTAAG	18-mer

Discussion

One of the most important applications for the identification of GSH loci is to use these regions for insertion of transgenes and generating transgenic animals with the ability to be used as bioproduction systems (Li et al., 2019; Ruan et al., 2015). It is possible to achieve a consistent and reliable expression of the transgene by stable chromosomal insertion of the exogenous DNA at a GSH locus (Shin et al., 2020). Since the generation of transgenic animals is expensive and time-consuming, the prediction of the potential GSH loci can be helpful, preventing a potential transgene-silencing over generations.

Traditionally, random integration of a given transgene followed by the screening of the transgene expression across the genome has been used to find the highly expressed regions (Zambrowicz et al., 1997). This method is accompanied by cumbersome and time-consuming steps, including screening of the integrated transgenes, analyzing their expression levels, and identification of reliable GSH regions. Moreover, in the random integration approach, lots of regions, including intergenic and intragenic regions, are targeted and screened, and some intragenic regions could be selected as potential GSH regions. In some previous studies, new GSH regions were identified by genome-wide comprehensive analyses (Ma et al., 2018) or using available bioinformatics data to search for potential GSH regions (Yang et al., 2016b; Irion et al., 2007; Kobayashi et al., 2012; Lee et al., 2019; Li et al., 2014; Liu et al., 2018; Rizzi et al., 2017; Ruan et al., 2015; Stanford et al., 2001; Tasic et al., 2011; Wu et al., 2016; Yang et al., 2016a; Zhu et al., 2014). It has been discussed that the utilization of intragenic regions to express a transgene may lead to transgene silencing, disruption of endogenous genes, or even inducing oncogenes (Oleg E. Tolmachov et al., 2013).

Whole transcriptome analysis has been performed to widely analyze gene expression levels in a range of organisms and tissues (Ma et al., 2018). Thus, an intergenic region between two highly expressed genes could be a potential GSH candidate (Tasic et al., 2011). Nowadays, with the advent of CRISPR/Cas technology, a transgene of interest can be precisely integrated into the candidate GSH region (Kimura et al., 2014). It has been demonstrated that the actively expressed gene-rich regions may support a reliable, consistent, and long-term expression of the transgene. For example, the intergenic region between the *DRG1* and *EIF4ENIF1* genes has been known as a GHS locus in several animals, including mice, humans, and pigs. It has been revealed that both *DRG1* and *EIF4ENIF1* genes have broad spatial and temporal EST (expression sequence tag) expression patterns (Hippenmeyer et al., 2010) and could reliably support transgene expression (Pryzhkova et al., 2020).

The DNA sequences between the *DRG1* and *EIF4ENIF1* genes in mice were compared with those from the same locus in humans to determine the level of sequence identity. Results showed that there was a 45% similarity (Zhu et al., 2014). Functional validation verified that the region was suitable as a safe location for the placement of transgenes in human cells. In another study, the prediction of the GSH locus was accomplished by the assessment of the similarity of adjacent genes and their intron/exon organization. For example, the intergenic sequence between the pig *DRG1* and *EIF4ENIF1* genes was predicted to be a GSH due to its similarity to the adjacent genes of mice (Ruan et al., 2015). Although the GSH locus between these two genes was successfully predicted in the human and pig genomes based on a similarity search, there are two caveats in these studies: ***i***) the levels of expression of these two genes were not evaluated, and ***ii***) the coordination of the *DRG1* and *EIF4ENIF1* genes related to the locations of TAD boundaries was not investigated.

It has been demonstrated that transcriptionally permissive chromatin structures can support the consistent and reliable expression of a transgene. For example, 10.9% of the Chinese hamster ovary (CHO) cell genome contains actively transcribed 3D

chromatin structures, leading to the stability of transgene expression during the cell development process (Hilliard and Lee, 2021). Therefore, the transcriptionally permissive 3D chromatin structures could be easily predicted using RNAseq and Hi-C data. Also, analyzing of NucMap data will make better predictions of GSH regions in the future (Zhao et al., 2019).

Here, we used a multi-faceted approach to predict a GSH region in the chicken genome based on similarity search, RNAseq data, and Hi-C data. The easy-to-use and fast pipeline for the prediction of GSH regions before generating the transgenic animals can facilitate industrial research and development procedures. In this study, for the first time, we introduce the GSH locus located between the *DRG1* and *EIF4ENIF1* genes in the chicken genome. It has been demonstrated that intergenic regions show less nucleosome occupancy than intragenic regions (Voong et al., 2016). So, it is less subjected to silencing. On the other hand, Tasic and colleagues showed that molecular integration tools could have better access to intergenic regions in comparison to intragenic regions in the mouse embryonic stem cells (Tasic et al., 2011). Also, consistent expression of the desirable transgene without silencing for over 30 passages has been reported (Zhu et al., 2014). Hence, the GSH locus located between the *DRG1* and *EIF4ENIF1* genes can be reliably applied to generate transgenic animals.

Acknowledgments
Hesam Dehghani would like to thank all members of his laboratory who have contributed to transgenesis and genome editing experiments.

Conflict of interest
The authors declare that they have no conflict of interest.

References

Fishman, V., Battulin, N., Nuriddinov, M., Maslova, A., Zlotina, A., Strunov, A., et al. (2019) 3D organization of chicken genome demonstrates evolutionary conservation of topologically associated domains and highlights unique architecture of erythrocytes' chromatin. Nucleic Acids Research 47:648–665.

Hilliard, W. and Lee, K.H. (2021) Systematic identification of safe harbor regions in the CHO genome through a comprehensive epigenome analysis.
Biotechnology & Bioengineering 118:659–675.

Hippenmeyer, S., Youn, Y.H. Moon, H.M., Miyamichi, K. Zong, H., Wynshaw-Boris, A., et al. (2010). Genetic mosaic dissection of Lis1 and Ndel1 in neuronal migration. Neuron 68: 695–709.

Irion, S., Luche, H., Gadue, P., Fehling, H.J., Kennedy, M. and Keller, G. (2007) Identification and targeting of the ROSA26 locus in human embryonic stem cells. Nature Biotechnology 25: 1477–1482.

Kimura, Y., Hisano, Y., Kawahara, A. and Higashijima, S. (2014) Efficient generation of knock-in transgenic zebrafish carrying reporter/driver genes by CRISPR/Cas9-mediated genome engineering. Scientific Report 4:6545.

Kobayashi, T., Kato-Itoh, M., Yamaguchi, T., Tamura, C., Sanbo, M., Hirabayashi, M. et al. (2012). Identification of rat Rosa26 locus enables generation of knock-in rat lines ubiquitously expressing tdTomato. Stem Cells Development 21:2981–2986.

Lee, E.-S., Moon, S., Abu-Bonsrah, K.D., Kim, Y.K., Hwang, M.Y., Kim, Y.J. et al. (2019) Programmable nuclease-based integration into novel extragenic genomic safe harbor identified from Korean population-based CNV analysis. Molecular Therapy Oncolytics 14:253–265.

Li, X., Yang, Y., Bu, L., Guo, X., Tang, C., Song, J. et al. (2014) Rosa26-targeted swine models for stable gene over-expression and Cre-mediated lineage tracing. Cell Research 24:501–504.

Li, Y.-S., Meng, R.-R., Chen, X., Shang, C.-L., Li, H.-B., Zhang, T.-J., et al. (2019) Generation of H11-albumin-rtTA Transgenic Mice: A tool for inducible gene expression in the liver. G3. 9:591–599.

Liu, T., Hu, Y., Guo, S., Tan, L., Zhan, Y., Yang, L., et al. (2018) Identification and characterization of MYH9 locus for high efficient gene knock-in and stable expression in mouse embryonic stem cells. PLoS One 13 (2):e0192641.

Ma, L., Wang, Y., Wang, H., Hu, Y., Chen, J., Tan, T., et al. (2018) Screen and verification for transgene integration sites in pigs. Scientific Report **8:**1–11.

Oleg E. Tolmachov, Subkhankulova, T. and Tolmachov, T. (2013) Silencing of transgene expression: a gene therapy perspective. Gene therapy tools and potential applications,

francisco martin molina, intechopen, doi: 10.5772/53379. available from: https://www.intechopen.com/chapters/43164

Papapetrou, E.P., Lee, G., Malani, N., Setty, M., Riviere, I., Tirunagari, L.M.S., et al. (2011) Genomic safe harbors permit high β -globin transgene expression in thalassemia induced pluripotent stem cells. Nature Biotechnology 29: 73–78.

Pryzhkova, M. V., Xu, M.J. and Jordan, P.W. (2020) Adaptation of the AID system for stem cell and transgenic mouse research. Stem Cell Research. 49.

Rizzi, N., Rebecchi, M., Levandis, G., Ciana, P. and Maggi, A. (2017) Identification of novel loci for the generation of reporter mice. Nucleic Acids Research 45(6): 37.

Ruan, J., Li, H., Xu, K., Wu, T., Wei, J. and Zhou, R. (2015) Highly efficient CRISPR / Cas9- mediated transgene knockin at the H11 locus in pigs. Scientific Reports 5:1–10.

Sadelain, M., Papapetrou, E.P. and Bushman, F.D. (2011) Safe harbours for the integration of new DNA in the human genome. Nature Reviews Cancer 12:51–58.

Shin, S., Kim, S.H., Shin, S.W., Grav, L.M., Pedersen, L.E., Lee, J.S., et al. (2020) Comprehensive analysis of genomic safe harbors as target sites for stable expression of the heterologous gene in HEK293 cells. ACS Synthetic Biology 9:1263–1269.

Stanford, W.L., Cohn, J.B., Cordes, S.P. and Lunenfeld, S. (2001) Gene-trap mutagenesis: past, present and beyond. Nature reviews genetics 2:756–768.

Tasic, B., Hippenmeyer, S., Wang, C., Gamboa, M., Zong, H., Chen-Tsai, Y., et al. (2011) Site-specific integrase-mediated transgenesis in mice via pronuclear injection. Proceedings of the National Academy of Sciences 108: 7902–7907.

Voong, L.N., Xi, L., Sebeson, A.C., Xiong, B., Wang, J.-P. and Wang, X. (2016) Insights into nucleosome organization in mouse embryonic stem cells through chemical mapping. Cell 167:1555-1570.

Wu, M., Wei, C., Lian, Z., Liu, R., Zhu, C., Wang, H., et al. (2016) Rosa26 -targeted sheep gene knock-in via CRISPR-Cas9 system. Scientific Reports. 6:1–7.

Yang, D., Song, J., Zhang, J., Xu, J., Zhu, T. and Wang, Z. (2016) Identification and characterization of rabbit ROSA26 for gene knock-in and stable reporter gene expression. Scientific Reports 6:1–8.

Yang, D., Song, J., Zhang, J., Xu, J., Zhu, T., Wang, Z., et al. (2016) Identification and characterization of rabbit ROSA26 for gene knock-in and stable reporter gene expression. Scientific Reports 6: 251-61.

Zambrowicz, B.P., Imamoto, A., Fiering, S., Herzenberg, L.A., Kerr, W.G. and Soriano, P. (1997) Disruption of overlapping transcripts in the ROSA beta geo 26 gene trap strain leads to widespread expression of beta-galactosidase in mouse embryos and hematopoietic cells. Proceedings of the National Academy of Sciences 94: 3789–3794.

Zhao, Y., Wang, J., Liang, F., Liu, Y., Wang, Q., Zhang, H., et al. (2019) NucMap: a database of genome-wide nucleosome positioning map across species. Nucleic Acids Research. 47: 163–169.

Zhu, F., Gamboa, M., Farruggio, A.P., Hippenmeyer, S., Tasic, B., Schüle, B., et al. (2014) DICE, an efficient system for iterative genomic editing in human pluripotent stem cells. Nucleic Acids Research. 42(5):e34.

Research Article

VEGF-C and p53 Gene Expression in the Normal and Neoplastic Mammary Gland of Canines: A Pilot Study

Mohammadreza Nassiri [1*], Azadeh Safarchi [2], Masoume Vakili-Azghandi [3], Vinod Gopalan [4], Mohammad Doosti [3], Shahrokh Ghovvati [5], Ahmad Reza Movassaghi [6]

[1] *Recombinant Proteins Research Group, The Research Institute of Biotechnology Group, Ferdowsi University of Mashhad, Mashhad, Iran*
[2] *School of Biotechnology and Biomolecular Science, University of New South Wales, Sydney, Australia*
[3] *Department of Animal Science, Faculty of Agriculture, Ferdowsi University of Mashhad, Mashhad, Iran*
[4] *School of Medicine and Medical Science, Menzies Health Institute Queensland, Griffith University, Gold Coast, 4222, Australia*
[5] *Department of Animal Science, Faculty of Agriculture, University of Guilan, Rasht, Iran*
[6] *Department of Pathobiology, Faculty of Veterinary Medicine, Ferdowsi University of Mashhad, Mashhad, Iran*

Received 1 July 2021 Accepted 14 August 2021

Abstract

The p53 is a tumor suppressor protein that plays an essential role in controlling the cell cycle. In addition, vascular endothelial growth factor (VEGF) is one of the most strong and specific angiogenic factors. The main objective of this study was to evaluate the impact of p53 and VEGF-C gene expression in the neoplastic and normal mammary glands of canines as an animal model. Eleven benign and malignant and five normal specimens were collected. After RNA extraction and cDNA synthesis, relative quantification of *p53* and *VEGF-C* genes was accomplished by real-time quantitative PCR (RT-qPCR), in which β-actin was used as a reference gene. The relative mRNA expression of the *p53* and *VEGF-C* genes was analyzed by GLM procedure of SAS software v9.2. The results indicated that the VEGF-C and p53 mRNA expression in neoplastic specimens was over-and down-expressed, respectively, compared with normal specimens. The p53 mRNA expression was significantly negatively associated with VEGF-C (~4 fold) in neoplastic specimens ($P < 0.01$). These findings emphasized that simultaneous evaluation of p53 and VEGF-C expression can be used as tumor biomarkers for the early diagnosis of malignancy in canines. Furthermore, RT-qPCR is a rapid and sensitive method for monitoring and investigating suspicious canines at the early stage of malignancy and may provide an alternative explanation for deregulated p53 signaling in breast cancer.

***Keywords*:** Canine mammary tumor, Breast cancer, p53, VEGF-C, Real-time PCR

Introduction

Breast cancer is one of the most prevalent types of human and canine neoplasia. Although there are numerous reports of mammary tumors in both man and male dogs (Li et al., 2012; Saba et al., 2007), it is rated the most common malignancy in women and female canines (Ghoncheh et al., 2016; Kaszak et al., 2018). The canine mammary tumor (CMT) is frequently diagnosed in dogs, accounting for 52% of all tumors, and is the most typical form of malignant neoplasia of the bitch (Kaszak et al., 2018). Due to the ethical issues and scarcity of human tissue sampling, various animals are used as human breast cancer models in current years (Abdelmegeed and Mohammed, 2018; Qiu et al., 2008a). Furthermore, recent studies showed clinical and molecular similarities between human breast cancer (HBC) and canine mammary tumors, including spontaneous tumor incidence, onset age, hormonal etiology, and molecular characteristics and gene expressions (Abdelmegeed and Mohammed, 2018; Queiroga et al., 2011; Visan et al., 2016). The etiology of BHC and CMT is multifactorial and includes factors such as genetic predisposition, the timing of onset of menarche and first pregnancy, and hormonal receptor activity in the mammary tissues (Abdelmegeed and Mohammed, 2018).

Meta-analysis studies revealed that gene expression of mammary tumor cells varies, and this can be used as a marker for early diagnosis of the disease that may help evaluate the cancer progression and increase the chance of a cure by chemotherapy (Bell et al., 2017). Two of the most common tumor biomarkers as proteins that can be measured in blood or cancer tissues to show the presence of the disease identified in humans and dogs are p53 and VEGF-C (Bell et al., 2017; Klopfleisch and Gruber, 2009; Santos et al., 2010).

*Corresponding author's e-mail address: *nassiryr@um.ac.ir*

p53 is an important tumor suppressor protein that plays an essential role in controlling the cell cycle by inducing apoptosis when cell damage cannot be repaired (Yang et al., 2013). It is located in the nucleus of the cell, which directly connects to the DNA. Following damage of DNA by various factors such as toxic chemicals, radiation, or ultraviolet (UV) rays from sunlight, p53, as a transcription factor, regulates the expression of genes involved in apoptosis (Levine, 2019). Mutations in the *p53* gene located in the chromosomes 17 and 5 of humans and dogs respectively seem to play a critical role as an oncogene in the carcinogenesis of mammary glands and tumor progression (Lee and Kweon, 2002). The vascular endothelial growth factor (VEGF) family is one of the most strong and specific angiogenic factors and is a well-known biomarker in oncologic studies [7]. VEGF proteins are encoded by four genes: *VEGF-A*, *VEGF-B*, *VEGF-C*, and *VEGF-D* (Kaszak et al., 2018). While *VEGF-A* and *VEGF-B* are responsible for angiogenesis, *VEGF-C* and *VEGF-D* have a key role in lymphangiogenesis (Karpanen et al., 2001). VEGFs mediates new vessel formation and regulates their functions and structures in healthy tissues (Karpanen et al., 2001; Millanta et al., 2010). Increased expression of VEGF in numerous human cancer cells is a main factor in the growth of malignant tumors and muscle destruction. Furthermore, overexpression of VEGF-C led to enhanced metastasis of regional lymph nodes and invasive lymphatic vessels in breast cancer in humans and canines (Karpanen et al., 2001; Qiu et al., 2008a).

In recent decades, real-time quantitative PCR (RT-qPCR) is one of the most useful biomolecular techniques that have been used for gene expression studies. In the present study, we established an RT-qPCR method to quantify the expression of *p53* and *VEGF-C* genes accurately and reproducibly in normal and neoplastic canine mammary glands.

Materials and Methods

Animals and Tissue Samples

A total of 11 adult intact bitches of various breeds bearing CMT that had not received any chemotherapy treatments before surgery were included in this study. All bitches were referred to the veterinary teaching hospital, the Ferdowsi University of Mashhad, for surgical excision of mammary tumors. Mammary tumor and normal mammary tissues were collected from the same bitch to avoid the different endocrine status among individual bitches.

Sample Collection and Histopathological Analysis

Both mammary tumors and contralateral normal mammary tissues from the same canines were obtained during the surgical procedure. Immediately after surgical excision, each tissue sample was divided into two parts. One part was maintained in liquid nitrogen for real-time PCR analysis. The other half of the sample was fixed in 10% neutral buffered formalin, dehydrated, and embedded in paraffin. Tissues were sectioned in 4 μm slices for hematoxylin and eosin staining and send for histopathology analysis. Tumor characteristics such as degree of differentiation and the other associated tumor properties were analyzed (Goldschmidt et al., 2011)

RNA Extraction and cDNA Synthesis

Total RNA was extracted from mammary gland specimens using Trizol kit (Iso Gene Company, Moscow, Russia) and treated with RNase-free DNase I to remove any DNA contamination. RNAs were reverse transcribed and cDNAs synthesized using RevertAid™ H minus Reverse Transcriptase kit (Fermentas Company, Burlington, USA). The quantity of RNA and cDNA samples was determined by Nano-Drop ND 2000 spectrophotometer (Thermo, Wilmington, USA). cDNAs were diluted at 300 ng/μl concentration for uniformity by DNase-free diluted water.

Primer Design

Primers for *β-actin*, as the reference gene, *p53*, and *VEGF-C*, as target genes, were designed by the Primer premier software, version5 (Table 1). Primers were blasted in the primer database such as RT (http://rtprimerdb.org) to confirm the total gene specificity of the nucleotide sequences chosen for the primers and the structure of primers.

Table 1. The Specifications of the primers used in the Real-Time PCR reactions

Gene	Primer sequence	Application size	The accession number of related genes

p53	Forward 5' TGACAGTAGTGACGGTCTTGCC 3'	117	NM_001003210.
	Reverse 5' TCATAAGGCACCACCACACTG 3'		1
VEGF-C	Forward 5' GAGCAGCAACAAACACCTTCTT 3'	110	
	Reverse 5' GAGGTGGCTTGTGCTGGTG 3'		XM-540047
beta-Actin	Forward 5' CAAATGTGGATCAGCAAGCAG 3'	103	
	Reverse 5' GAAAGGGTGTAACGCAACTAAAG 3'		XM-544346

Real-time Quantitative Reverse Transcriptase PCR Assay

300 ng of cDNA were amplified in a real-time quantitative polymerase chain reaction (RT-qPCR) using TaqMan Universal Master Mix (PE Applied Biosystems), 0.8 ng primers for p53, β-actin, and VEGF-C. The RT-qPCRs were performed in an ABI PRISM Model 7300 sequence detector by using the fluorescent dye SYBR Green I. The optimum concentration of primers was determined in preliminary experiments. Thermal cycling conditions included initial denaturation in 1 cycle of 10 minutes at 95°C, followed by 45 cycles of 30 seconds at 95°C, 30 seconds at 60°C, and 30 seconds at 72°C and melting curve in 1 cycle of 15 seconds at 95°C, one minute at 60°C, 15 seconds at 95°C and 15 seconds at 60°C. A melting curve was performed after qPCR cycles to verify amplification specificity. Reactions without reverse transcriptase or template served as controls for p53 and VEGF-C genomic DNA contamination. The specificity of the amplified products was confirmed by gel electrophoresis (1.5% agarose gels).

Quantification of Target Gene Expression

PCR efficiency and data analysis were performed using the Pfaffle method (Pfaffl, 2001). The standard curve simplifies calculations and avoids practical and theoretical problems currently associated with relative real-time PCR-efficiency assessment. p53 and VEGF-C standard curve by real-time PCR was plotted by serial dilution of Ct values vs. log of input cDNAs. A standard curve slope of –3.32 indicates a PCR reaction with 100% efficiency. The slope of this curve was –3.1, and it was in the expected range. In this study, PCR efficiency was noted 95% for p53, VEGF-C, and β-actin genes. After determining the expression content of the *VEGF-C* and *p53* genes for each cancerous sample, the obtained value is divided into the mean internal control of normal samples (β-actin) and the relative expression of these genes obtained according to mean ± SD for each cancerous sample.

Statistical Analysis

All samples were analyzed in triplicate. Statistical analysis was performed using the SDS software (v1.4). Fisher's exact test was used for categorical variables. Student t-test procedure was performed in SAS (v9.2) and Microsoft Excel to determine statistical significance. The level of significance was 5% ($P < 0.05$).

Results

Histopathological Analysis

Of eleven dogs, four had benign mammary gland tumors, including two benign mixed-type tumors and two fibroadenomas (Table 2). From seven malignant mammary gland tumors (Figure.1. A-D), one showed carcinosarcoma features with malignant epithelial and myoepithelial cells with connective tissues (Figure.1A). Another case showed complex carcinoma features with proliferated myoepithelial cells and abundant chondromucinous substance (Figure.1B). Among the cases, extensive necrosis was noted in one with features of a solid tumor (Figure.1C). Tubulopapillary subtype was also noted in one case (Figure.1D), which showed papillary projections with hyperchromatic nuclei.

Table 2. Histopathological classification of tumor

Histological diagnosis	Number of cases
Benign tumor	
Benign mixed tumor	2
Fibroadenoma	2
Malignant tumor	
Tubulopapillary carcinoma	1
Simple carcinoma	2
Cystic papillary carcinoma	1
Complex-type carcinoma	3

Total	11

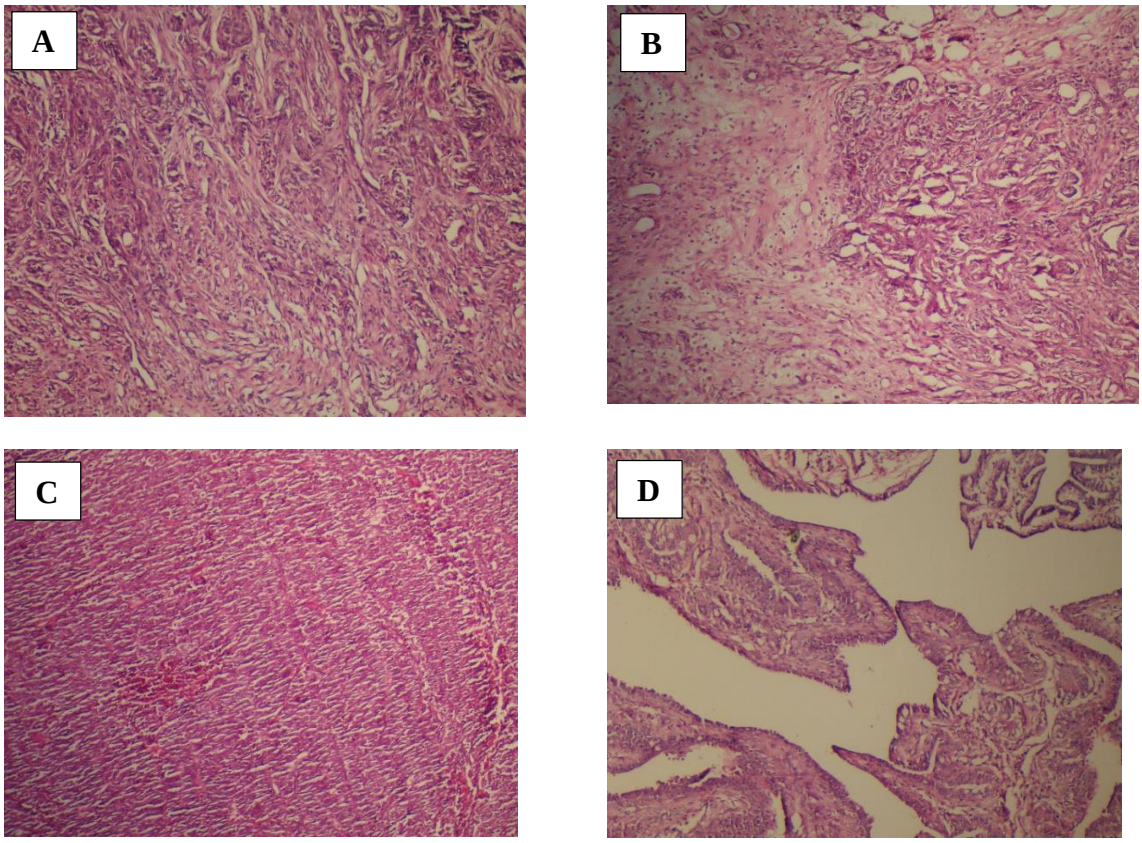

Figure 1. Histopathology of different types of malignant canine mammary glands.
A: Carcinosarcoma, a tumor composed of cells morphologically resembling malignant epithelial and myoepithelial cells with malignant connective tissue B: Complex carcinoma showed proliferation of luminal epithelial cells with pleomorphic and hyperchromatic nuclei and also the proliferation of spindle-shaped myoepithelial cells arranged in a stellate pattern with chondromucinous substance C: Caudal mammary gland as Solid carcinoma, tumor cells were arranged in solid sheets. Some tumor cells showed vacuolated cytoplasm. There were scattered necrotic foci. D: Large mammary gland, Tubulopapillary carcinoma. There are tubules with papillary projections consist of tumor cells with hyperchromatic nuclei. Mitotic figures were 8 per 10 HPF.

Gene Expression

To test the VEGF-C and p53 expression in CMT compared to the normal mammary gland of the same dogs, mRNA copy numbers (Ct) of VEGF-C per mRNA the reference gene was determined using RT-qPCR. The results showed that VEGF-C was overexpressed significantly (approximately 4-fold change) in the neoplastic tissue compared to normal tissues (Figure 2). On the other hand, tumor suppressor p53 gene expression in cancerous tissues was significantly lower than normal mammary glands.

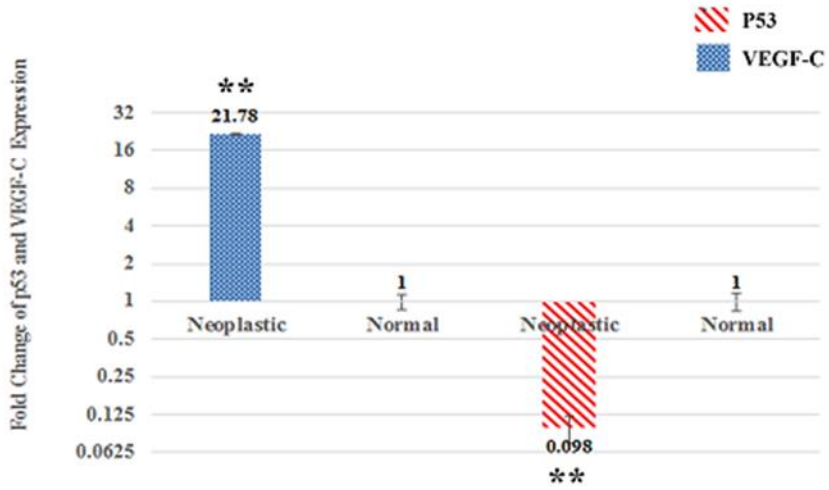

Figure 2. Normalized expression fold change indicates the mean expression of VEGF-C and p53 in the normal and neoplastic mammary glands. While VEGF-C was overexpressed in CMT samples, p53 was down-expressed in neoplastic tissues (* $P < 0.05$, ** $P < 0.01$).

Discussion

Canine mammary tumors (CMT) are usually reported in female elderly dogs (8-10 years old) and may vary depending on different breeds and lifestyles (Raposo et al., 2017; Sorenmo et al., 2011). The second global leading cause of death due to cancer among women is breast cancer. Common clinical and epidemiological features between HBC and CMT, including incidence rate and mortality, age of onset and an identical course of the disease, histopathological symptoms, hormonal etiology, as well as molecular markers, have been described in recent years (Visan et al., 2016; Garcia et al., 2021). These common clinical and epidemiological features make canine a suitable animal model to investigate different diagnoses and therapies of breast neoplasia, leading to comparative oncological studies (Abdelmegeed and Mohammed, 2018; Raposo et al., 2017; Visan et al., 2016). So far, surgery and removal of the affected glands are the main available treatment for HBC and CMT. In most malignant cases, follow-up chemotherapy or radiotherapy is performed, which is costly and might not be efficient (Kaszak et al., 2018). Therefore, the early detection of neoplasia seems essential in the disease prognosis in humans and dogs. Nowadays, biomarker investigation is suggested as a suitable way for the early diagnosis and evaluation of the risk assessments and prognosis of HBC and CMT (Chen et al., 2017; Ma et al., 2010).

Immunohistochemistry (IHS) analysis has been vastly used to investigate and evaluate the expression of proteins as biomarkers in breast cancer, either in humans or canines. However, quantification of biomarker expression by IHS is difficult. The fluorescence-based detection methods, like real-time quantitative PCR, have emerged as an accurate and sensitive technique to investigate the mRNA expression of different genes, including tumor biomarkers. The expression of p53 and VEGFs, two of the most studied common biomarkers, in dog normal and neoplastic mammary glands have been evaluated. Here, we conducted RT-qPCR as a rapid and precise method targeting mRNA using the fluorescent dye SYBR Green I.

Some specific protein biomarkers expressed by cancerous cells can be detected in serum or tissues and are reported to be common in humans and dogs (Kaszak et al., 2018; Pena et al., 2014; Qiu et al., 2008c; Raposo et al., 2017). VEGFs and p53 have an essential role in HBC and CMT (Howard et al., 2004; Karpanen et al., 2001; Levine, 2019). The *p53* is a tumor suppressor gene that acts as a transcription factor and plays a vital role in genome stability by regulating cell proliferation, cellular death, and repairing damaged DNA (Wijnhoven et al., 2005). The amino acid sequence of the p53 protein in dogs is approximately 87% homologous to the human one. Like humans, it is mutated in different types of canine tumors, including CMT (Zhang et al., 2009).

Several studies showed numerous mutations leading to a different level of p53 expression in HBC as well as CMT and its direct correlation with tumor prognosis (Bae et al., 2018; Gasco et al., 2002; Howard et al., 2004; Lee et al., 2004; Levine, 2019;

Wang, 2017). Dolka et al. reported that expression of p53 was positive in only 30% of CMTs, depending on the tumor malignancy and the breed of the dogs (Dolka et al., 2016). Klopfleisch and Gruber showed the heterogeneous expression of p53 in lymph nodes metastasizing canine mammary adenocarcinoma and normal gland using real-time PCR and questioned the prognostic significance of p53 (Klopfleisch and Gruber, 2009). They only found a few significantly increased expressions of p53 in a low sample size (20% of adenomas and 10% of adenocarcinomas). Our results confirmed the previous findings by Ripoli et al. in 2016, which showed the lower expression of p53 in malignant tissues compared to normal tissues (Lüder Ripoli, 2016). The controversial reports of the p53 expression levels in canines might be due to a correlation between its expression and differences in dog breed (Veldhoen et al., 1999). It is demonstrated that expression of p53 is mainly associated with the weight of breed dogs as it was found in 67% of large breed dogs with CMTs in the study of Dolka et al. (Dolka et al., 2016). Since p53 plays as a tumor suppressor protein, its lower expression in cancerous tissues found in our study might lead to uncontrolled cell cycles and hyperplasia in mammary glands. It is reported that the less expression or inactivation of p53 in neoplastic tissues is due to numerous mechanisms mainly caused by mutations in the gene (Gasco et al., 2002; Muto et al., 2000).

The vascular endothelial growth factor (VEGF) family, which includes VEGF-A - D, in many human tumor types, plays an essential role in the induction of angiogenesis and uses as the most frequent biomarker in human clinical medicine (Kaszak et al., 2018). VEGF-C is believed to be a critical factor in lymph angiogenesis, leading to a poor prognosis of aggressive breast cancer (Karpanen et al., 2001). Overexpression of VEGF-C in HBC and CMT is associated with malignant tumors and a bad prognosis. It can be detected in serum and tissue, making it a useful biomarker in early HBC and CMT (Santos et al., 2010; Zajkowska et al., 2016). Higher expression of VEGF-C in malignant cases of both HBC and CMT is demonstrated (Mohammed et al., 2007; Qiu et al., 2008a). Furthermore, Thammineni et al. recommend VEGF-C evaluation as a diagnostic biomarker of lymph node metastasis in patients with breast cancer (Thammineni et al., 2019). The VEGF expression was significantly higher in malignant CMT cases than benign using IHS and RT-qPCR (Anadol et al., 2017; Qiu et al., 2008a; Queiroga et al., 2011). The use of immunohistochemistry showed that VEGFs increased in cancer tissues, serum, and plasma of animals with cancer compared to normal (Kato et al., 2007). Our results confirm that previous studies showed significant VEGF-C overexpression in malignant CMT compared to benign CMT using RT-qPCR. Furthermore, high VEGF-C expression was observed in CMTs with lymph node metastasis compared to the tumors without one (Qiu et al., 2008b). The correlation between the higher expression of VEGF-C and lymph node metastasis and its prognosis was also observed in human breast cancer (Chen et al., 2017; Li et al., 2012; Liang and Li, 2014; Saba et al., 2007). In our results, the expression of VEGF-C was more (4-fold overexpression) in tumor tissues than normal.

In HBC, the correlation between the expression of p53 and VEGF was controversial. While Lu et al. and Howard et al. found no correlation between the expression of p53 and VEGF in invasive breast cancer and primary breast tumor respectively (Howard et al., 2004; Lu et al., 2008), some studies found a positive correlation in patients with breast cancer and suggested it as the higher risk factor. (Linderholm et al., 2000; Noranizah et al., 2010). Iovino et al. showed a significant positive correlation between VEGF serum level and p53 overexpression in primary endocrine-positive breast cancer patients (Iovino et al., 2008). To the best of our knowledge, it seems that this is the first study investigating the simultaneous expression of p53 and VEGF in canines. Our findings showed the correlation between the higher expression of VEGF-C and lower expression of p53 in canine neoplastic mammary glands, which might be due to the mutation in p53 and its effect on VEGF and can cause poor prognosis (Linderholm et al., 2000; Linderholm et al., 2001).

In summary, our results showed that quantitative real-time PCR could be used as a sensitive and rapid method to investigate the quantification of biomarker expression, including p53 and VEFG-C, in different types of CMT. Furthermore, our finding suggested that overexpression of VEGF-C and down-expression of p53 may contribute to the malignancy of CMT and help the researchers for early diagnosis of malignant tumors, which help to prevent the metastasis of CMTs.

Acknowledgments

This work was supported financially by the Ferdowsi University of Mashhad, Iran.

Conflict of interest statement

The authors declare that they have no conflicts of interest.

References

Abdelmegeed S.M. and Mohammed S. (2018) Canine mammary tumors as a model for human disease. Oncology Letter 15:6, 8195-8205.

Anadol E., Yar Saglam A.S., Gultiken N., Karakas K., Alcigir E., Alkan H. et al. (2017) Expression of iNOS, COX-2 and VEGF in canine mammary tumours and non-neoplastic mammary glands: Association with clinicopathological features and tumour grade. Acta Veterinaria Hungarica 65:3, 382-393.

Bae S.Y., Nam S.J., Jung Y., Lee S.B., Park B.W., Lim W. et al. (2018) Differences in prognosis and efficacy of chemotherapy by p53 expression in triple-negative breast cancer. Breast Cancer Research and Treatment 172, 437-444.

Bell R., Barraclough R. and Vasieva O. (2017) Gene expression meta-analysis of potential metastatic breast cancer markers. Current Molecular Medicine 17:3, 200-210.

Chen Y., Liu Y., Wang Y., Li W., Wang X., Liu X. et al. (2017) Quantification of STAT3 and VEGF expression for molecular diagnosis of lymph node metastasis in breast cancer. Medicine (Baltimore) 96, e8488.

Dolka I., Krol M. and Sapierzynski R. (2016) Evaluation of apoptosis-associated protein (Bcl-2, Bax, cleaved caspase-3 and p53) expression in canine mammary tumors: An immunohistochemical and prognostic study. Research in Veterinary Science 105, 124-133.

Garcia A.P.V., Reis L.A., Nunes F.C., Longford F.G.J., Frey J.G., de Paula A.M. and Cassali G.D. (2021) Canine mammary cancer tumour behaviour and patient survival time are associated with collagen fibre characteristics. Scientific Reports 11: 5668.

Gasco M., Shami S. and Crook T. (2002) The p53 pathway in breast cancer. Breast Cancer Research 4, 70-76.

Ghoncheh M., Pournamdar Z. and Salehiniya H. (2016) Incidence and mortality and epidemiology of breast cancer in the world. The Asian Pacific Journal of Cancer Prevention 17, 43-46.

Goldschmidt M., Pena L., Rasotto R. and Zappulli V. (2011) Classification and grading of canine mammary tumors. Veterinary Pathology 48:1, 117-131.

Howard E.M., Lau S.K., Lyles R.H., Birdsong G.G., Tadros T.S., Umbreit J.N. et al. (2004) Correlation and expression of p53, HER-2, vascular endothelial growth factor (VEGF), and e-cadherin in a high-risk breast-cancer population. International Journal of Clinical Oncology 9, 154-160.

Iovino F., Ferraraccio F., Orditura M., Antoniol G., Morgillo F., Cascone T. et al. (2008) Serum vascular endothelial growth factor (VEGF) levels correlate with tumor VEGF and p53 overexpression in endocrine positive primary breast cancer. Cancer Investigation 26:3, 250-255.

Karpanen T., Egeblad M., Karkkainen M.J., Kubo H., Yla-Herttuala S., Jaattela M. et al. (2001) Vascular endothelial growth factor C promotes tumor lymphangiogenesis and intralymphatic tumor growth. Cancer Research 61:5, 1786-1790.

Kaszak I., Ruszczak A., Kanafa S., Kacprzak K., Krol M. and Jurka P. (2018) Current biomarkers of canine mammary tumors. Acta Veterinaria Scandinavica 60: 66.

Kato Y., Asano K., Mogi T., Kutara K., Teshima K., Edamura K. et al. (2007) Clinical significance of circulating vascular endothelial growth factor in dogs with mammary gland tumors. Journal of Veterinary Medicine Science 69:1, 77-80.

Klopfleisch R. and Gruber, A.D. (2009) Differential expression of cell cycle regulators p21, p27 and p53 in metastasizing canine mammary adenocarcinomas versus normal mammary glands. Research in Veterinary Science 87:1, 91-96.

Lee C.H., Kim W.H., Lim J.H., Kang M.S., Kim D.Y. and Kweon O.K. (2004) Mutation and overexpression of p53 as a prognostic factor in canine mammary tumors. Journal of Veterinary Science 5:1, 63-69.

Lee C.H. and Kweon, O.K. (2002) Mutations of p53 tumor suppressor gene in spontaneous canine mammary tumors. Journal of Veterinary Science 3: 4, 321-325.

Levine A.J. (2019) The many faces of p53: something for everyone. Journal of Molecular Cell Biology 11:7, 524-530.

Li X., Dang X. and Sun X. (2012) Expression of survivin and VEGF-C in breast cancer tissue and its relation to lymphatic metastasis. European Journal of Gynaecological Oncology 33: 2, 178-182.

Liang B. and Li Y. (2014) Prognostic significance of VEGF-C expression in patients with breast cancer: A meta-analysis. Iranian Journal of Public Health 43: 2, 128-135.

Linderholm B., Lindh B., Tavelin B., Grankvist K. and Henriksson R. (2000) p53 and vascular-endothelial-growth-factor (VEGF) expression predicts outcome in 833 patients with primary breast carcinoma. International Journal of Cancer 89: 51-62.

Linderholm B.K., Lindahl T., Holmberg L., Klaar S., Lennerstrand J., Henriksson R. et al. (2001) The expression of vascular endothelial growth factor correlates with mutant p53 and poor prognosis in human breast cancer. Cancer Research 61:5, 2256-2260.

Lu X., Gu Y., Ding Y., Song W., Mao J., Tan J. et al. (2008) Correlation of ER, PgR, HER-2/neu, p53, and VEGF with clinical characteristics and prognosis in Chinese women with invasive breast cancer. The Breast Journal 14: 308-310.

Lüder Ripoli F., Conradine Hammer S., Mohr A., Willenbrock S., Hewicker-Trautwein M., Brenig B. et al. (2016) Multiplex gene expression profiling of 16 target genes in neoplastic and non-Neoplastic canine mammary tissues using branched-DNA assay. International Journal of Molecular Sciences 17, 9.

Ma H., Wang Y., Sullivan-Halley J., Weiss L., Marchbanks P.A., Spirtas R. et al. (2010) Use of four biomarkers to evaluate the risk of breast cancer subtypes in the women's contraceptive and reproductive experiences study. Cancer Research 70:2, 575-587.

Millanta F., Caneschi V., Ressel L., Citi S. and Poli A. (2010) Expression of vascular endothelial growth factor in canine inflammatory and non-inflammatory mammary carcinoma. The Journal of Comparative Pathology 142: 36-42.

Mohammed R.A., Green A., El-Shikh S., Paish E.C., Ellis I.O. and Martin S.G. (2007) Prognostic significance of vascular endothelial cell growth factors -A, -C and -D in breast cancer and their relationship with angio- and lymphangiogenesis. British Journal of Cancer 96: 1092-1100.

Muto T., Wakui S., Takahashi H., Maekawa S., Masaoka T., Ushigome S. et al. (2000) p53 gene mutations occurring in spontaneous benign and malignant mammary tumors of the dog. Veterinary Pathology 37:3, 248-253.

Noranizah W., Siti-Aishah M.A., Munirah M.A., Norazlin M.H., Rohaizak M., Naqiyah I., Sharifah N.A. et al. (2010) Immunohistochemical expression of vascular endothelial growth factor (VEGF) and p53 in breast lesions. Clinical Therapeutics 161:2, 129-137.

Pena L., Gama A., Goldschmidt M.H., Abadie J., Benazzi C., Castagnaro M. et al. (2014) Canine mammary tumors: a review and consensus of standard guidelines on epithelial and myoepithelial phenotype markers, HER2, and hormone receptor assessment using immunohistochemistry. Veterinary Pathology 51: 127-145.

Pfaffl M.W. (2001) A new mathematical model for relative quantification in real-time RT-PCR. Nucleic Acids Research 29: 9, e45.

Qiu C., Lin D., Wang J. and Wang L. (2008a) Expression and significance of PTEN in canine mammary gland tumours. Research Veterinary Science 85:2, 383-388.

Qiu C., Lin D.D., Wang H.H., Qiao C.H., Wang J., Zhang T. (2008b) Quantification of VEGF-C expression in canine mammary tumours. Australian Veterinary Journal 86:7, 279-282.

Qiu C.W., Lin D.G., Wang J.Q., Li C.Y., Deng G.Z. (2008c) Expression and significance of PTEN and VEGF in canine mammary gland tumours. Veterinary Research Communications 32:6, 463-472.

Queiroga F.L., Pires I., Parente M., Gregorio H., Lopes C.S. (2011) COX-2 over-expression correlates with VEGF and tumour angiogenesis in canine mammary cancer. Veterinary Journal 189:1, 77-82.

Raposo T.P., Arias-Pulido H., Chaher N., Fiering S.N., Argyle D.J., Prada J. et al. (2017) Comparative aspects of canine and human inflammatory breast cancer. Seminars in Oncology 44: 4, 288-300.

Saba C.F., Rogers K.S., Newman S.J., Mauldin G.E. and Vail D.M. (2007) Mammary gland tumors in male dogs. Journal of Veterinary Internal Medicine 21: 5, 1056-1059.

Santos A.A., Oliveira J.T., Lopes C.C., Amorim I.F., Vicente C.M., Gartner F.R. et al. (2010)

Immunohistochemical expression of vascular endothelial growth factor in canine mammary tumours. The Journal of Comparative Pathology 143: 4, 268-275.

Sorenmo K.U., Rasotto R., Zappulli V. and Goldschmidt M.H. (2011) Development, anatomy, histology, lymphatic drainage, clinical features, and cell differentiation markers of canine mammary gland neoplasms. Veterinary Pathology 48: 85-97.

Thammineni K.L., Thakur G.K., Kaur N. and Banerjee B.D. (2019) Significance of MMP-9 and VEGF-C expression in North Indian women with breast cancer diagnosis. Molecular and Cellular Biochemistry 457:1-2, 93-103.

Veldhoen N., Watterson J., Brash M., Milner J. (1999) Identification of tumour-associated and germ line p53 mutations in canine mammary cancer. British Journal of Cancer 81: 3, 409-415.

Visan S., Balacescu O., Berindan-Neagoe I. and Catoi C. (2016) In vitro comparative models for canine and human breast cancers. Clujul Medical 89: 38-49.

Wang L. (2017) Early diagnosis of breast cancer. Sensors17:7, 1572.

Wijnhoven S.W., Zwart E., Speksnijder E.N., Beems R.B., Olive K.P., Tuveson D.A. et al. (2005) Mice expressing a mammary gland-specific R270H mutation in the p53 tumor suppressor gene mimic human breast cancer development. Cancer Research 65: 8166-8173.

Yang P., Du C.W., Kwan M., Liang S.X. and Zhang, G.J. (2013) The impact of p53 in predicting clinical outcome of breast cancer patients with visceral metastasis. Scientific Reports 3, 2246.

Zajkowska M., Glazewska E.K., Bedkowska G.E., Chorazy P., Szmitkowski M. and Lawicki S. (2016) Diagnostic power of vascular endothelial growth factor and macrophage colony-stimulating factor in breast cancer patients based on ROC analysis. Mediators of Inflammation 2016: 5962946.

Zhang J., Chen X., Kent M.S., Rodriguez C.O. and Chen X. (2009) Establishment of a dog model for the p53 family pathway and identification of a novel isoform of p21 cyclin-dependent kinase inhibitor. Molecular Cancer Research 7: 67-78.

Research Article

Molecular Screening of Nitrate Reductase Enzyme in Native Halophilic Bacteria of Iran

Saeedeh Sibevieh [1¶], Ensieh Salehghamari [2¶*], Mohammad Ali Amoozegar [3], Mohammad Reza Zolfaghari [1], Mohammad Soleimani [4], Zohre Nasrollahzadeh [2], Sara Eftekhari Yazdi [3]

[1] *Department of Microbiology, Qom Branch, Islamic Azad University, Qom, Iran*
[2] *Department of Cell and Molecular Sciences, Faculty of Biological Sciences, Kharazmi University, Tehran, Iran,*
[3] *Extremophiles Laboratory, Department of Microbiology, Faculty of Biology and Center of Excellence in Phylogeny of Living Organisms, College of Science, University of Tehran, Tehran, Iran*
[4] *Department of Microbiology, Faculty of Medicine, AJA University of Medical Sciences, Tehran, Iran*

Received 13 September 2020 Accepted 5 May 2021

Abstract

With the increased usage of nitrate fertilizers, the removal of their stable ionic and water-soluble end products is a challenge for human health. Several physicochemical methods have been examined for nitrate removal of water, but biological treatments are mostly preferred due to a higher efficiency and lower cost. To remove nitrogen from water, we investigated the potential of nitrate-reducing halophilic and halotolerant bacteria. A total of 50 strains from different saline and hypersaline environments of Iran, including the Incheboron wetland, Aran-Bidgol salt-lake, and Urmia endorheic salt-lake, were screened for nitrate reductase production. Among investigated bacteria, 60% and 19% of strains obtained from Urmia lake, and Incheboron wetland produced nitrate reductases, respectively. The nitrate reductase coding genes *narG*, and *napA* were analyzed in all strains with confirmed nitrate-reducing capacity. The *napA* gene was successfully amplified from a gram-negative halophilic strain, and the *narG* gene was detected in ten halophilic strains. Among nitrate-reducing isolates with the *narG* gene expression, the *Kocuria rosea* strain R3A34 showed the highest nitrate reductase production level. This strain was selected to optimize for its denitrifying activity. Results showed that 32°C, pH 7.0, NaCl 8% (w/v), and mannitol (as a carbon source) provide the optimal environmental conditions for the efficient production of nitrate reductase by the *Kocuria rosea* strain R3A34. As these are compatible with wastewaters conditions, this bacterium can be a proper candidate for bioremediation of wastewaters from nitrate pollutants.

***Keywords*:** Halophiles, *Kocuria*, *napA*, *narG*, Nitrate Reductase

Introduction

Increased frequency of water eutrophication has made the issue of nitrate removal from the ecosystem more important. With the increased usage of nitrate fertilizers, the amount of nitrate uptake in the body has quadrupled compared to the past (Luvizotto et al., 2018, Pastorelli et al., 2013). As nitrate is a stable ion with a high water-solubility and low precipitation or adsorption capacity, its removal is remained as a challenge for human health. Several methods have been examined, such as reverse osmosis, ion exchange, distillation, electrodialysis, and biodenitrification. Among which, the latter one is widely applied in the removal of different pollutions such as nitrogen because of its high efficiency and low cost (Duan et al., 2015). Heterotrophic denitrification is the process of nitrate reduction to nitrite, nitric oxide, nitrous oxide, and nitrogen (N_2). This process is carried out by denitrifying bacteria and eukaryotic microorganisms (Baggs, 2011). Nitrate reductase is one of the most important enzymes which reduces nitrate to nitrite. The membrane-bound Nar and the periplasmic Nap enzymes are two types of bacterial nitrate reductases (Argandona et al., 2006).

The previously known heterotrophic denitrifying bacteria are mostly isolated from freshwater or soil. Hence, they may not work efficiently in wastewaters with a high salinity (>1%), mostly originated from various industrial activities such as seafood processing, tanning, and petroleum production. As ***i***) high salinity can cause cell plasmolysis, and ***ii***) several nitrate-contaminated environments contains high amounts of salts, the utilization of salt-tolerant/halophilic microorganisms are of great significance. The majority of the reports about isolated halophilic microorganisms have focused on

* Corresponding author's e-mail address: esaleh@khu.ac.ir
¶ *These authors are equally contributed to this article.*

the degradation of organic substances (Paniagua-Michel et al., 2018), while halophilic strains which are capable of heterotrophic nitrification have been rarely reported.

According to above explanations, halophilic, or halotolerant strains can be considered as valuable candidates to remove nitrate from saline or hypersaline environments. To remove nitrogen from such wastes, we studied several nitrate-reducing halophilic, and halotolerant bacteria and found a novel strain with the nitrate contamination-reducing capacity of such saline environments. The newly-identified bacterial strain *Kocuria rosea* R3A34 IBRC-M 11008 with such a high level of denitrifying activity in a short time, has not been reported before. So, considering its capacity, it can be proposed as a valuable candidate for industrial treatment of saline wastes. Moreover, bacterial isolates were screened for the *narG*, and *napA* nitrate-reducing responsible genes. It was confirmed that the selected halophilic bacterium *Kocuria rosea* strain R3A34 has *narG*, and *napA* genes. Furthermore, different conditions of the culture medium affecting the heterotrophic denitrification capacity of the strain R3A34 were investigated to find the optimal condition.

Materials and Methods

Bacterial strains, and culture medium conditions

A Total of 50 halophilic bacterial strains were received from the Iranian Biological Resource Center (IBRC) (Supplementary Table 1). The strains belong to the different saline environments of Iran, including Incheboron wetland, Aran-Bidgol lake, and Urmia lake. Halophilic bacterial strains were recovered in the moderate halophilic medium with total salt of 8% (MH 8%) (Biswas et al., 2018). The strains were then cultured and incubated at 34°C for 5 days. Pure cultures of each strain were then streaked on slants of MH 8% media, and stored at 4°C for further studies.

Measurement of nitrate reductase production, a point-assay

Nitrate broth medium with total salt concentration of 8% (w/v), which was applied to perform a point-assay enzyme production for all strains with nitrite positive results, contains the following compounds: NaCl (67.33g/L), $MgCl_2.6H_2O$ (4.6g/L), KCl (1.33g/L), $NaHCO_3$ (0.04g/L), $CaCl_2.2H_2O$ (0.17g/L), $MgSO_4.7H_2O$ (6.4g/L), potassium nitrate (1g/L), yeast extract (3g/L), peptone (5g/L), and glucose (1g/L).

1ml of 0.5 McFarland suspension of each of the strains was transferred into the nitrate-containing broth medium and incubated at 28°C for 72h. Then, a crude extract of the cells was prepared by breaking washed cells in a French pressure cell press, and unbroken cells were removed by sedimentation. Then, the supernatant was mixed with sodium formate (1M) (1:20), and 2 µg nitrate was added to the mixture (1.5 ml). 4h later the reaction was stopped using the equal volumes of sulfanilamide (1%, w/v) in HCl (1.5N), and N-(1-Naphthyl) ethylene diamine dihydrochloride (0.02%, w/v; Griess reagent) (Boon et al., 2018). The tubes that developed a red/pink color in 15min belongs to the strains with the nitrate-reductase activity. Thereafter, a toothpick full zinc powder was added to non-pink color tubes incubated for 15min. Tubes with no color changes were assumed as further denitrification, which means that no nitrate was present. No color change at this point considered as positive result. Strains with positive result, were selected for the point assay of nitrate reductase production. The test was repeated three times for all strains with nitrite positive results.

In order to measure the nitrate reductase production of different bacterial isolates quantitatively, the above mentioned steps were repeated again to prepare red/pink color tubes. Then, all the tubes were examined by the UV-vis spectrophotometry at 540 nm (Boon et al., 2018). The nitrite concentration was calculated by comparing the absorbance of each sample (at 540 nm) to the standard curve which was obtained for known nitrite concentrations. One unit of the nitrate reductase activity is considered equal to a 1 µmol of nitrite release per minute at pH 7.0 in the room temperature (Kroneck et al., 2018).

To obtain the growth curve for the most potent nitrate-reducing strain, and to determine the optimum time of reducing nitrate to nitrite, the selected strain was cultured in the nitrate broth medium with a total salt concentration of 8% (w/v), and incubated at 28°C for 90h. The monitoring period was 4h.

Effects of different factors on the growth and heterotrophic denitrification of R3A34 strain

To study the heterotrophic denitrification characteristics of the bacterial strain R3A34 under different circumstances it was cultured in replicates by changing one factor at a time method (Javaheri-Kermani and Asoodeh 2019). To do so, they were inoculated into the nitrate broth medium (150 ml), and incubated at 28°C for 72 h. Studying the effects

of salinity on the nitrite release was conducted by the adjustment of the NaCl concentration in the medium to provide different salinity percents (0-20%, w/v). The effect of the initial pH on the denitrification was conducted by adjusting pH in the medium between 5 to 10. Different ranges of incubation temperatures (20-50°C) were also examined. In addition, the consequences of the utilization of different carbon sources, including glucose, mannitol, citrate, acetate, and succinate (1 g/L) were investigated on the nitrite release. All experiments were carried out in triplicates. Analysis of variance (ANOVA) was used to study the variation of the data (with a 5% level of significance).

DNA extraction and amplification of *napA*, and *narG* genes

The genomic DNA of the selected halophilic strain with the best reductase activity was extracted as described by Marmur (Marmur, 1961). Degenerated Primer pairs S.F1173d (5'-TGGT/AG/CG/CATGGGT/G/CT/ATT/G/CAACC -3'), and S.R2294 (5'-GT/AG/ATGCCAG/ATGA/T/C/GTC -3') (Klatte et al., 2011) and degenerated primer pairs NarG1960F (5' TAT/CGTG/CGGG/CCAG/AGAG/AAA -3'), and NarG2650R (5'-TTT/CTCG/ATACCAT/G/AGTT/G/AGC -3') (Ma et al., 2019) were used respectively for the *napA*, and *narG* amplification. The reaction mix (25 µl) contained 50ng of genomic DNA, 12.5 µl of Taq Master Mix (2X), 0.5 mM of each primer, and 5% (v/v) DMSO. The reaction was started with an initial denaturation at 95°C for 5min followed by 30 cycles of denaturation at 94°C for 60s, annealing at 53°C for 60s, and 72°C for 60s with a final extension at 72°C for 420s. The PCR products were purified and sequenced by Macrogen Inc. (Seoul, Korea). To identify phylogenetic neighbors and to calculate pairwise *16S rDNA* sequence similarities, the BLAST software (https://blast.ncbi.nlm.nih.gov/Blast.cgi) was used. To align sequences, the Clustal X software (version 2.0, Conway Institute, USA) was used. The Phylogenetic tree was constructed by the neighbor-joining method using the MEGA software (version 6.0, Biodesign Institute, USA). The bootstrap value was calculated from 1000 replicates.

Results

Selection of nitrate reductase-producing strains

In the current study, 50 halophilic isolates were screened for their nitrate reductase production capacity. Twelve isolates produced a red-pink color in the medium from the nitrite test, and 5 strains were colorless in the zinc powder test. They were selected for comparing their nitrate reductase production (supplementary table 1).

Among bacteria from different regions, 60% and 19% of the strains which were isolated from the Urmia lake, and the Incheboron wetland produced nitrate reductase, respectively. None of the strains from the Aran-Bidgol lake produce this enzyme. Among all nitrate-reducing strains, 69% were gram-positive bacilli form, 19% were gram-negative bacilli form, and 12% were coccus.

The *presence of napA* and *narG* genes in the nitrate-reducing strains

The *napA*, and *narG* genes were analyzed in all nitrate-reducing strains. In this study, the *napA* gene (1121bp) was amplified successfully from *Marinobacter adhaerens* as a gram-negative strain. The *narG* gene (690bp) was detected in 7 gram-positive and 3 gram-negative strains belonging to *Oceanobacillus caeni*, *Staphylococcus saprophyticus*, *Bacillus daliensis*, *Oceanobacillus pictuare*, *Kocuria rosea*, *Virgibacillus necropolis*, *Saliteribacillus persicus*, and *Halomonas fontilapidosi* species. The amplified genes from two different strains are shown in the figure 1.

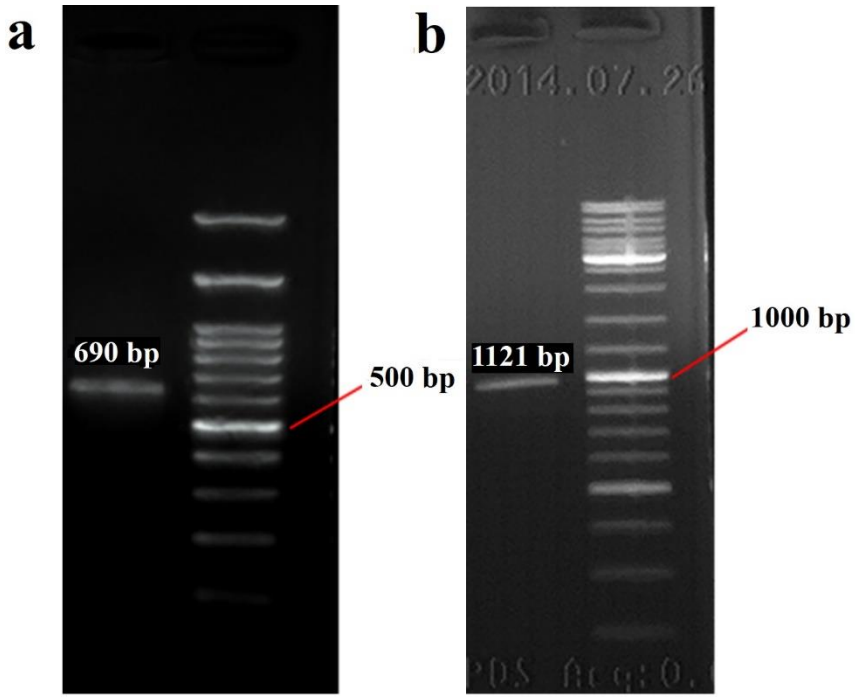

Figure 1. The amplified *narG* gene of *K. rosea* (a), and *napA* gene of *M. adhaerens* (b).

Nitrate reductase production of *K. rosea* strain R3A34 during the growth phases

Among five selected nitrate reductase-producing strains, a halophilic strain, called *K. rosea* strain R3A34 displayed the highest nitrate reductase production (0.006 U/ml, 7.8mg nitrite/L) in three days as it was measured by the spectrophotometric assay. Nitrate reductase activity of the other four selected strains including *Oceanobacillus* IBRC-M 11331, *S. saprophyticus* IBRC-M 10635, *Marinobacter sp.* IBRC-M 10904 and *Gracilibacillus sp.* IBRC-M 4252 were 0.005, 0.004, 0.004, 0.003 U/ml, respectively.

Figure 2 illustrates the growth curve, and the nitrite concentration curve of the R3A34 strain during 90h in the nitrate broth medium under aerobic conditions.

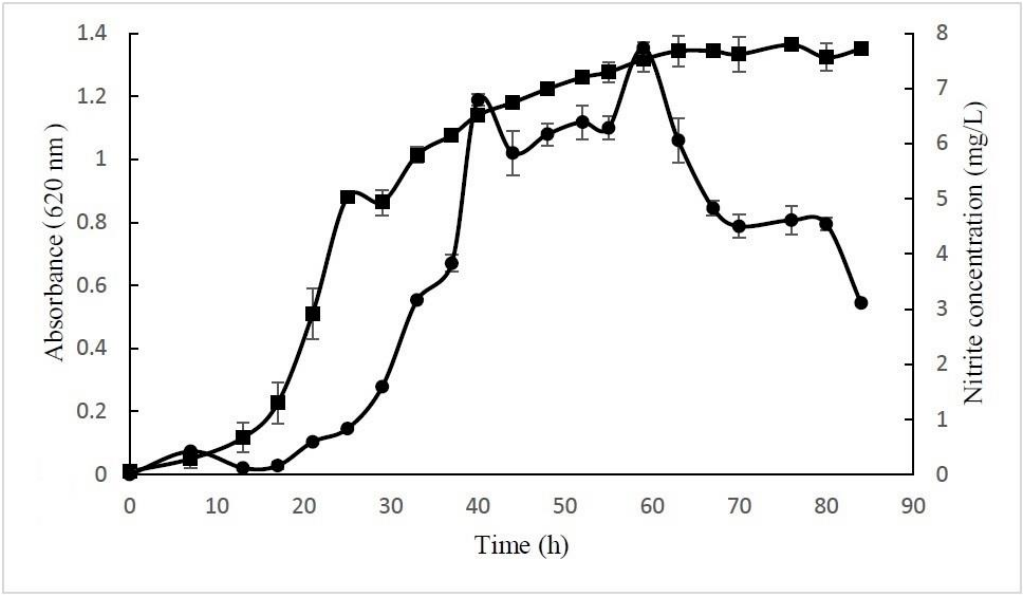

Figure 2. The growth curve (square), and nitrite production (circle) of *K. rosea* R3A34 in nitrate broth medium at 28°C for 90h.

As it is shown in the figure, along with its growth curve, the concentration of the nitrate reductase enzyme increases during the time, and reaches to its maximum concentration in the middle of the stationary phase (40h). Furthermore, as it was indicated in the figure, the growth was approximately remained constant after 60h, while the reduction ability dropped at 65h (Figure 2).

Different factors affect the growth and denitrification

Investigating the growth rate, and enzyme production of strain R3A34 in the MH medium with an extensive range of 0 to 20% (w/v) of salt concentrations demonstrated that this strain grows well in the presence of 3.5 to 8% (w/v) of NaCl, while the maximum denitrification (5.95 mg/L) occurs in 8% (w/v) of NaCl (Figure 3a). Also, the effect of initial pH was checked on the growth and enzyme production. It was revealed that the maximum growth, and denitrification occurs in pH 7.0 (Figure 3b).

Growth and enzyme production assays in a range of temperatures demonstrated that the strain grows in 25 to 40°C and the maximum denitrification (5.95 mg/L) occurs at 32°C (Figure 3c). Moreover, the effects of different carbon sources were checked on the growth and enzyme production. The maximum growth and denitrification occurs in the medium containing mannitol as the carbon source (Figure 3d).

Phylogenetic analysis of nitrate reductase genes in *K. rosea*

The genomic DNA of the selected strain was isolated and its *napG* gene was PCR amplified with specific forward and reverse primers. Based on the *napG* gene sequence, it has a high level of sequence similarity (76%) with the *narG* gene of *Kocuria flava*. The phylogenetic tree based on the *napG* sequences was constructed with the neighbor-joining (NJ) method (Figure 4).

Discussion

Iran is among the countries where saline ecosystems, especially saline lakes, are found to be abundant in. Hence, many arid and semi-arid regions of the country have salty soil and water. These lakes are the origins of halophilic or halotolerant microorganisms with a high biodiversity. These microorganisms, with a biodenitrification capacity, have the ability to produce nitrate reductase enzymes that are resistant to extreme environmental conditions, such as temperature, pH, and high salt concentrations. These microorganisms are of a great value in the fields of biotechnology, and more particularly in industrial decontamination of wastewaters since they contain a large amount of salt and nitrate (Beeler and Singh, 2016). For this reason, halophilic denitrifying bacteria investigated in our study could play a major role in the treatment of such nitrate-contaminated wastewaters. Previous studies have shown that several genes are responsible for encoding denitrifying activated enzymes in microorganisms, and detecting responsible genes (*narG* and *napA*) in halophilic bacteria can be useful as biotechnological tools for denitrification (Duan et al., 2015). Bacteria can harbor either or both of these nitrate reductases (Asamoto et al, 2021). In the present study, a membrane-bound nitrate reductase gene (*narG*) was found in ten halophilic strains, and a periplasmic nitrate reductase gene (*napA*) was found in one halophilic strain, all of which have never been reported before. We have also examined denitrification ability of 50 strains and discovered the best strain with the nitrate reductase production capacity, which is belonged to the *K. rosea* strain R3A34.

The results revealed a positive correlation among bacterial growth and nitrate reductase activity (Figure 2). The same result was reported by Eltarahony et al. (2020). It was mentioned in the results section (Figure 3) that the nitrite release by the strain R3A34 is stabilized at a relatively high level under 3.5–8% of salinity. As the highest rate of the denitrification activity was detected in 8% of NaCl concentration, it is evident that this enzyme has a better function in high-saline media. The same result was reported by Li et al. (2013) for *M. hydrocarbonoclasticus.* However, strain R3A34 does not release nitrite in the absence of NaCl. It can be explained that due to the strain's origin (i.e. the saline ecosystem) the presence of NaCl is essential for its enzymatic activity. Upon increasing the salinity to 10%, no nitrite is released by the strain; because too high salinity may cause microorganisms /cells plasmolysis and loss of activity as Duan et al., (2015) reported. Since the highest nitrite release was occurred in 3.5–8% of salinity, strain R3A34 could be identified as a halophilic bacterium (Kushner and Kamekura, 1988). This characteristic determined its application scope for the treatment of wastewater with high salinity, such as aquaculture wastewater

and seafood processing wastewater. Strain R3A34 grows in temperatures of 20-40°C and the optimum temperature of growth was recorded as 32°C, where the best nitrate-reductase production can take place.

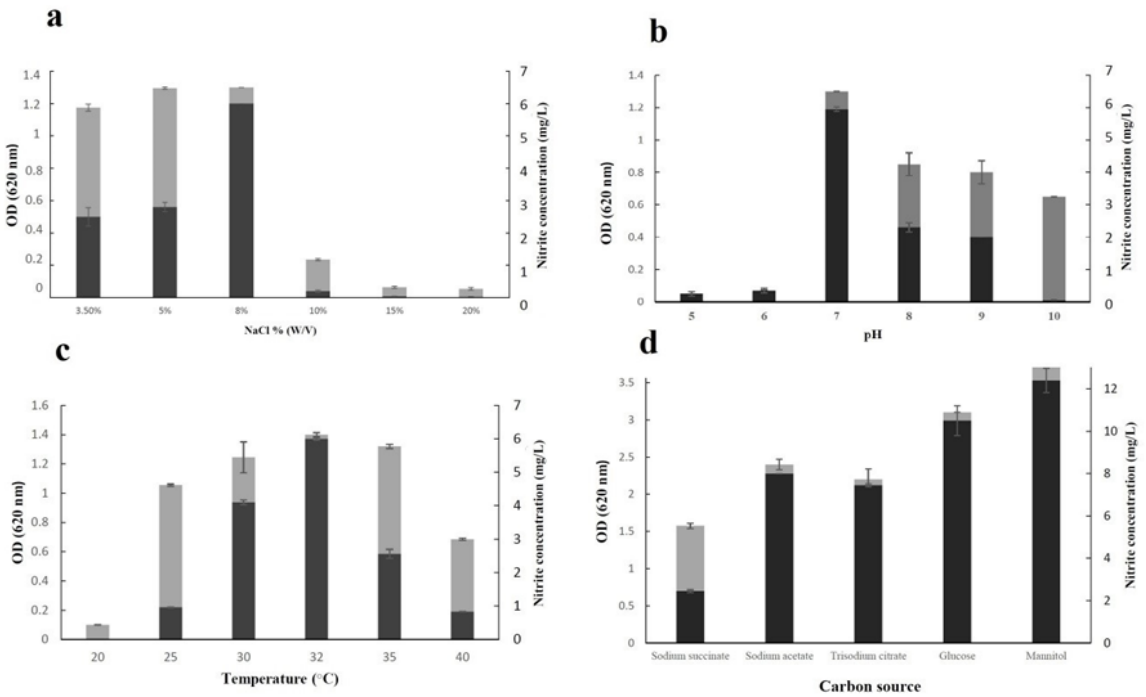

Figure 3. Effects of various culture conditions, including salinity (a), pH (b), temperature (c), and carbon source (d) on the nitrate reductase production/nitrate concentration (black color) and growth (gray color) of *K. rosea* R3A34, incubated at 28°C for 72 h. The difference between data was significant $P<0.05$.

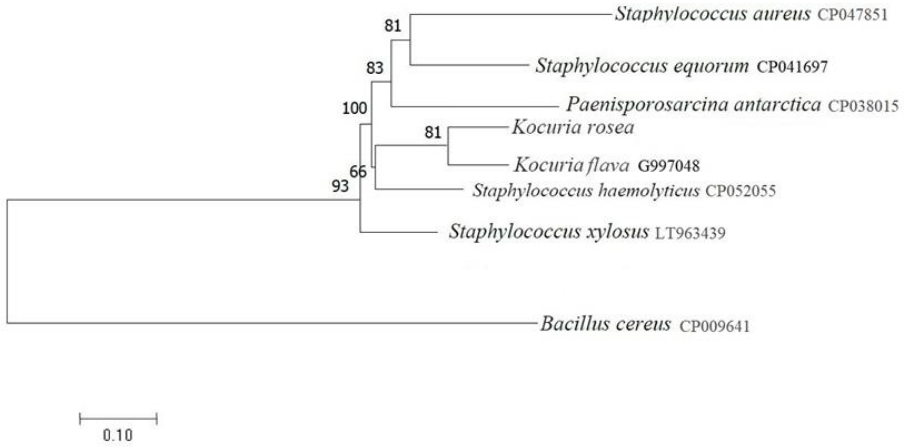

Figure 4. The phylogenetic relationship of *narG* genes. Phylogenetic distances were determined by the neighbor-joining (NJ) analysis. The *Bacillus cereus narG* gene was used as an outgroup. The bootstrap value was calculated from 1000 replicates.

This indicates that the growth of this strain is directly affected by its denitrification activity. Similar effects of the temperature on the nitrate reduction was examined by Cyplik et al., (2007), and the best temperature was reported as 37°C. The optimized pH for nitrate reduction of strain R3A34 was 7. Li et al, reported the optimized Ph 8 for nitrate reduction of *M. hydrocarbonoclasticus* (Li et al., 2013). The source of carbon in the culture media is one of the most critical factors affecting the denitrification capacity during which bacterial cells use a carbon source as an electron donor and finally reduce nitrate to nitrite. Since the molecular structure of carbon sources plays a significant role in the efficiency of denitrification, evidently, sources with simpler and smaller molecular structures are more favorable (Li et al., 2013). Hence, glucose, mannitol, citrate, acetate, and succinate were also investigated as carbon sources to evaluate the denitrification efficiency of the strain R3A34. Finally, it was concluded that among various sources mannitol was the best source. The best reduction was occurred following the 40h of bacterial culture, which is in the middle of the stationary phase of the growth curve, meaning that the highest reduction of nitrate to nitrite occurs when the cell mass is in its maximum level.

One of the objectives of this study was to determine bacterial strains which can grow in saline environments and reduce nitrate to nitrite efficiently. Here we report the *K. rosea* strain R3A34 as the best strain which is active in the saline media. The strain can carry out the denitrification in a proper time. Hence, it could be a suitable candidate for the biological treatment of wastewaters.

References

Argandona M., Martínez-Checa F., Llamas I., Arco Y., Quesada E., & Del Moral A. (2006). A membrane-bound nitrate reductase encoded by the narGHJI operon is responsible for anaerobic respiration in Halomonas maura. Extremophiles 10: 411-419.

Asamoto C. K., Rempfert K. R., Luu V. H., Younkin A. D. & Kopf S. H. (2021). Enzyme-Specific Coupling of Oxygen and Nitrogen Isotope Fractionation of the Nap and Nar Nitrate Reductases. Environmental Science and Technology, 55(8): 5537-5546.

Baggs E. M. (2011). Soil microbial sources of nitrous oxide: recent advances in knowledge, emerging challenges and future direction. Current Opinion in Environmental Sustainability 3: 321-327.

Baker S. C., Ferguson S. J., Ludwig B., Page M. D., Richter O. M. H., & van Spanning R. J. (1998). Molecular genetics of the genus *paracoccus*: metabolically versatile bacteria with bioenergetic flexibility. Microbiology and Molecular Biology Reviews 62:1046-1078.

Beeler E., & Singh O. V. (2016). Extremophiles as sources of inorganic bio-nanoparticles. World Journal of Microbiology and Biotechnology 32: 156-167.

Biswas J., Bose P., Mandal S., & Paul A. K. (2018). Reduction of hexavalent chromium by a moderately halophilic bacterium, Halomonas smyrnensis KS802 under saline environment. Environmental Sustainability 1: 411-423.

Boon N et al. (2018). Microbiome analysis and-omics studies of microbial denitrification processes in wastewater treatment: recent advances. Science China Life Sciences 61: 753-761.

Boujida N., Palau M., Charfi S., Manresa À., Senhaji N. S., Abrini J., & Miñana-Galbis D. (2019). Marinobacter maroccanus sp. nov., a moderately halophilic bacterium isolated from a saline soil. International Journal of Systematic and Evolutionary Microbiology 69: 227-234.

Cyplik P., Grajek W., Marecik R., & Kroliczak P. (2007). Effect of macro/micro nutrients and carbon source over the denitrification rate of Haloferax denitrificans archaeon. Enzyme and microbial technology 40: 212-220.

Duan J., Fang H., Su B., Chen J., & Lin J. (2015). Characterization of a halophilic heterotrophic nitrification–aerobic denitrification bacterium and its application on treatment of saline wastewater. Bioresource technology 179: 421-428.

Eltarahony M., Zaki S., & Abd-El-Haleem D. (2020). Aerobic and anaerobic removal of lead and mercury via calcium carbonate precipitation mediated by statistically optimized nitrate reductases. Science Report 10: 4029.

Gao H., Yang Z. K., Barua S., Reed S. B., Romine M. F., Nealson K. H., ... & Zhou J. (2009). Reduction of nitrate in Shewanella oneidensis depends on atypical NAP and NRF systems with NapB as a preferred electron transport protein from CymA to NapA. The ISME journal 3: 966-976.

He T., Xie D., Li Z., Ni J., & Sun Q. (2017). Ammonium stimulates nitrate reduction during simultaneous nitrification and denitrification process

by Arthrobacter arilaitensis Y-10. Bioresource technology 239: 66-73.

Javaheri-Kermani M., & Asoodeh A. (2019). A novel beta-1, 4 glucanase produced by symbiotic Bacillus sp. CF96 isolated from termite (Anacanthotermes). International journal of biological macromolecules 131: 752-759.

Klatte T., Evans L., Whitehead R. N., & Cole J. A. (2011). Four PCR primers necessary for the detection of periplasmic nitrate reductase genes in all groups of Proteobacteria and in environmental DNA 39: 321-326.

Kroneck P. M. (2018). Walking the seven lines: binuclear copper A in cytochrome c oxidase and nitrous oxide reductase. JBIC Journal of Biological Inorganic Chemistry 23: 27-39.

Kushner D. J. (1988). Physiology of halophilic eubacteria. Halophilic bacteria. 109-138.

Li R., Zi X., Wang X., Zhang X., Gao H., & Hu N. (2013). Marinobacter hydrocarbonoclasticus NY-4, a novel denitrifying, moderately halophilic marine bacterium. SpringerPlus 3: 1-9.

Luvizotto D. M., Araujo J. E., Silva M. D. C. P., Dias A. C., Kraft B., Tegetmeye H., ... & Andreote F. D. (2019). The rates and players of denitrification, dissimilatory nitrate reduction to ammonia (DNRA) and anaerobic ammonia oxidation (anammox) in mangrove soils. Anais da Academia Brasileira de Ciências 91: 1-14.

Ma Y., Zille , J. L., & Kent A. D. (2019). An evaluation of primers for detecting denitrifiers via their functional genes. Environmental microbiology 21: 1196-1210.

Marmur J. (1961). A procedure for the isolation of deoxyribonucleic acid from micro-organisms. Journal of molecular biology 3: 208-IN1.

Li R., Zi X., Wang X., Zhang X., Gao H., & Hu N. (2013). Marinobacter hydrocarbonoclasticus NY-4, a novel denitrifying, moderately halophilic marine bacterium. SpringerPlus 2: 1-9.

Paniagua-Michel J., & Fathepure B. Z. (2018). Microbial consortia and biodegradation of petroleum hydrocarbons in marine environments. In Microbial Action on Hydrocarbons Springer, Singapore. 1-20.

Pastorelli R., Piccolo R., Simoncini S., & Landi S. (2013). New primers for denaturing gradient gel electrophoresis analysis of nitrate-reducing bacterial community in soil. Pedosphere 23: 340-349.

Supplementary Table 1. Bacterial strains, accession number from the Iranian Biological Resource Center (IBRC) and nitrite absorption (A)

Bacterial species	Accession number	Nitrite absorption (A)
Alkalibacterium sp.	IBRC-M 11371	-*
Halomonas ventosae	IBRC-M 10566	0.91
Halobacillus sp.	IBRC-M 10952	0.13
Marinobacter sp.	IBRC-M 10904	2.1
Bacillus cohnii	IBRC-M 4079	-
Halomonas sp.	IBRC-M 10886	0.32
Planococcus sp	IBRC-M 11377	-
Thalassobacillus hwangdonensis	EU817571	-
Pontibacillus marinus	IBRC-M 10973	0.78
Piscibacillus salipiscarius	IBRC-M 10562	0.11
Bacillus safensis	NZ_UWJF00000000.1	-
Alkalibacterium putridalgicola	IBRC-M 11371	-
Gracilibacillus sp.	IBRC-M 4252	1.62
Bacillus sonorensis	IBRC-M 4099	-
Staphylococcus saprophyticus	IBRC-M 10635	2.1
Planococcus rifietoensis	IBRC-M 4022	-
Marinobacter hydrocarbonoclasticus	IBRC-M 10592	-
Kocuria rosea	IBRC-M 11008	3
Marinobacter sp.	IBRC-M 11306	-
Aeromocrobium halocynthiae	IBRC-M 4042	-
Virgibacillus salaries	IBRC-M 4091	-
Desmospora active	NZ_PZZP01000001.1	-
Marinobacter szutsaonensis	IBRC-M 11378	-
Bacillus mojavensis	AY212986.1	-
Rhodococcus corynebacterioides	MZ477522.1	-
Micrococcus yunnanensis	NZ_SMVL00000000.1	-
Micrococcus luteus	IBRC-M 10691	-
Martelella mediterranea	IBRC-M -4040	-
Bacillus vietnamensis	IBRC-M 10877	-
Halobacillus profundi	NR_041246.1	0.19
Salicola sp.	IBRC-M 4044	0.11
Marinobacter persicus	IBRC-M 10445	-
Alteribacillus iranensis	IBRC-M 10446	-
Halomonas andesensis	IBRC-M 4081	1.5
Kocuria Polaris	IBRC-M 10207	-
Halobacillus yeomjeoni	IBRC-M 10952	-
Halomonas sp	IBRC-M 4013	0.79
Oceanobacillus	IBRC-M 11331	2.4
Chromohalobacter israelensis	IBRC-M 10835	-
Halobacillus litoralis	IBRC-M 10222	-
Bacillus halosaccharovorans	IBRC-M 10095	-
Bacillus daliensis	MN713774.1	0.19
Bacillus circulans	IBRC-M 4069	-
Saliteribacillus sp.	IBRC-M 4457	0.24
Bacillus horikoshii	MW332512.1	-
Bacillus circulans	IBRC-M 10697	-
Bacillus pocheonensis	AB245377.1	-
Virgibacillus necropolis	IBRC-M 10959	0.25

*Negative Nitrite test

Journal of Cell and Molecular Research (2021) 13(1), 27-35 DOI: 10.22067/JCMR.2021.69999.1005

Research Article

Comparative Analysis of Commercial CCL21 and CCL21/IL1β Recombinant Proteins by *in silico* Tools

Ahdiyeh Shahtaghi[1¶], Ali Alam Shahnabadi[1¶], Kamelia Kohannezhad[1], Neda Amini[1], Maria Beihaghi[1,2*]

[1]*Department of Biology, Kavian Institute of Higher Education, Mashhad, Iran*
[2]*Faculty of Science, Ferdowsi University of Mashhad, Mashhad, Iran*

Received 11 March 2020 Accepted 16 May 2020

Abstract

One of the newest diagnostic methods and treatment of cancer is to design new drugs. It is now possible to design a drug with desired properties in theory and evaluate its therapeutic effects through bioinformatics tools. Among the studied drugs, those based on cytokine genes, which increase the body's immunity against cancer, are of great interest. Cytokines are small proteins that play an essential role in cell signaling and can affect the function and behavior of surrounding cells. CCL21 chemokine is one of the cytokines that possess antitumor properties has the potential for chemoattraction of T lymphocytes and dendritic cells. Interleukin 1 beta (IL1β) is a cytokine involving different cellular activities such as the activation of neutrophils, B-Cells, and T-Cells. In the present study, we designed a drug-based cytokine gene to activate T cells and B cells by inserting defined CCL21 epitope and IL1β peptide sequences into a protein construct. Molecular dynamics simulation was performed in Linux space using Gromex software. Results of RMSD, RMSF, and the radius of gyration obtained from the simulation showed the stability of both proteins, which indicated that there are no significant conformational differences between the commercial CCL21 and recombinant form. The interaction of synthetic construct and human CCL21 with the CCR7 receptor was also investigated by HADDOCK software. Obtained results showed no differences between these proteins, and recombinant protein has the same structural and conformational characteristics as human commercial CCL21.

***Keywords*:** Cytokine, Chemokine, CCL21, Docking, Molecular Dynamics Simulation

Introduction

Nowadays, immunotherapy is a well-known method for understanding the problems related to the side effects of chemical drugs, analyzing the functional immune system during treatment, thus preventing tumor production. Among the drugs being studied for immunotherapy are cytokine-based drugs that increase immunity against cancer. Cytokines are small proteins that play an important role in cell signaling and affect surrounding cells' function and behavior. Cytokines include interferons, tumor necrosis factors, lymphokines, chemokines, and interleukins secreted by immune cells, mast cells, and various stromal cells (Akhter, Wu, Memon, & Mohsin, 2015).

Chemokines are a family of cytokines involved in the direct migration of leukocytes and activation of inflammatory stimuli. Chemokines and their receptors play a vital role in the growth, survival, or death of tumor cells as well as their metastasis (Jorgensen et al., 2019; Moore, 2001). Chemokine C-C motif ligand 21 (CCL21) is a cytokine that binds specifically to the CCR7 chemokine receptor, which has antitumor properties and can predict tumorigenesis in cancer (Madej et al., 2013; McHugh, 2019). CCL21/CCR7 has essential roles in immune cell and lymph-node homing, peripheral tolerance, development and function of T regulatory cells, and lymphoid neogenesis (Joutoku et al., 2019; Zhao et al., 2014). Increased CD8+ T cells can reduce the progression of viral diseases such as HIV and COVID-19. High expression of these genes acts as biomarkers in various diseases such as cancers and viral infections like HIV infection and pneumonia (Cyster, 1999; Gollmer et al., 2009; Jorgensen et al., 2019). CCL21 is known as a base for cancer immunotherapy since it can chemoattract T lymphocytes and DCs (Beemiller, Jacobelli, & Krummel, 2012). DCs receive tumor antigens and migrate to T-cell zones of lymphoid organs for particular antitumor T-cell activity (Zhao et al., 2014). Interleukin-1 beta (IL1β) belongs to the family of cytokines with severe proinflammation and, the *IL1β* gene encodes it in humans. IL1β is involved in various cellular

*Corresponding author's e-mail address: *maria_beihaghi@yahoo.com*
¶These authors contributed equally to this work.

activities such as activation of neutrophils, T and B lymphocytes, production of cytokines, antibodies, collagen, and fibroblast proliferation. (Van Damme et al., 1985). VQGEESNDK epitope is a part of IL-Iβ that acts as a potent adjuvant by binding to secretory protein sequences. This peptide sequence possesses all of the IL-Iβ adjuvant activity without any inflammatory response, such as induction of a fever response. (Boraschi, Tagliabue, & Miller, 2009).

Molecular dynamic simulation (MD) is a computer simulation method used to understand the conformational changes in recombinant proteins due to mutations comparatively(Musiani et al., 2014). In addition, its dynamics information can be used to analyze the highly fluctuating and complex nature of protein dynamics (Gaieb & Morikis, 2017).

The project's goal was to use immunoinformatic methods based on drug design algorithms to simulate and produce a drug based upon cytokine genes. Therefore, due to the complexity of the discovery process and the efficiency of neural network techniques, in addition to molecular docking, neural network techniques with neurophase rules were used to design an efficient diagnostic model in the immune system.

Materials and Methods

Construction of Amino acid Cassette

The epitope of human CCL21 (Accession No: CAG29322.1) and epitope of human IL-1β (PDB ID: 4G6M_A) were designed as the principal part of the recombinant protein cassette. So, the best T cell epitope of CCL21, EAAAK sequence as beta-defensins linker, the epitope of human IL-1 beta, RRVR as sensitive foreign protease linker, the signal SEKDEL for effectual agglomeration of the plant recombinant protein in the endoplasmic reticulum (ER), RVLAEA sequence as HIV protease linker and 6xHis tags was possessed (Figure 1)

Prediction of T- and B-Cell Epitopes of the Recombinant Protein

T-cell and B-cell epitopes of this recombinant protein were identified by BepiPred 2.0, BCpreds, ABCpreds, SVMTrip, and MAPPP online servers (Table 1 and 2). These bioinformatic tools have been used to prognosticate antigenic epitopes presented on the T-cell and B-cell surface by major histocompatibility complex class I and II molecules (MHC I, MHCII) (O'Donnell, Rubinsteyn, & Laserson, 2020). TAPPred server was used to verify the recombinant protein binding affinity of peptides toward the TAP transporter. This online service is based on cascade SVM and uses the amino acids sequence and properties.

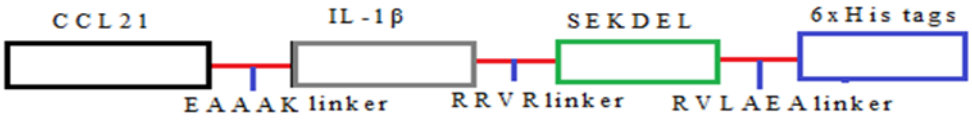

Figure 1. A) Schematic representation of CCL21/IL1β protein construct.

Table 1. Prediction of T- cell epitopes of human CCL21 (PDB ID: 2L4N). A covering score over 90% and IC50 below 50 were the best binder epitopes

MHCI			MHCII		
Epitope peptide	**allel HLA**	**score**	**Epitope peptide**	**allel HLA**	**IC50**
IPAKVVRSY	HLA-B*35:01	99.4%	LWVQQLMQH	HLA-DRB4*01:01	15.60
LPRKRSQAEL	HLA-B*07:02	95.7%	ELWVQQLMQ	HLA-DRB4*01:01	17.10
LCADPKELW	HLA-B*58:01	95.4%	PKELWVQQ	HLA-DRB4*01:01	18.50
LCADPKELW	HLA-B*57:01	93.4%	AKVVRSYRK	HLA-DRB4*01:01	19.20
IPAKVVRSY	HLA-B*53:01	90.3%	QQLMQHLDK	HLA-DRB4*01:01	21.40

Table 2. Prediction of T-cell epitopes of CCL21/IL1β protein.

MHCI			MHCII		
Epitope peptide	**allel HLA**	**score**	**Epitope peptide**	**allel HLA**	**IC50**
IPAKVVRSY	HLA-B*35:01	99.4%	SGTNDAEDCCLSVTQ	HLA-DRB1*08:02, HLA-DRB5*01	14.20
KELWVQQLM	HLA-B*40:01	93%	CAPPDQPWVERIIQR	HLA-DRB1*04:01	16.20

A covering score over 90% w and IC50 below 50 were the best binder epitopes of MHCI and MHCII-related HLAs, respectively.

Prediction of Physicochemical Characterization of Recombinant Protein

The SOLpro server measured the solubility of recombinant protein. Furthermore, ProtParam online server was used to identify various physicochemical parameters, including amino acid composition, pI, aliphatic index (II), instability index, in vivo and in vitro half-life, molecular weight (MW), and grand average of hydropathicity (GRAVY). The SignalP 5.0 server predicts the presence of signal peptides and the location of their cleavage sites in recombinant and commercial proteins. Localization of protein was analyzed by DeepLoc online server. The allergenicity of this recombinant protein was assessed by the AlgPred web server, which was used to show the post-translational modifications of CCL21/IL1β. NetOGlyc 4.0 Server was used to show the O-glycosylation and NetNGlyc 1.0 Server to show the N-glycosylation site of this recombinant protein. NetPhos 3.1 Server was used to find the phosphorylation sites of the protein (Safavi et al., 2019).

Molecular Dynamic Simulation and the Prediction of the Stability and Flexibility of the Recombinant Protein

PSIPRED webserver was used for computational modeling and getting the PDB file of the CCl21/IL-1β construct. Molecular dynamic (MD) simulations were utilized using GROMACS-4.5 and GROMOS96 (ffG45a3) force fields to assess the conformational changes of the protein. In order to neutralize the system in terms of charge, 5 counter Cl- ions for CCl21 and 7 counter Cl- ions for CCl21/IL-1β simulation were added to the solvated system. Pressure and temperature were kept at 1 bar and 300 K, and the system ran for 20 nanoseconds. The root-mean-square deviation (RMSD), the root-mean-square fluctuation (RMSF), and the radius of gyration of C-alpha atoms were calculated and analyzed using the Grace software. Also, the PDB files of the two proteins were aligned using the Pymol software.

Homology Modeling Structure Using *in silico* Tools

Since the 3D structure of this recombinant protein is not available, the comparative modeling method was used to create its three-dimensional

structure. Comparative modeling is one of the best methods for obtaining the three-dimensional structure of a target protein, where three-dimensional structures that have very similar sequences to the target sequence are used as a model. One of the online software used for comparative modeling is the Swiss Model. We also used the 1.7.0 version of Pymol software for modeling our target recombinant protein.

Molecular Docking of Cytokine Ligands and CCR7 Receptor

HADDOCK software was used to compare the interaction of CCR7 - CCl21/IL-1β and CCR7 - CCL21. HADDOCK software can use biochemical and biophysical information obtained from laboratory methods to predict interaction. This program performs protein-protein docking in a completely flexible manner. Amino acids obtained from these methods are defined as ambiguous interaction constraints (AIRs). AIR is then used to perform molecular docking. This energy is the sum of electrostatic energies, Van der Waals. In this method, amino acids that more than 50% of their external surfaces are exposed to water are considered active amino acids. The active amino acids of the cytokine ligands were identified according to mentioned protocol. Also, extracellular amino acids of CCR7 protein were considered as active amino acids.

Results and Discussion

Evaluation of the Physicochemical Properties of Recombinant Protein

Previously mentioned servers predicted the physicochemical analysis of the recombinant protein. The presence of signal peptides in commercial CCL21 and CCL21/IL1β recombinant proteinS was predicted by The SignalP 5.0 server. As shown in figure 2, the presence of signal peptides in 23 primary amino acids and the location of their cleavage sites in the 24th amino acid of commercial CCl21 was detected. However, there is no signal peptides in 65 primary amino acids of CCL21/IL1β recombinant protein were reported; obtained results was based on the fact that 23 primary amino acids as signal peptide were removed from CCL21/IL1β construct and the sequences of the signal SEKDEL for effectual agglomeration of the plant recombinant protein in the endoplasmic reticulum was replaced at the end of the construct. The molecular weight (Mw) of both native and recombinant proteins was estimated as 14'884.5504 Da and 14'893.834 Da. Isoelectric point values (pI) were 9.377 and 9.231, respectively, and both proteins' solubility was about 0.84.

Furthermore, the instability index of native protein was 37.8, and recombinant protein was 38.03, which confirms the stability of these proteins. In both proteins, the computed half-life in the mammalian, yeast, and E. coli cells was more than 30 h, 20 h, and 10 h, respectively. Aliphatic index and GRAVY were determined to be about 49 and -1.2, respectively, which shows that both proteins possess hydrophilic properties. As shown in Figure 3 and Table 3, this protein is localized in the nucleus. The allergenicity of recombinant protein was assessed, and the prediction accuracy was 94% at the -0.4 threshold. Therefore, unlike commercial CCL21 protein, recombinant protein has no allergenic effects.

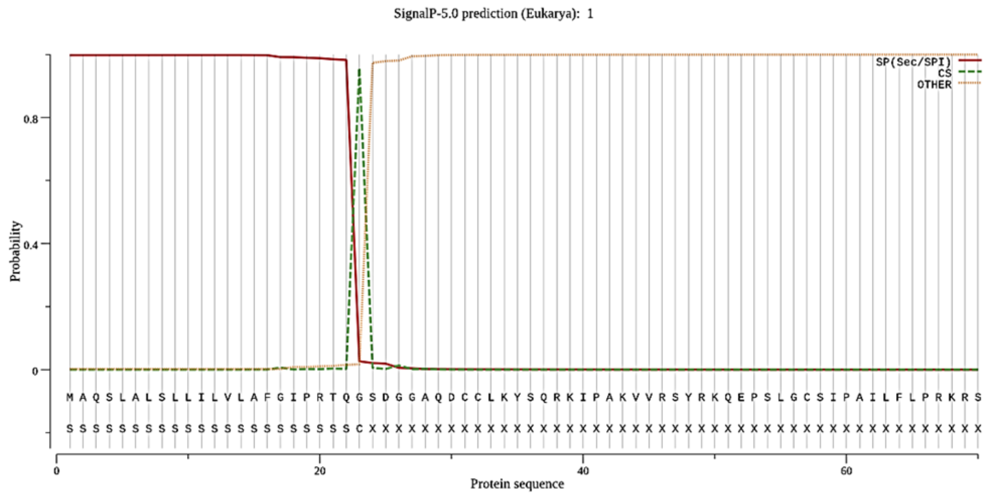

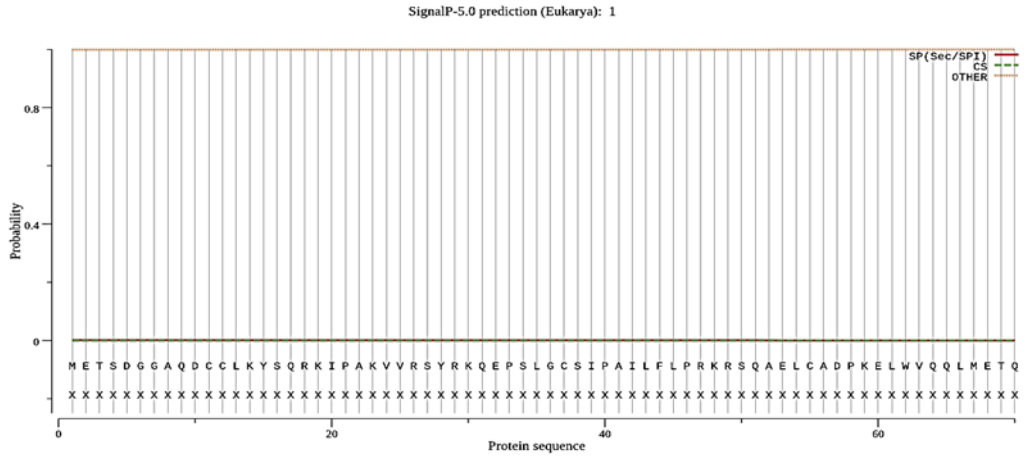

Figure 2. Prediction of the presence of signal peptides in commercial CCl21 and CCL21/IL1β recombinant protein by the SignalP 5.0 server; A) presence of signal peptides in 23 primary amino acids the location of their cleavage sites in 24th amino acid of commercial CCl21 were detected. B) as shown in this figure, no signal peptides in 65 primary amino acids of CCL21/IL1β recombinant protein.

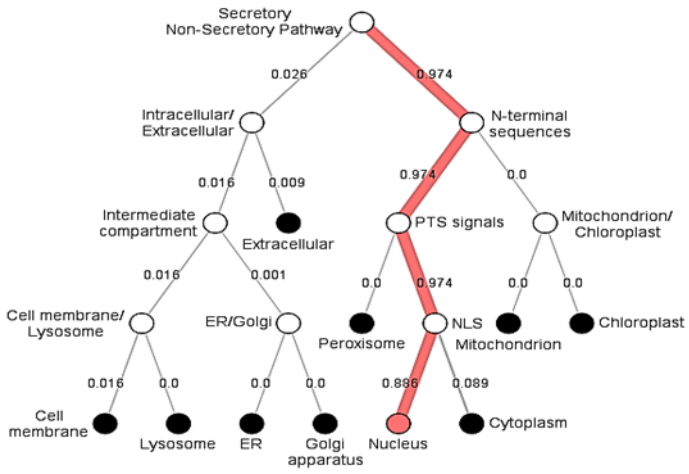

Figure 3. Schematic representation of subcellular localizations CCL21/IL1β protein construct. This soluble and extracellular protein that localized in the nucleus with a Likelihood of 89.9 percent.

Table 3. Prediction of subcellular localization of CCL21/ Il1β constructs in human cells.

Localization	Nucleus	Cytoplasm	Cell membrane	Extracellular	Mitochondrion	Endoplasmic reticulum	Golgi apparatus	Plastid	Peroxisome	Lysosome/ Vacuole
Likelihood	0.8918	0.093	0.015	0.0079	0.0009	0.0005	0.0005	0.0002	0.0001	0

Type	Soluble	Membrane
Likelihood	0.8434	0.1566

Prediction of T- cell and B-cell Epitopes of the Recombinant Protein

T-cell and B-cell epitopes of recombinant protein were identified. All T cell epitopes of human CCL21 and CCL21/IL1β were illustrated in

Tables 1 and 2. There were no B cell epitopes predicted in human CCL21, but the VQGESNDK sequence of IL1β was predicted as a B cell epitope.

Protein Structure Conformational Flexibility and Stability Analysis

In this project, we used MD simulations to compare the conformational changes of native and recombinant proteins. Multiple were analyzed throughout the simulation project, chiefly root mean square deviation (RMSD), root mean square fluctuations (RMSF), and the radius of gyration of the proteins with the time-dependent function of MD. Obtained results proved that the dynamic motions of the two proteins are very similar.

RMSD values of CCl21 commercial antigen, native protein, CCL21/IL-1β recombinant antigen, and mutant proteins were analyzed to identify the effect of mutations on recombinant protein structure. We calculated RMSD for protein backbones and found RMSD values from the mutant structures to be quite stable, like the native protein.

The CCl21 antigen and recombinant protein were stabilized at an RMSD value of around 5 Å, demonstrating that the mutations did not destabilize the protein structure (Figure 4A).

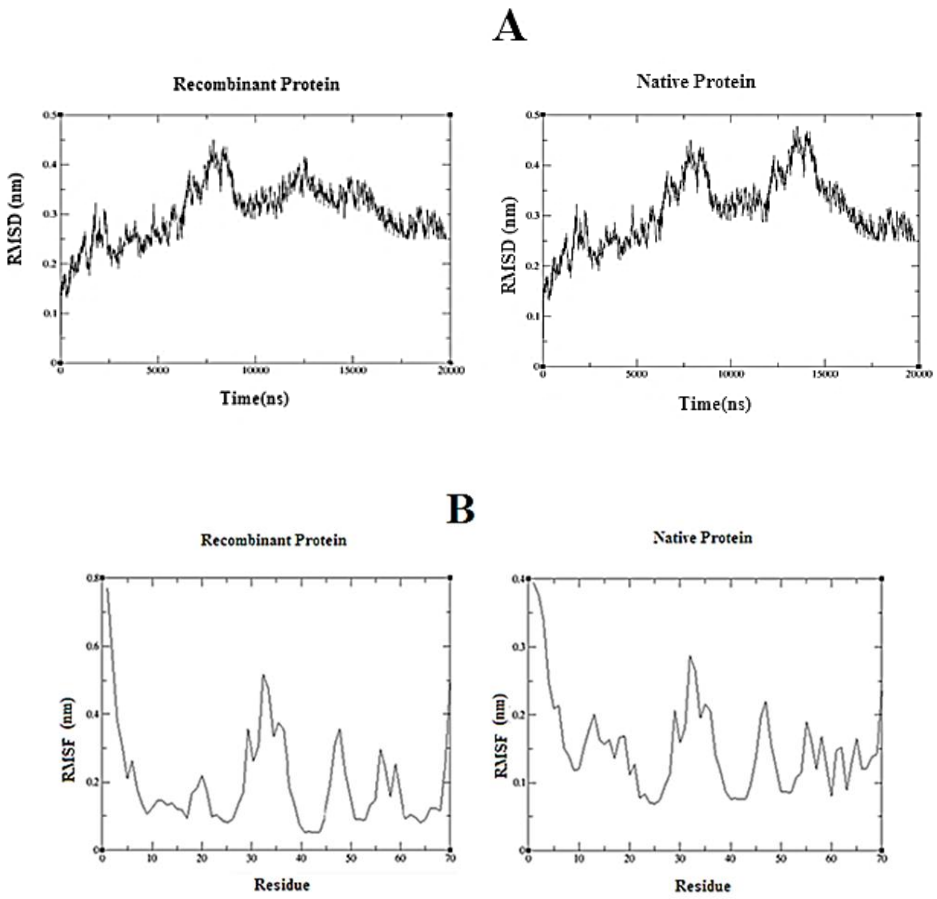

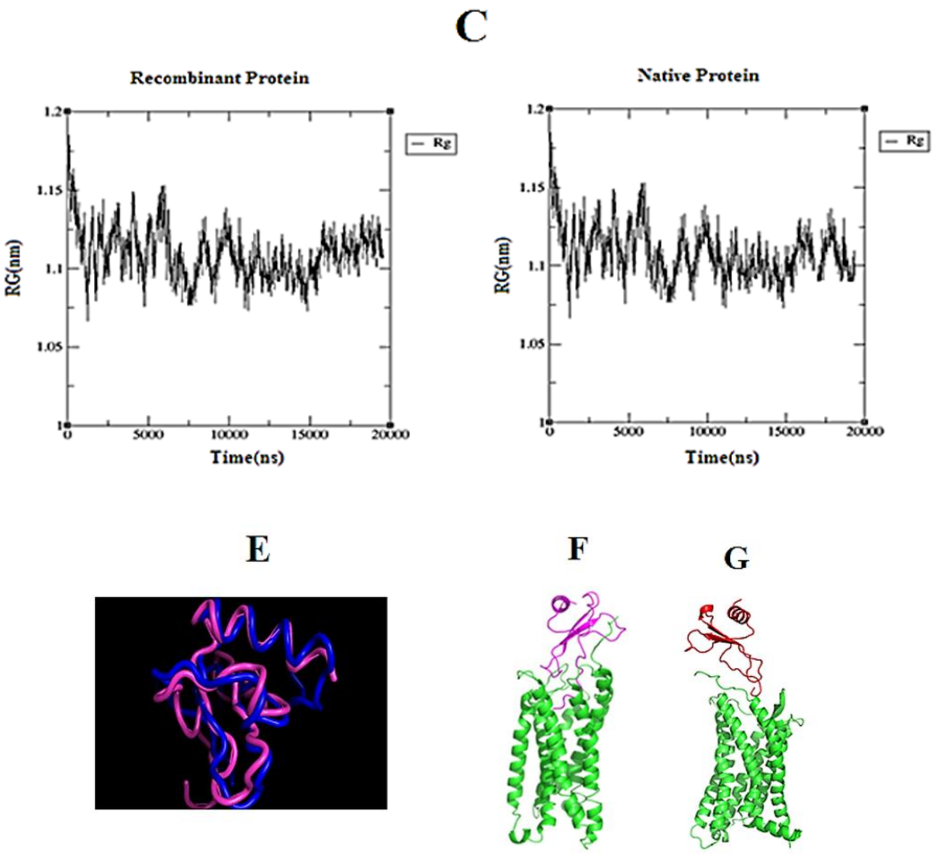

Figure 4. Protein structure conformational flexibility and stability analysis of CCl21 constructs, as the recombinant protein, and commercial CCl21, as the native protein, for 20 ns MD simulations. A) RMSD values during MD simulations of the recombinant protein and native protein structure. CCl21 antigen and recombinant protein were stabilized at an RMSD value of around 5 Å. B) Calculated average RMSF for Cα atoms of the recombinant and native protein structure, residues located between Positions 30 and 60, residue fluctuations for CCL21/IL-1β were similar to CCl21 commercial antigen and fairly low C) Radius of Gyration for the recombinant and native protein. The results of the radius of gyration indicated that CCl21/IL-1β and CCl21 commercial antigen have the minimum compactness of their structures with 11.8 Å value. E) Visualization of the native (blue) and mutant (red) PDB files, aligned with PyMol software to show the same structure and conformational characteristics of these two proteins. F) The molecular docking of the complex of CCR7 and CCl21/IL-1β. G) The molecular docking of the complex of CCR7 and human CCl21.

We also analyzed the RMSF fluctuations of each residue to specify the effect of mutations on protein residues. As Figure 4B demonstrates for residues located between positions 30 and 60, residue fluctuations for CCL21/IL-1β were similar to CCl21 commercial antigen and fairly low.

The results of the radius of gyration indicated that CCl21/IL-1β and CCl21 commercial antigen have the minimum compactness of their structures with 11.8 Å value. These data show that CCl21 mutations did not cause structural destabilizing effects, and no significant alterations were found for either protein's compactness during the simulation (Figure 4C).

Visualization Analysis of Native and Recombinant Protein

The PDB files of two proteins were aligned together by PyMol software to compare the conformational differences of the native and recombinant proteins (Figure 4E). Put together. Our findings verify that these proteins have the same structural and conformational characteristics.

Comparative Analysis of Molecular Docking of these Two Proteins with CCR7 Receptor

This project aimed to investigate and comparative analysis of interactions between these proteins and CCR7 receptors. As shown in Table 3, molecular docking of human CCL21 was determined, and the best cluster had a score of -27, with a size of 34 complexes. In addition, Z-score was equal to -2.3. Molecular docking of CCl21/IL-1β was also determined. The score of the best

Table 4. The best cluster of molecular docking result

protein	HADDOCK score	Cluster size	**Z-Score**
human CCL21	-27	34	**-2.3**
CCL21/IL1β	-30	38	**-2.8**

cluster was -30, with a size of 38 complexes. In addition, Z-score was equal to -2.8 (Table 4). Results obtained from molecular docking of these two proteins were so similar, and as mentioned before, there were interactions between CCL21/IL1β ligands and CCR7 receptors as human CCL21. The image of the complex of CCR7 - CCl21/IL-1β and CCR7 -CCl21 has been shown in Figures 4 F & 4 G.

Conclusion

The findings of this experiment confirmed that the recombinant protein and commercial CCL21 have the same structural and conformational characteristics. Therefore, this recombinant protein maybe has the same function as commercial CCl21, like anti-metastatic and cytotoxicity effects on cancer cell lines. Also, it has a chemotactic response on lymphocyte cells and is a potential treatment option in cancer immunotherapy. We have achieved our predetermined goals: to produce the recombinant protein in different expression hosts like yeast and plant to improve the production of CCL21 recombinant protein. Other diagnostic tests should be performed before the clinical application and commercialization of this protein.

Acknowledgments

This study was financially supported by the Biotechnology Development Council of the Islamic Republic of Iran. We would also like to thank faculty of science, Ferdowsi university of Mashhad, Mashhad, Iran.

References

Akhter, N., Wu, B., Memon, A. M., and Mohsin, M. (2015). Probiotics and prebiotics associated with aquaculture: a review. Fish & shellfish immunology, 45(2), 733-741 .

Beemiller, P., Jacobelli, J., and Krummel, M. F. (2012). Integration of the movement of signaling microclusters with cellular motility in immunological synapses. Nature immunology, 13(8), 787-795 .

Boraschi, D., Tagliabue, A., and Miller, A. D. (2009). The immunostimulatory effect of IL-1β in vivo is blocked by antisense peptides complementary to the loop sequence 163–171. FEBS letters, 583(4), 792-796 .

Cyster, J. G. (1999). Chemokines and the homing of dendritic cells to the T cell areas of lymphoid organs. Journal of Experimental Medicine, 189(3), 447-450 .

Gaieb, Z., & Morikis, D. (2017). Detection of Side Chain Rearrangements Mediating the Motions of Transmembrane Helices in Molecular Dynamics Simulations of G Protein-Coupled Receptors. Computational and structural biotechnology journal, 15, 131-137 .

Gollmer, K., Asperti-Boursin, F., Tanaka ,Y., Okkenhaug, K., Vanhaesebroeck, B., Peterson, J. R., et al. (2009). CCL21 mediates CD4+ T-cell costimulation via a DOCK2/Rac-dependent pathway. Blood, 114(3), 580-588 .

Jorgensen, A. S., Rosenkilde, M. M., Hjortø, G. M., Larsen, O., Legler, D. F., Uetz-von Allmen, E., et al. (2019). Biased signaling of CCL21 and CCL19 does not rely on N-terminal differences, but markedly on the chemokine core domains and extracellular loop 2 of CCR7. Frontiers in immunology, 10, 2156 .

Joutoku, Z., Onodera, T., Matsuoka, M., Homan, K., Momma, D., Baba, R., Hishimura, R. (2019). CCL21/CCR7 axis regulating juvenile cartilage repair can enhance cartilage healing in adults. Scientific reports, 9(1), 5165 .

Madej, T., Lanczycki, C. J., Zhang, D., Thiessen, P. A., Geer, R. C., Marchler-Bauer, A., and Bryant, S. H. (2013). MMDB and VAST+: tracking structural similarities between macromolecular complexes. Nucleic acids research, 42(D1), D297-D303 .

McHugh, J. (2019). CCL21–CCR7 axis in RA: linking inflammation and bone erosion. Nature Reviews Rheumatology, 15(10), 576-576 .

Moore, M. A. (2001). The role of chemoattraction in cancer metastases. Bioessays, 23(8), 674-676 .

O'Donnell, T. J., Rubinsteyn, A., and Laserson, U.

(2020). MHCflurry 2.0: Improved Pan-Allele Prediction of MHC Class I-Presented Peptides by Incorporating Antigen Processing. Cell Systems, 11(1), 42-48. e47 .

Van Damme, J., De Ley ,M., Opdenakker, G., Billiau, A., De Somer, P., and Van Beeumen, J. (1985). Homogeneous interferon-inducing 22K factor is related to endogenous pyrogen and interleukin-1. Nature, 314(6008), 266-268 .

Zhao, D.-x., Li, Z.-j., Zhang, Y., Zhang, X.-n., Zhao, K-.c., Li, Y.-g., et al. (2014). Enhanced antitumor immunity is elicited by adenovirus-mediated gene transfer of CCL21 and IL-15 in murine colon carcinomas. Cellular immunology, 289(1), 155-161 .

Journal of Cell and Molecular Research (2021) 13 (1), 36-43 DOI: 10.22067/JCMR.2021.68523.1000

Research Article

Royal Jelly Decreases MMP-9 Expression and Induces Apoptosis in Human 5637 Bladder Cancer Cells

Narges Fazili[1,2], Zahra Soheila Soheili[1*], Saeid Malekzadeh-Shafaroudi[2], Shahram Samiei[3], Shamila D. Alipoor[1], Nasrin Moshtaghi[2], Abouzar Bagheri[4]

[1] *Department of Molecular Medicine, National Institute of Genetic Engineering and Biotechnology, Tehran, Iran*
[2] *Department of Biotechnology and Plat Breeding, Faculty of Agriculture, Ferdowsi University of Mashhad, Mashhad, Iran*
[3] *Blood Transfusion Research Center High Institute for Research and Education in Transfusion Medicine, Tehran, Iran*
[4] *Department of Clinical Biochemistry and Genetics, Mazandaran University of Medical science, Iran*

Received 25 January 2021 Accepted 30 June 2021

Abstract

Royal jelly (RJ) as a traditional medicinal agent has a variety of pharmacological benefits. In the present study, the effects of the royal jelly were investigated on the urinary bladder cancer cell line 5637 (HTB-9). MTT assay was performed to determine the percent of cell viability at different concentrations of the royal jelly. Moreover, *in vitro* wound-healing assay was applied to investigate the effects of RJ on cell migration. The activities and gene expression levels of matrix metalloproteinase 2 and 9 were assessed by zymography and Real time PCR, respectively. It was confirmed that royal jelly (RJ) at the concentration of 0.7 mg/ml exerted a significant inhibitory effect on HTB 5637 cells and reduced cell viability to 72% in comparison to the control cultures (P-value<0.009) during the first 72h of treatment. Furthermore, royal jelly Significantly decreased the bladder cancerous cell migration capacity, and induced a significant decrease in the transcriptional level of the MMP9 after 72h (50% of the controls; P-value<0.049). However, R.J.S did not impose any effect on the expression level and activity of matrix metalloproteinase 2. The results indicated the potential of RJ as a promising natural anti-proliferative and anti-metastatic drug.

***Keywords*:** Bladder Cancer, Royal jelly, MMP-9, MMP2

Introduction

Bladder cancer (BC) is one of the most widely spread malignancies of the genitourinary tract all over the world. Despite of considerable achievements in its treatment, the global control of the disease remains problematic (Saginala et al., 2020) .

Currently, chemotherapy of bladder tumors is considered as an efficient therapeutic method, but most of the chemotherapy regimens are associated with acute systemic toxicity and cause the pain, irritation, myelosuppression, and neuropathy (Saini et al., 2011; Volpe et al., 2013). The establishment of new innovative approaches of cancer treatment still remains a challenge. In this regard, natural products with anticancer properties are in the focus of studies (Cieckiewicz et al., 2012).

Royal jelly (RJ), as a natural product, is well known for its beneficial pharmacological effects, and has received particular attention in the treatment of different cancers (Didar et al., 2019; Izuta et al., 2009; Miyata and Sakai, 2018; Ramanathan et al., 2018; Zhang et al., 2017). RJ is the food of queen bees and larvae for the first three days, but after that, just queen larvae are fed with it (Shi et al., 2011). RJ consists of a family of proteins called major RJ protein (MRJP), which constitute 80-90% of total RJ protein (Zhang et al., 2012). Chemically RJ includes water (50-60%), protein (18%), carbohydrates (15%), lipids (3-6%), mineral salt (5%), and vitamins; together with a large number of bioactive substances such as 10-hydroxy-2-decenoic acid (Viuda-Martos et al., 2008).

It has been shown that RJ has anti-allergic, anti-inflammatory, and antioxidant activities (Ramanathan et al., 2018). In addition it has relieving effects of damaged tissues with high levels of oxidative stress and inflammation (Didar et al., 2019). RJ also can stimulate antibody production, immune cell proliferation, and immunomodulatory mechanisms in inflammatory conditions (Karadeniz et al., 2011).

* Corresponding author's e-mail address: soheili@nigeb.ac.ir, zssoheili@gmail.com

Tumor cells are characterized by an enhanced rate of cell proliferation and loss of apoptosis. Mixing the whole RJ with AKr leukemia cells, Ehrlich carcinoma, TA3 mammary carcinoma, and 6C3HED lymphosarcoma, suppresses the tumor growth (Bincoletto et al., 2005).

Digestion of a type IV collagen, an essential component of the basement membrane, provides the initial step of cell invasion, and matrix metalloproteinases (MMPs) play the crucial role in this process. MMPs belong to the zinc-dependent family of endo-peptidases. They can induce tumor cell proliferation by recruiting growth factors (Sugiyama et al., 2012). Among the matrix metallic proteinases, the gelatinases MMP-2 (72KDa) and MMP-9 (92KDa) have key roles, and promote the degradation of physical barriers of the cell invasion (Gialeli et al., 2011; Kessenbrock et al., 2010). Overexpression of MMP-2 and MMP-9 in different types of human cancers such as breast, colon, prostate, bladder, and ovarian cancers have been illustrated (Aparna and Brundha, 2020; Ricci et al., 2015)

In this study, we tried to investigate the effects of RJ on 5637 cells' migration, gene expression pattern of metalloproteinases, and enzymatic activities of MMP-2 and MMP-9. These cells are considered as a highly metastatic and differentiated type of the transitional cell carcinoma (TCC) (Ricci et al., 2015).

Materials and Methods

Preparation of soluble extract of royal jelly

Fresh RJ was collected from the Kazeroon, Iran. The RJ was obtained from four days old larvae of queen honeybees, and was prepared as follows: Briefly, neutral RJ was suspended in PBS at the concentration of 0.01g/ml. The suspension was then centrifuged at 15000*g* for 15min at 4°C and separated into three layers; the clear top layer was pooled and sterilized using 0.22µm filters (Millipore, Munich, Germany) and stored at -80°C freezer until use.

Cell culture and cell viability assay

The 5637 cells were obtained from the ATCC (Manassas, VA, USA), and cultured in the Roswell Park Memorial Institute medium (RPMI 1640) (Gibco; Carlsbad, CA, USA) supplemented with 10% of heat-inactivated fetal bovine serum (FBS) (Gibco), 25 mM HEPES (Gibco), 100units/ml penicillin (Sigma, Munich, Germany), and 100ug/ml streptomycin (Sigma) in the presence of 5% CO_2 at 37°C. For the experimental procedure, cells were seeded at a primary density of 10^3 cells/cm^2 in 96-well plates (Costar, Munich, Germany), and exposed to 0.05 to 0.7 mg/ml of RJS or PBS as control. Cell proliferation assay was performed 72h post treatment according to the study performed by Nakayaet et al. (Nakaya et al., 2007) .

Cellular viability was measured using the colorimetric MTT assay based on their metabolic activities. Briefly, the medium was refreshed, and 20µl MTT solution (5 mg/ml in PBS) was added per well. The cells were then incubated for 4h. Formazan crystals were dissolved in dimethyl sulfoxide (100µl/well) (Sigma). The absorbance intensities were measured at 490 nm with a reference wavelength of 620 nm (Titertek Multiskan ELISA reader, Labsystems Multiskan, Roden, Netherlands).

In vitro wound-healing assay

Cells were seeded at a primary density of 10^4 cells/cm^2 in a 12-well plate (Costar, Munich, Germany) overnight, and were treated with RJS. A plastic blue micropipette tip was used to introduce a scratch in a straight line. Cells were exposed to 0.7 mg/ml RJS or RPMI for another 24h (RJ/RJ and RJ/RPMI groups respectively). Cell migration towards the wound closure was monitored by a phase-contrast microscope (OLYMPUS, Japan). Images were captured 24-hours later using an inverted light microscope to observe cellular migration and to count the migrated cells.

Zymography

Concentrated conditioned media from 5637 cells culture were collected, centrifuged and concentrated using Whatman centrifuge tube filters 6, 12, 24, 48, and 72h post RJ-treatment, and were run on 10% polyacrylamide gel containing 20mg/ml gelatin. Following the electrophoresis, a renaturing buffer (2.5% Triton X-100 in distilled water) was used for washing the gel. Then, the gel was incubated in the zymography buffer (0.15M NaCl, 10mM $CaCl_2$, 0.02% NaN3 in 50mM Tris–HCl, pH 7.5) for 72h at 37°C. In the next step, the gel was incubated in the Coomassie brilliant blue (0.05% Coomassie blue R-250, 25% ethanol, and 10% acetic acid in distilled water) for 1h, and finally, it was de-stained (20% isopropanol and 10% acetic acid in distilled water). Bands densities were measured by the by image J software. (Rasband, 2011).

Quantitative Real-time PCR

Total RNA extraction and cDNA synthesis were performed using an RNA extraction kit (Qiagen,

Table 1. Primers that have been used in the quantitative RT-PCR experiments.

Gene Accession Number	Name	Primers (Qiagen)
P04406	GAPDH	Q101192646
P14780	MMP-9	Q100040040
P08253	MMP-2	QT00088396

Hilden, Germany) and cDNA synthesis kit (Invitrogen Corp., Carlsbad, CA), according to the manufacturer's instructions. SYBR Green PCR Master Mix (Invitrogen) was used to perform quantitative RT-PCR experiments with the following program: an initial denaturation (95°C for 15min); 40 cycles of amplification, including (95°C for 15s, 52–60°C for 17s, and 72°C for 25s). The gene expression levels were normalized to the expression level of the glyceraldehyde 3-phosphate dehydrogenase (GAPDH) as the internal control using the $2^{-\Delta\Delta Ct}$ method. The primer sequences are shown in Table 1.

Statistical Analyses

Two-tailed Student's t-test (Microsoft Excel 2010) was used to evaluate the statistical significance of the data, and *P*-values less than 0.05 were considered statistically significant. All data were expressed as mean ± standard error (SE).

Results

The Effects of RJS on 5637 cells viability

Based on the result obtained by MTT assay, a significant reduction in the viability of 5637 cells was detected (72%) following the treatment by RJS at the concentration of 0.7mg/ml (Figure 1). This RJ concentration (0.7mg/ml) was used in subsequent experiments.

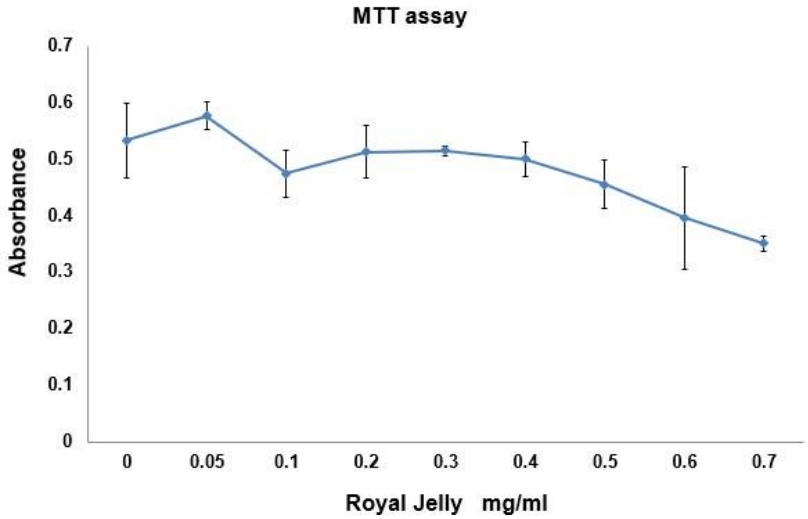

Figure 1. The Effect of RJS on 5637 cells viability, MTT assay. Dose-dependent effect of the RJ against the 5637 cells viability is shown following 72h exposure to 0.05-0.7mg/ml of RJS according the study performed by Nakayaet et al (Nakaya et al., 2007). The maximum effect was observed in 0.7mg/ml concentration.

The effects of RJS on 5637 cells migration and wound healing capabilities

Upon RJS treatment, 5637 cells' migration was significantly inhibited in comparison to control samples (Figure 2). The cells in both treatment groups (RJ/RJ and RJ/RPMI) were treated with RJS, 24h before scratching. In RJ/RJ group; RJS treatment was continued for another 24h following the introduction of the wound. The rate of cell migration decreased significantly (0.25- and 0.5-fold decrease in RJ/RJ and RJ/RPMI groups, respectively) (P-value <0.049). Based on the results, RJS treatment reduced cell migration irrespective of the superiority or precedence of RJ application (Figure 2).

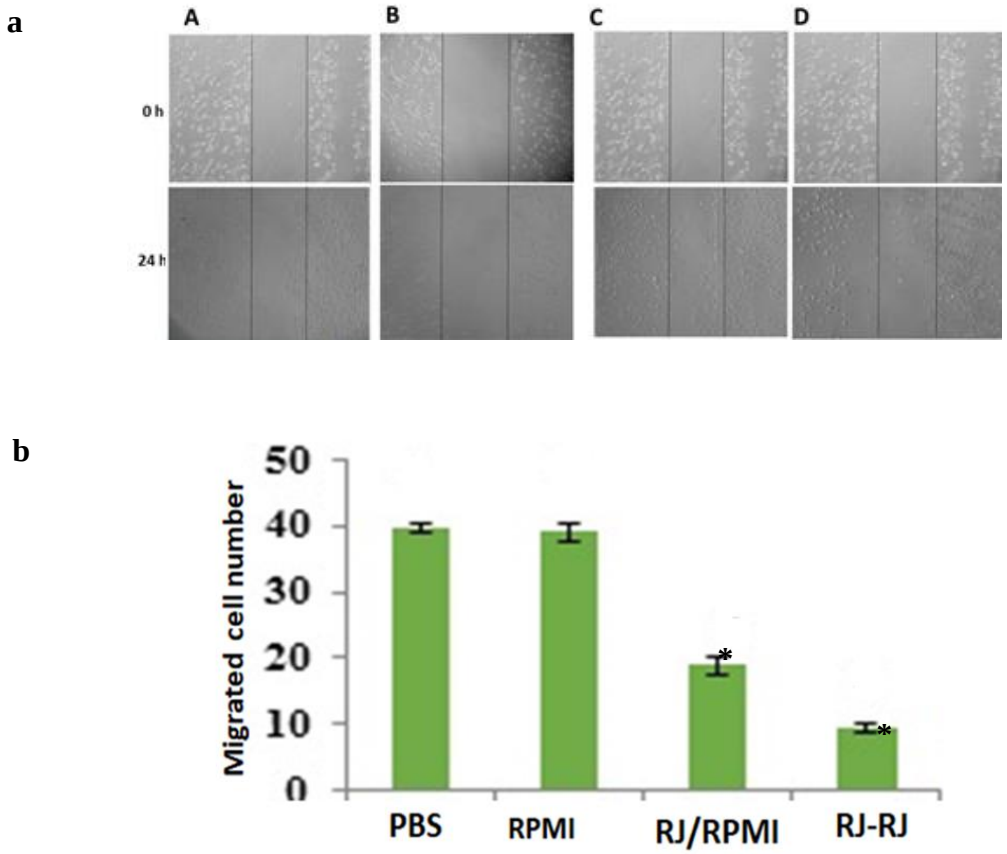

Figure 2. 5637 cells' migration is negatively affected by the RJS treatment. a: Results from the scratch assay: (A) untreated cells, (B) PBS-treated cells, (C) RJ-RJ treated cells (RJS concentration 0.7mg/ml; continued RJS treatment 24h after scratching), and (D) RJ-RPMI treated cells (treated with RJS only before scratching). The first photographs were taken at the zero-time point and the second ones were taken 24h later. Representative images are shown for each group (magnification ×100). b: Quantitative results of migration assay. The cells that had been migrated from the edge of scratched area were counted following the imaging by the inverted microscope. PBS: PBS treated cells, RPMI: untreated cells; RJ-RPMI: treated with RJS only before scratching. RJ-RJ: continued RJS treatment 24h after scratching.

The effects of RJS on MMP gelatinolytic activity

Zymography was used to assess the MMP gelatinolytic activity upon the treatment of 5637 cells with 0.7mg/ml of RJS (Figure 3a). No significant changes were detected in MMP-2 activity levels 6, 12, 24, 48, and 72h post-treatments (Figure 3b). Due to the long exposure time, MMP-9 was digested, and its activity was not detectable.

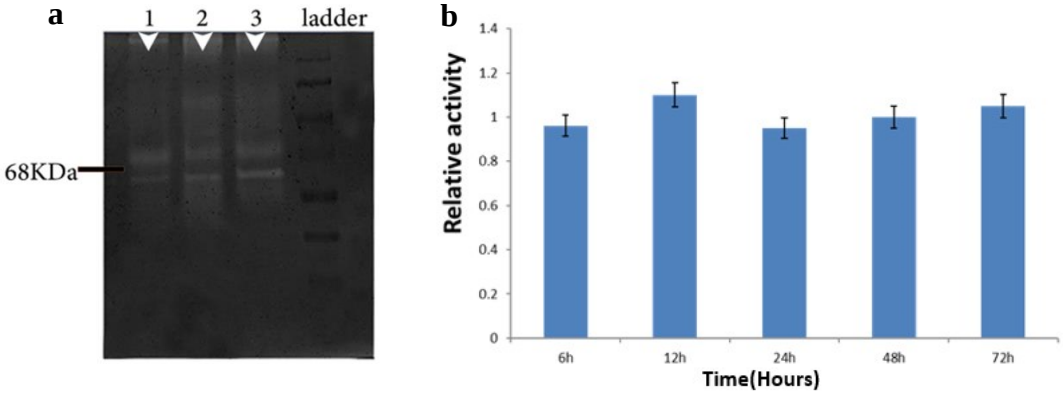

Figure 3. Zymography of conditioned media from 5637 cells. (a) Representative image of MMP-2 activity, gelatin zymography, 12h post-treatment: 1) PBS, 2) untreated, and 3) RJS treated cells. (b) Quantitative results from the zymography experiments on samples collected from 6h to 72h post treatment (p value<0.05). The relative activity in each band was estimated by image J software. (Rasband, 2011).

The effect of RJS treatment on MMP-2 and MMP-9 gene expressions

Real time PCR revealed that RJ induced a significant increase in the transcriptional level ofMMP-9 after 6h (2.8-fold *p-value* <0.02 respectively). However, a decreasing trend started from 24h post-treatment and continued until 72h. The maximum reduction was observed 72 h post treatment (0.5-fold, *p-value* <0.049) (Figure 4).

No significant changes were detected in MMP-2 mRNA level upon RJS treatment at different time points (Figure 4).

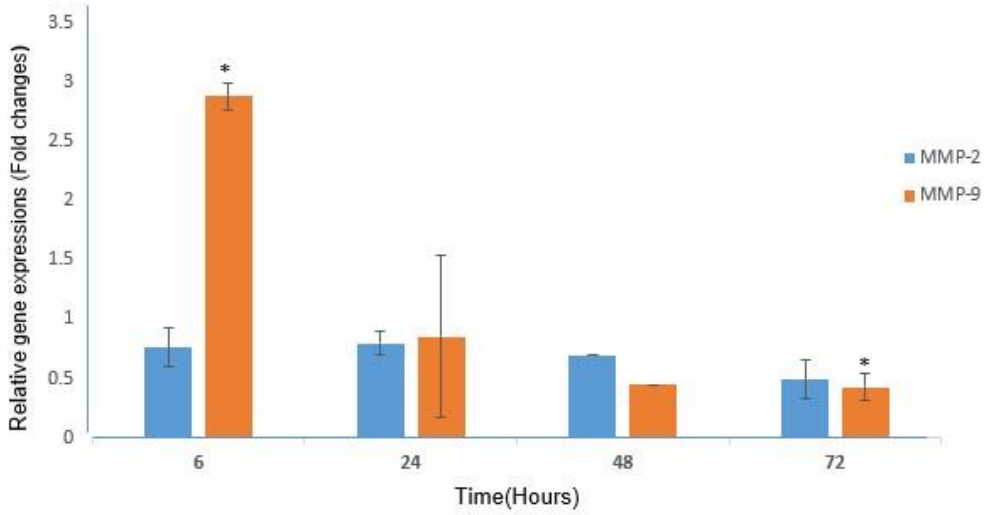

Figure 4. The Effect of RJS on MMP-2 and MMP-9 gene expressions. Relative expression of MMP-2 and MMP-9 in RJS treated samples were compared to PBS treated ones. The target genes expression was normalized to the GAPDH. Statistical significance was determined by Student's t-test (p<0.05).

Discussion

This study set out to determine the effect of RJ on the proliferation of the bladder cancer cell line 5637 and their invasiveness secretory indicators: MMP-2 and MMP-9. The anti-tumor activity of RJ has been suggested to be related to its fatty acid content, mainly $10H_2DA$, which is not a water-soluble compound. Here we investigated the inhibitory effects of the soluble supernatant of the RJ on the characteristics of the bladder cancer cells.

To determine the effects of RJS on the proliferation of 5637 cells, they were treated with different concentrations of the RJ supernatant (0.05 to 0.7mg/ml). Results from MTT assay showed that RJS decreases bladder cancer cell proliferation at the concentration of 0.7mg/ml. These anti-proliferative effects were dose-dependent. Furthermore, it was shown that 72h treatment of the cells with 0.7 mg/ml of RJS induces apoptosis. In a similar study, Erem et al (2006) reported that the addition of 0.02 to 0.5 mg/ml of the RJS to lymphocyte cultures, decline cell proliferation rates. However, the higher concentrations (more than 5mg/ml), conversely, increase cell proliferation capacities (Erem et al., 2006). Although, treatment of HeLa cells by RJ. P_{30} (a fraction of RJ protein extract) reduces the cells' proliferation on the first day of treatment (Salazar-Olivo and Paz-Gonzalez, 2005). Pervious experiments confirmed that of RJ decreases the number of human breast cancer cells (MCF-7), 72h. in our study based on scratch assay experiments, revealed that pretreatment of cells with 0.7mg/ml of RJS significantly reduces wound healing (p<0.01). On the contrary, another study reported that RJS at different concentrations (0.05, 0.001, and 0.00001mg/ml) could enhance cell migration in human dermal fibroblasts (Kim et al., 2010).

Our study has shown that RJS-treated 5637 cells induced no significant change in the MMP-2 gene expression. while, 6h following the treatment, the expression of MMP-9 was increased significantly. This is in accordance with the previous study reported the increased human dermal fibroblast cell migration 8h post-treatment. (Bergers et al., 2000).

In the present study, 24h post-treatment, the MMP-9 gene expression was down regulated, and within 72h it was declined to 0.5fold (P<0.049). The increasing level of MMP-9 (up to 6h) in RJS-treated cells could be attributed to the treatment duration. In accordance with our

data, a previous study revealed that the migration capacity of RJ-treated human dermal fibroblasts just increased up to 8h post-treatment and thereafter (up to 48h), it was remained equal to the migration capacity of control cells (Erem et al., 2006; Kim et al., 2010) in this study the whole RJ suspended in PBS was used. In another study, analyzing the protein content of the RJ demonstrated that defensin-1 peptide of the royal jelly induced an enhanced level of MMP-9 expression and wound healing in keratinocyte s, *in vitro*. In this study we apply RJ prepared in sterile deionized water at a concentration of 100 mg/ml as it was proposed previously (Bucekova et al., 2017). As a result, it may be concluded that RJ may exert distinct effects based on method of extraction.

According to the last updates, the effects of RJ extensively depend on the method of extraction and the treatment duration. In the current study, the upper soluble part of the RJS was utilized to determine its anti-proliferative and anti-migration potentials. It was reported that this soluble fraction of RJS contains major royal jelly protein 2 and 3 (MRJP2, MRJP3) (GUO et al., 2005; Nagai and Inoue, 2004).

Several mechanisms may be responsible for the observed decrease in the cell proliferation and migration upon the treatment. It is well known that tumor cells induce the production of inflammatory factors (Nagai and Inoue, 2004). The presence of inflammatory messenger polypeptides, such as tumor necrosis factor-alpha (TNF-α) and interleukins in the tumor microenvironment plays a critical role in the genomic rearrangement and angiogenesis (Zidi et al., 2010). TNF-α can induce 5637 cells' growth and MMP-9 gene expression, which is one of the major enzymes involve in cell migration and invasiveness. However, it has been suggested that it doesn't impose any effect on the MMP-2 expression levels (Lee et al., 2008). Moreover, it causes tumor cells to be tolerant against apoptosis (Huerta-Yepez et al., 2006). TNF-α induces pro-inflammatory cytokines, such as interleukin-1 (IL-1), interleukin-6 (IL-6), and interleukin-8 (IL-8) (Zidi et al., 2010). Interestingly, a few studies indicated that RJS decreases some of the pro-inflammatory cytokines. Kohno (2003) showed that RJS inhibited TNF-α, IL-1, and IL-6 in the cultures of mouse peritoneal macrophages in a dose-dependent manner (Kohno et al., 2004). Also, the reduction of TNF-α in the human peripheral blood lymphocytes cultures were reported upon 72h incubation with RJS (Erem et al., 2006). It was reported that the water-soluble extract of RJ possesses the most potent immunomodulatory properties *in vitro*. It can decrease interleukin-2 (IL-2), and increase apoptosis in rat T-cells (Gasic et al., 2007). As mentioned before, MRJP3 is enriched in the water-soluble fraction of the RJ, and inhibits the production of some cytokines, such as IL-4, IL-2, and IFN-g, through the inhibition of the T cells proliferation (Okamoto et al., 2003).

Taken together, it can be concluded that RJS may indirectly affect MMP-9 expression levels by decreasing the TNF-α and IL-6 production. Reduced MMP-9 expression can reduce cell proliferation, and inhibit cell migration. It is also very interesting that decreasing the levels of TNF-α, diminishes cell tolerance against apoptosis

Collectively, these findings provide some further evidences that the soluble fraction of the RJS decreases 5637 cells' proliferation and migration. It reduces MMP-9 expression, which is commonly over-expressed in 60% of high-grade urothelial bladder tumors, and it is responsible for tumor invasiveness (Reis et al., 2012). Similar results are expected to be observed for other cell lines from the identical tissue. As well as, some differences which are inevitable.

Conclusion

Based on the results from the present study, RJS can promote apoptosis and decrease cell migration through the inhibition of cell proliferation and concurrent reduction of the MMP-9 gene expression in 5637 cells. RJ could be considered as a promising natural medication candidate. Its potential should be further investigated to be applied in combination with chemotherapeutics in advanced stages of bladder cancers.

Acknowledgments

We would like to thank all the biochemistry laboratory staff of the National Institute of Genetic Engineering and Biotechnology for their generous help.

References

Aparna J. and Brundha M. (2020) Matrix Metalloproteinases (MMPS) and its Role in Cancers-A Review. Indian Journal of Forensic Medicine & Toxicology 14.

Bergers G., Brekken R., McMahon G., Vu T. H., Itoh T., Tamaki K., and et al. (2000) Matrix metalloproteinase-9 triggers the angiogenic switch during carcinogenesis. Nature cell biology 2:737-744.

Cieckiewicz E., Angenot L., Gras T., Kiss R. and Frédérich M. (2012) Potential anticancer activity of young< i> Carpinus betulus</i> leaves. Phytomedicine 19:278-283.

Didar G., Delpazir F., Kaviani M., Azarpira N., Sepehrara L., Ebadi P. and Koohpeyma F. (2019) Influence of mesenchymal stem cells and royal jelly on kidney damage triggered by ischemia-reperfusion injury: comparison with ischemic preconditioning in an animal model. Comparative Clinical Pathology 28:311-320.

Erem C., Deger O., Ovali E. and Barlak Y. (2006) The effects of royal jelly on autoimmunity in Graves' disease. Endocrine 30:175-183.

Gasic S., Vucevic D., Vasilijic S., Antunovic M., Chinou I. and Colic M. (2007) Evaluation of the immunomodulatory activities of royal jelly components in vitro. Immunopharmacology and immunotoxicology 29:521-536.

Gialeli C., Theocharis A. D. and Karamanos N. K. (2011) Roles of matrix metalloproteinases in cancer progression and their pharmacological targeting. FeBS Journal 278:16-27.

Huerta-Yepez S., Vega M., Garban H. and Bonavida B. (2006) Involvement of the TNF-α autocrine–paracrine loop, via NF-κB and YY1, in the regulation of tumor cell resistance to Fas-induced apoptosis. Clinical immunology 120:297-309.

Izuta H., Chikaraishi Y., Shimazawa M., Mishima S. and Hara H. (2009) 10-Hydroxy-2-decenoic acid, a major fatty acid from royal jelly, inhibits VEGF-induced angiogenesis in human umbilical vein endothelial cells. Evidence-based complementary and alternative medicine 6:489-494.

Karadeniz A., Simsek N., Karakus E., Yildirim S., Kara A., Can I., and et al. (2011) Royal jelly modulates oxidative stress and apoptosis in liver and kidneys of rats treated with cisplatin. Oxidative medicine and cellular longevity 2011.

Kessenbrock K., Plaks V. and Werb Z. (2010) Matrix metalloproteinases: regulators of the tumor microenvironment. Cell 141:52-67.

Kim J., Kim Y., Yun H., Park H., Kim S. Y., Lee K.-G., Han S.-M. and Cho Y. (2010) Royal jelly enhances migration of human dermal fibroblasts and alters the levels of cholesterol and sphinganine in an in vitro wound healing model. Nutrition research and practice 4:362-368.

Kohno K., Okamoto I., Sano O., Arai N., Iwaki K., Ikeda M. and Kurimoto M. (2004) Royal jelly inhibits the production of proinflammatory cytokines by activated macrophages. Bioscience, biotechnology, and biochemistry 68:138-145.

Lee S.-J., Park S.-S., Lee U.-S., Kim W.-J. and Moon S.-K. (2008) Signaling pathway for TNF-α-induced MMP-9
expression: mediation through p38 MAP kinase, and inhibition by anti-cancer molecule magnolol in human urinary bladder cancer 5637 cells. International immunopharmacology 8:1821-1826.

Miyata Y. and Sakai H. (2018) Anti-cancer and protective effects of royal jelly for therapy-induced toxicities in malignancies. International journal of molecular sciences 19:3270.

Okamoto I., Taniguchi Y., Kunikata T., Kohno K., Iwaki K., Ikeda M. and Kurimoto M. (2003) Major royal jelly protein 3 modulates immune responses in vitro and in vivo. Life sciences 73:2029-2045.

Ramanathan A. N. K. G., Nair A. J. and Sugunan V. S. (2018) A review on Royal

Jelly proteins and peptides. Journal of Functional Foods 44:255-264.

Reis S. T., Leite K. R. M., Piovesan L. F., Pontes-Junior J., Viana N. I., Abe D. K., and et al. (2012) Increased expression of MMP-9 and IL-8 are correlated with poor prognosis of Bladder Cancer. BMC urology 12:18.

Ricci S., Bruzzese D. and Di Carlo A. (2015) Evaluation of MMP-2, MMP-9, TIMP-1, TIMP-2, NGAL and MMP-9/NGAL complex in urine and sera from patients with bladder cancer. Oncology letters 10:2527-2532.

Saginala K., Barsouk A., Aluru J. S., Rawla P., Padala S. A. and Barsouk A. (2020) Epidemiology of bladder cancer. Medical Sciences 8:15.

Saini S., Arora S., Majid S., Shahryari V., Chen Y., Deng G., and et al. (2011) Curcumin modulates microRNA-203-mediated regulation of the Src-Akt axis in bladder cancer. Cancer Prev Res (Phila) 4:1698-1709.

Salazar-Olivo L. and Paz-Gonzalez V. (2005) Screening of biological activities present in honeybee (< i> Apis mellifera</i>) royal jelly. Toxicology in vitro 19:645-651.

Shi Y. Y., Huang Z. Y., Zeng Z. J., Wang Z. L., Wu X. B. and Yan W. Y. (2011) Diet and cell size both affect queen-worker differentiation through DNA methylation in honey bees (Apis mellifera, Apidae). PloS one 6:e18808.

Sugiyama T., Takahashi K. and Mori H. (2012) Royal jelly acid, 10-hydroxy-trans-2-decenoic acid, as a modulator of the innate immune responses. Endocrine, Metabolic & Immune Disorders-Drug Targets (Formerly Current Drug Targets-Immune, Endocrine & Metabolic Disorders) 12:368-376.

Viuda-Martos M., Ruiz-Navajas Y., Fernández-López J. and Pérez-Álvarez J. (2008) Functional properties of honey, propolis, and royal jelly. Journal of food science 73:R117-R124.

Volpe A., Racioppi M., D'Agostino D., D'Addessi A., Marangi F., Totaro A., and et al. (2013) Advanced bladder cancer: new agents and new approaches. A review. *In* Urologic Oncology: Seminars and Original Investigations. Vol. 31. Elsevier. 9-16.

Zhang L., Fang Y., Li R., Feng M., Han B., Zhou T. and Li J. (2012) Towards posttranslational modification proteome of royal jelly. Journal of proteomics 75:5327-5341.

Zhang S., Shao Q., Geng H. and Su S. (2017) The effect of royal jelly on the growth of breast cancer in mice. Oncology letters 14:7615-7621.

Zidi I., Mestiri S., Bartegi A. and Amor N. B. (2010) TNF-α and its inhibitors in cancer. Medical Oncology 27:185-198.

Journal of Cell and Molecular Research (2021) 13 (1), 44-53 DOI: 10.22067/JCMR.2021.71863.1017

Research Article

Effect of Glutamine Stability on the Long-term Culture and Line Establishment of Chicken Primordial Germ Cells

Sara Yousefi Taemeh [1,2], Jalil Mehrzad [3], Hesam Dehghani [1,2,4] *

[1] *Division of Biotechnology, Faculty of Veterinary Medicine, Ferdowsi University of Mashhad, Mashhad, Iran*
[2] *Stem Cell Biology and Regenerative Medicine Research Group, Research Institute of Biotechnology, Ferdowsi University of Mashhad, Mashhad, Iran*
[3] *Department of Microbiology and Immunology, Section of Immunology, Faculty of Veterinary Medicine, University of Tehran, Tehran, Iran*
[4] *Department of Basic Sciences, Faculty of Veterinary Medicine, Ferdowsi University of Mashhad, Mashhad, Iran*

Received 6 August 2021 Accepted 14 September 2021

Abstract

Primordial germ cells (PGCs) are precursors of mature gametes, which transmit genetic information to the next generation. Due to the importance of PGCs in many fields, including developmental biology, genome editing, transgenesis, and conservation of avian genetic resources, various research aspects have focused on the cultivation of PGCs. Despite considerable progress in the establishment of specified culture media for the expansion of PGCs, a well-defined PGC culture medium has not yet been developed. This might be due to the complexity of the nutritional requirements of PGCs in the culture. Besides the nutritional needs, including vitamins, amino acids, salts, carbohydrates, and growth factors, a particular source of energy must be provided to sustain growth and viability. Glutamine is a major energy source for cultured cells, commonly added in cell culture media at higher concentrations than other amino acids. However, glutamine is very labile and rapidly degrades in solutions such as culture media. This generates ammonia as a by-product, which is toxic to the cultured cells and can affect cell viability and protein glycosylation. Therefore, the stability of glutamine in culture conditions is another concern for the long-term culture of PGCs. Here, we study the effect of glutamine stability on PGC culture using glutamine and GlutaMax (a commercial stabilized dipeptide form of glutamine). We found that the addition of GlutaMax in the medium promotes PGC proliferation. This effect might be exerted by minimizing production of toxic ammonia that results in maximizing cell performance and media stability.

***Keywords*:** Primordial Germ Cells, Long-term Culture, Glutamine Supplementation, Culture Media, Transposon, Germ Cell-specific Promoter

Introduction

Primordial germ cells (PGCs) are the embryonic precursors of germline cells that produce male and female gametes in adults. Due to the importance of chicken PGCs (cPGCs) in many fields, including developmental biology, genome editing, transgenesis, and conservation of avian genetic resources, a cost-effective and efficient *in vitro* cultivation of PGCs is necessary. In the early development of the chicken embryo, cPGCs arise from the epiblast and migrate to the germinal ridges through blood circulation during HH stages 13–17 (Hamburger and Hamilton 1992; Naito, Harumi, and Kuwana 2015). The cPGCs can be isolated from the bloodstream or the gonads in low numbers. They can be enriched by appropriate *in vitro* culture conditions (Macdonald et al. 2010; Whyte et al. 2015). Despite progress in cPGC culture methods, problems such as low proliferation rates and the low germline specification rates exist in the long-term *in vitro* culture and establishment of cPGCs (Kong et al. 2018; van de Lavoir et al. 2006).

The basic composition of culture medium has been identified by Eagle in the 1950s. Culture media provide the mixtures of substances and nutrients, including vitamins, amino acids, salts, carbohydrates, and growth factors that support the growth and propagation of cells. Reduction of any one of these factors affects cell viability and proliferation (Eagle 1959). Amino acids are the raw material for the cells to synthesize protein and thus are necessary ingredients of cell culture media. Nine essential amino acids cannot be synthesized by cells and must be included in the culture media. Glutamine is considered a conditionally essential amino acid required 10- to 100-fold greater than any other amino acid in the culture medium. Glutamine

* Corresponding author's e-mail address: dehghani@um.ac.ir

functions at low concentrations to support the energy required for the growth and proliferation of cells, but rapidly dividing cells such as cancer cells require much larger concentrations to survive (Chen and Cui 2015).

Glutamine (L-glutamine) is very labile in solution (including culture media) and degrade in a temperature-dependent manner during the culture period. The degradation of glutamine generates toxic by-products such as ammonia which negatively affect cell survival. Dipeptide derivatives of glutamine such as GlutaMax (a commercial stabilized dipeptide form of glutamine) are degradation-resistant and more stable during long-term culture. This stability can be important for the sensitive and challenging cultivation of cPGCs. In this study, we assayed the long-term culture and compared the establishment of chicken PGC lines using two different culture media containing glutamine (Gmin medium) and GlutaMax (Gmax medium).

Materials and Methods

Isolation, Establishment, and Maintenance of Chicken Primordial Germ Cell

The fresh fertile chicken eggs were used for the establishment of primordial germ cell lines. Blood was collected from each embryo between HH stages 13 to 16 (2.5 days old). Using a glass microcapillary attached to a pipettor, about 2µl blood was taken from the dorsal aorta under the stereomicroscope and was immediately transferred into a well of the 48-well plates containing media with glutamine (Gmin) or GlutaMax (Gmax). Gmin-containing and Gmax-containing media were prepared for feeder-free culture of cPGCs. The base medium was avian KO-DMEM basal medium (a custom modification of knockout-DMEM produced by Gibco®, USA; 250 mOsm/kg, 12.0 mM glucose, without calcium chloride), supplemented with B-27, NEAA, 0.1 mM β-mercaptoethanol, nucleosides, 1.2 mM pyruvate, 0.2% ovalbumin (Sigma-Aldrich, USA), 0.2% sodium heparin (Sigma-Aldrich, USA), 10 mg/ml ovotransferrin (Sigma-Aldrich, USA), 25 ng/ml human BMP4 (ABM, US), and 4 ng/ml human FGF2 (Sigma-Aldrich, USA). For the Gmin-containing medium, glutamine (Gibco®, USA) was added at the concentration of 2.0 mM. For the Gmax-containing medium, GlutaMax (Gibco®, USA) was added at the final concentration of 2.0 mM. All components were purchased from Gibco company unless specifically indicated.

Evaluation of Proliferation Rate

To evaluate the proliferation rate of long-term cultured cPGCs, 0.5 x 10^5 cells were seeded in 300 ul of the Gmin and Gmax media in triplicates (in 48-well culture plates). On the day 2, 4, 6, 8, and 10, the cells were pipetted gently, and 15µl of suspended cells were mixed with 15µl of trypan blue dye (0.4%). The cells were counted using a hemocytometer slide. The average of counted live cells obtained from three repeats each day was used to generate proliferation plots for each medium.

Sex Determination

Sex-determination was performed on cPGCs cultured in the Gmin and Gmax media. To this end, after the extraction of genomic DNA using genomic DNA purification kit (New England Biolabs, Ipswich, MA, USA) from cPGCs, and previously described specific primers (Fridolfsson and Ellegren 1999) (Table 1), the W-specific and Z-specific bands were amplified using Hot Start Taq DNA Polymerase (New England Biolabs, Ipswich, MA, USA) according to the manufacturer's instructions. Electrophoresis was done on 2% agarose gel at 90V for 1h.

Table 1. Primers used in this study

GenBank accession number	Primer Sequence (5' to 3')	Product (bp)	Application
DAZL (NC_052533)	**DAZL-F:** GGCgctagcacagtcaagagtttgtcacagcatcc **DAZL-R:** GGCgctgaggtgtcagcgttagaatagcagataccg	1833	Promoter assay
W Chr. (NC_052571.1) **Z Chr.** (NC_052572.1)	**Sexing_F:** gttactgattcgtctacgaga **Sexing_R:** attgaaatgatccagtgcttg	Z Chr.: 594 W Chr.: 447	Sex determination

Underlined sequences indicate restriction sites: *NheI* in primer DAZL-F and *BbvcI* in primer DAZL-R.

Plasmid Construction, Transfection, and Promoter Assay

The functionality of germ-line-specific promoters was assessed to ensure the germ-line competency of the cells during the long-term culture of cPGCs. An expression vector containing a PGC-specific promoter (DAZL) driving tdTomato was constructed. To this end, the DAZL promoter was amplified from the chicken genome using DAZL-F, and DAZL-R primers containing *NheI* and *BbvCI* cut sites at the 5' end of each primer, respectively (Table 1). The amplified 1833-bp DAZL promoter was cloned into a plasmid at the upstream of tdTomato reporter gene containing *NheI* and *BbvCI* cut sites between two internal terminal repeats (ITRs) of the *piggyBac* transposon. The plasmid backbone was cut with *NheI- BbvCI* for 3 hrs at 37 °C, followed by dephosphorylation with fast alkaline phosphatase for 10 min at 37 °C, and heat-inactivation for 30 min at 70 °C. The amplified 1833-bp DAZL promoter was cut with the same enzymes for 3 hrs at 37 °C. A 1:3 vector to insert molar ratio was used to ligate the amplified 1833-bp DAZL promoter into the plasmid backbone by T4 ligase. 5µl of the ligation mix was transformed into chemically competent DH5alpha bacteria followed by overnight incubation at 37 °C. Colony PCR was performed on transformants by vector-specific, and insert-specific primers, and positive clones were liquid-cultured overnight for plasmid extraction using the Plasmid Isolation Kit (New England Biolabs, Ipswich, MA, USA). Plasmid subcloning was verified using restriction enzyme digestion.

To transfect cPGCs, 0.5×10^6 cells were suspended in 10µl of R buffer containing 10µg DAZL-tdTomato transposon and 10µg transposase plasmids. Using the Neon tip attached to the Neon pipette, the suspended cells were placed in a pipette station filled with buffer E. Electroporation was performed at 1000 volt, 100 ms, and 1 pulse. Immediately after, the cPGCs were transferred into a well with 300µl medium. Transfected cPGCs were evaluated for tdTomamto expression after 24h.

Results

Morphological Characteristics of freshly isolated circulating cPGCs

Initial identification of cPGCs is based on morphological features. Circulating cPGCs are distinguished by their large round-shape nuclei and glycogen granules in the cytoplasm (Meyer 1964). We examined the morphological features of freshly isolated cPGCs with an inverted microscope. A few cPGCs with previously described features were found in blood-derived samples. As the culture progressed, the proliferating cPGCs became much more visible and prominent due to the disappearance of the red blood cells, and doublets indicative of dividing cPGCs appeared in the cultured blood samples (Figure 1 A & B).

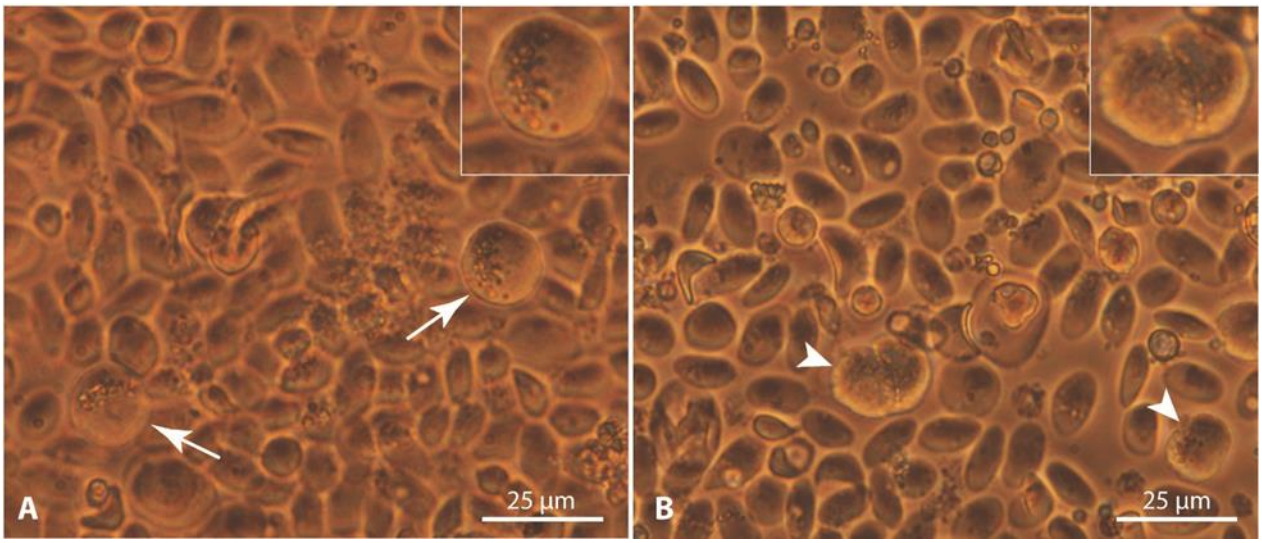

Figure 1. Morphology of circulating cPGCs in the freshly-isolated sample of embryonic blood. Circulating cPGCs, isolated from the embryonic blood (stage 13-H.H), which can easily be distinguished from red blood cells by their large size, large nuclei, and accumulated granules in the cytoplasm (arrows, inset). (B) Arrowheads (and inset) pinpoint two dividing cPGCs (doublets) in the freshly isolated embryonic blood. Scale bar = 25 µm. Magnification = ×400

Derivation of cPGCs in The Gmin and Gmax Media

To study the effects of glutamine stability on the long-term culture and establishment of chicken PGC lines, we cultured circulating-cPGCs in two different media with different energy sources. Circulating-cPGCs were grown in L-glutamine-containing (Gmin) and GlutaMAX-containing (Gmax) media.

Blood samples collected from 20 chicken embryos at stages 13–16 were individually transferred to each well of 48-well culture plates containing Gmin or Gmax media. From day 2 onward, half of the Gmin and Gmax media in each well was exchanged with the fresh medium every other day. After ~ 2 weeks of culture, from a total of 20 cPGC lines cultured in each medium, 13 and 16 lines of cPGCs were successfully derived in the Gmin and Gmax media, respectively. Apoptotic cells were more frequently observed in the Gmin-cultured wells, whereas the glycogen granules were more abundant in the derived lines cultured in the Gmax medium (Figure 2).

Evaluation of Proliferation and Viability of cPGCs Cultured in The Gmin and Gmax Media

To evaluate the cell proliferation status of derived cPGCs in the Gmin and Gmax media, a total of 0.5 x 10^5 cells were seeded in each well in 48-well culture plates in triplicates. The cPGCs were counted on culture days 2, 4, 6, 8, and 10. The results showed that on day 4 onward, cells in the Gmax medium proliferate with higher efficiency than cells in the Gmin medium (Figure 3).

Long-term Culture of cPGCs in The Gmin and Gmax Media.

To evaluate the long-term self-renewal capacity of cPGCs during *in vitro* culture, first, we determined the sex of the Gmin and Gmax cultured cPGC lines, and then we cultured one male and one female in each medium to ensure that the long-term culture of the cPGC is not sex-dependent (Figure 4).

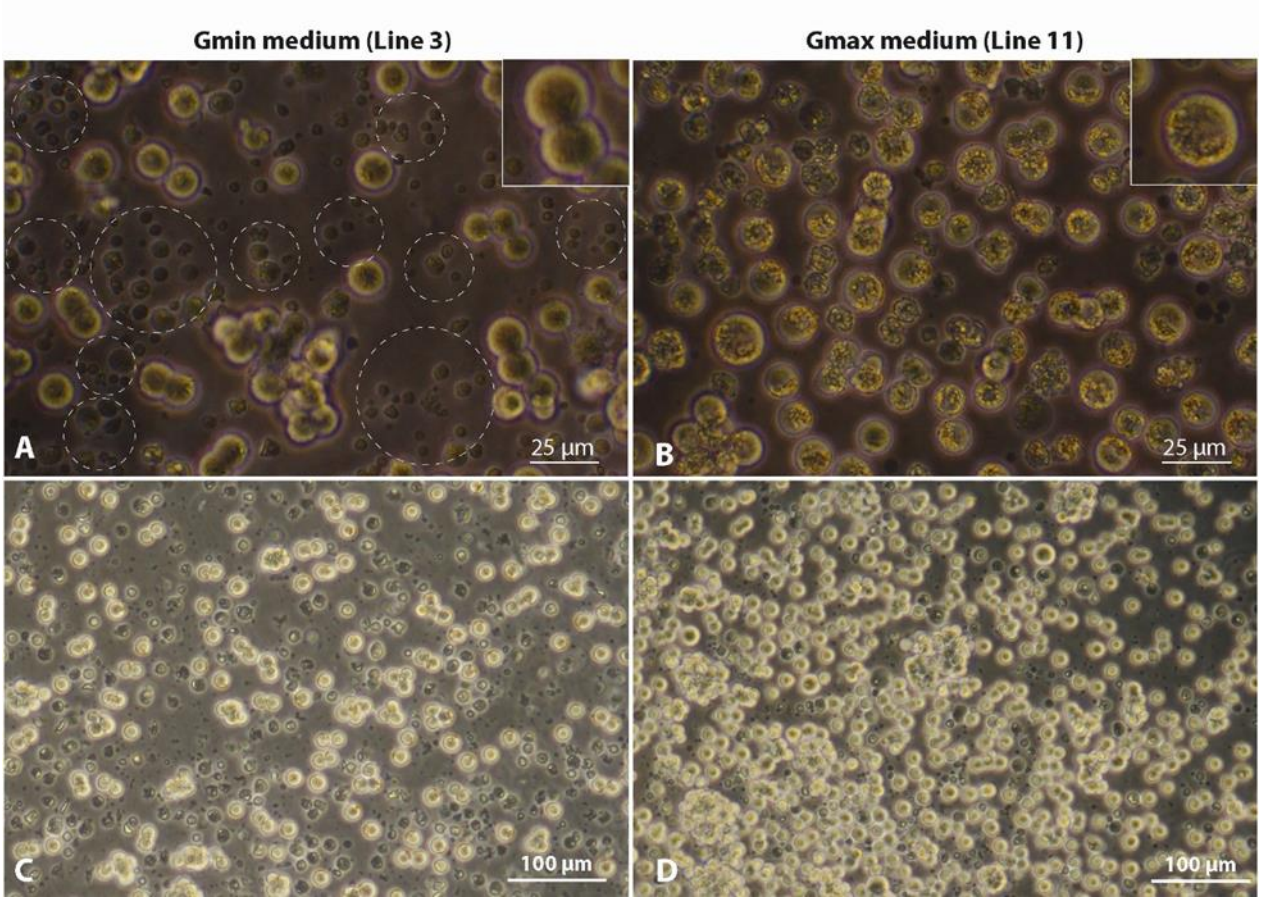

Figure 2. Derivation of cultured cPGCs in the Gmin and Gmax media. Two lines of derived cPGCs after 2 weeks of culture in the Gmin (A & C), and Gmax (B & D) media. The dashed enclosed areas in panel A show apoptotic cPGCs. The granular pattern of cytoplasm is much more prominent in panel B. The insets in panels A and B show a digitally magnified doublet and a PGC with granular cytoplasm, respectively. Scale bar = 25 µm. Magnification = ×200 (A & B). Scale bar = 100 µm. Magnification = ×100 (C & D).

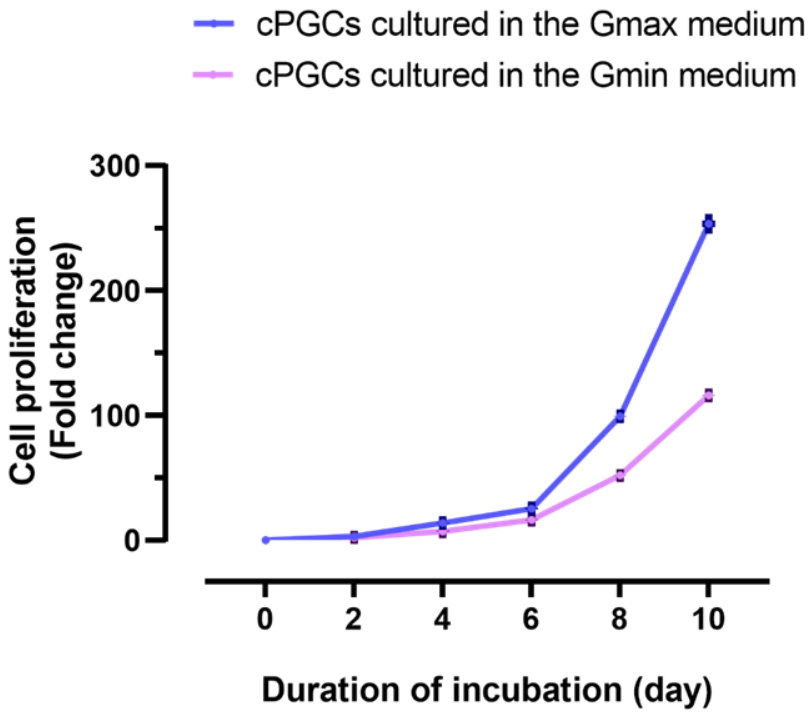

Figure 3. Growth curve of cultured cPGCs in the Gmin and Gmax media. The cPGCs cultured in the Gmin and GMax media were counted at various time points (days 2, 4, 6, 8, and 10). To calculate fold-change, the number of cells at each time point has been divided by the number of cells seeded at day 0. The results for each data point are based on 3 independent experiments. Error bars are standard deviations based on three biological replicates.

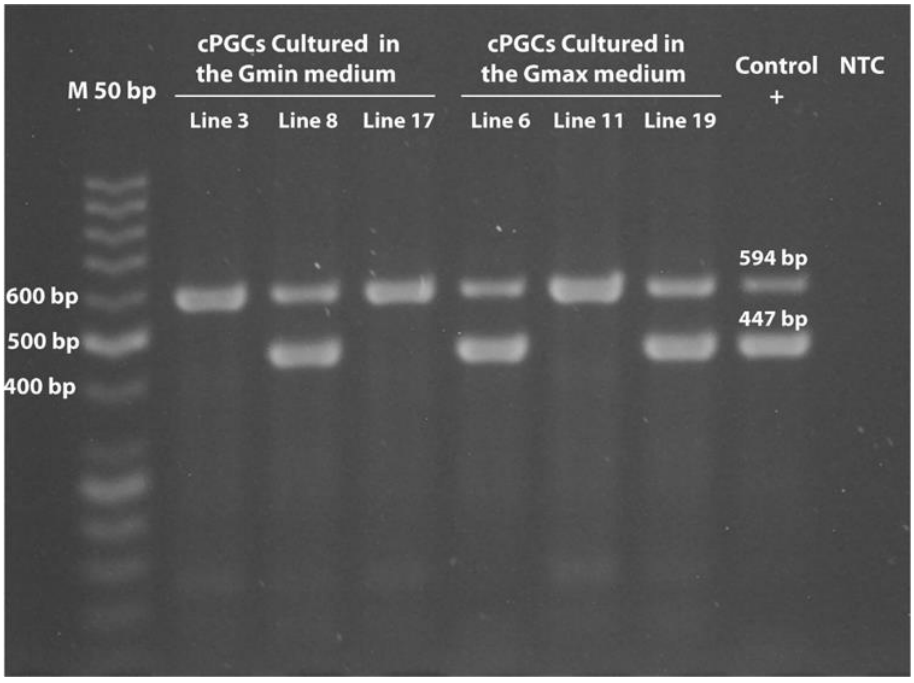

Figure 4. Sex determination of cPGCs cultured in the Gmin and Gmax media. The amplified fragments with the sexing primer set from a female's W and a male's Z chromosome were 447 bp and 594 bp, respectively. In each lane, one PCR band indicates male genotype, and two PCR bands a female genotype of the PGC line.

Selected derived-cPGCs were cultured in the Gmin and Gmax media for more than 3 months. In a long-term culture of 100 days, cultured cPGCs in the Gmin medium underwent around 21 passages, whereas cultured cPGCs in the Gmax medium underwent around 33 passages. Although the rate of proliferation in cPGCs cultured in the Gmin medium was slow with an extremely significant difference, no apparent difference was observed in the morphological characteristics of the cell lines (Figure 5 A & B).

Germ Cell-specific Promoter Assay

To examine whether our long-term cultured cPGCs in the Gmin and Gmax media are amenable to genetic modification and whether genetically manipulated cPGCs retain their germline features in the long-term culture, a promoter assay was carried out. To this end, we constructed an expression vector with a PGC-specific (DAZL) promoter driving tdTomato expression (Figure 6 A). The reporter cassette allowed the visualization of tdTomato in long-term cPGCs. These cells were successfully transfected and retained their germline features. Our results demonstrated that the long-term culture of cPGCs cultured in both the Gmin and Gmax media does not affect the transfectability of these cells (Figure 6 B).

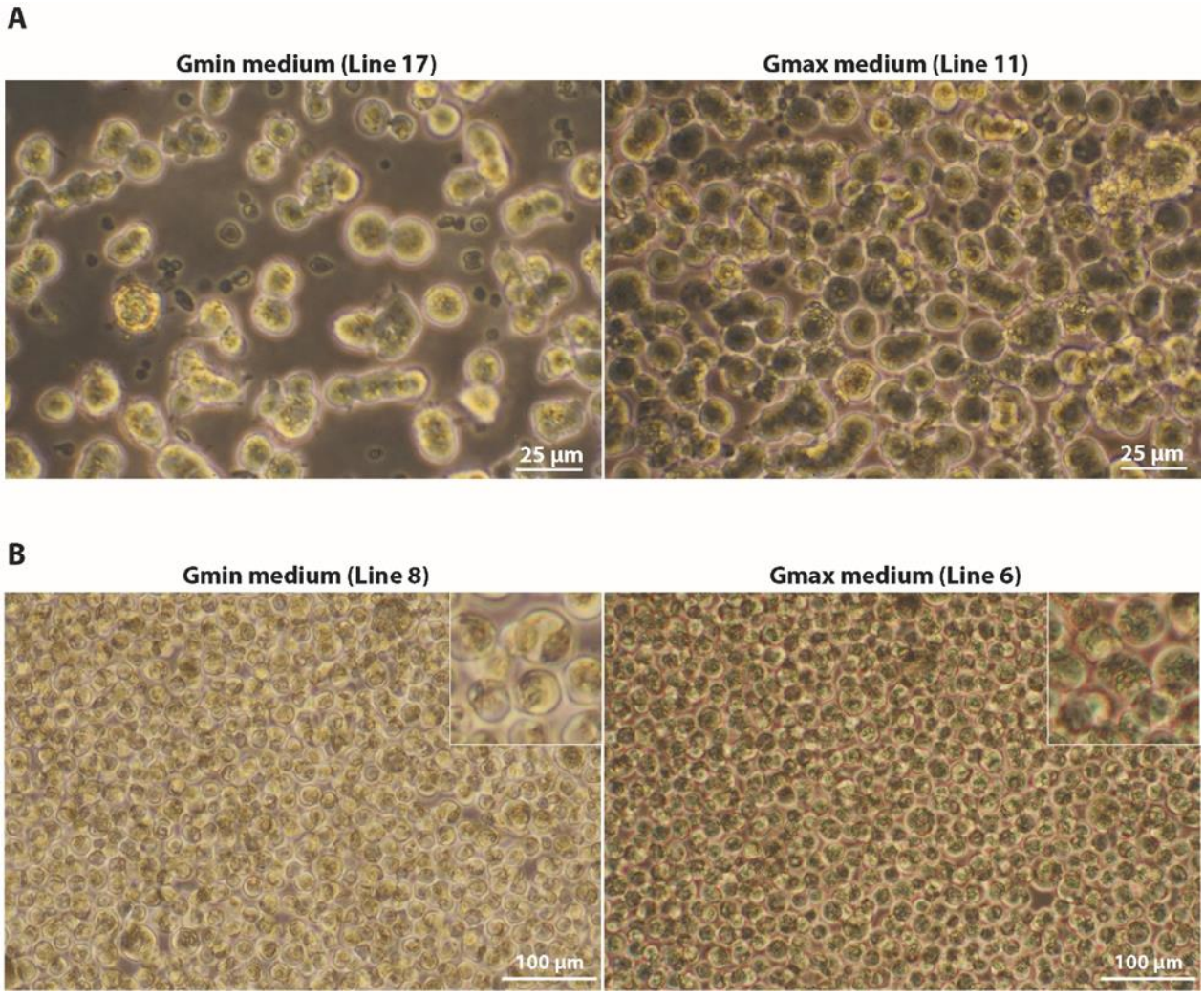

Figure 5. Morphology of the long-term cultured cPGCs in the Gmin and Gmax media. (A) Two lines of male PGCs, cultured for more than one month in the Gmin and the Gmax media. Scale bar = 25 µm. Magnification = ×200. (B) Two lines of female cPGCs, cultured for more than 3 months in the Gmin and the Gmax media. The insets in the left and right panels of B show digitally magnified long-term cultured cPGCs. Scale bar = 100 µm. Magnification = ×100

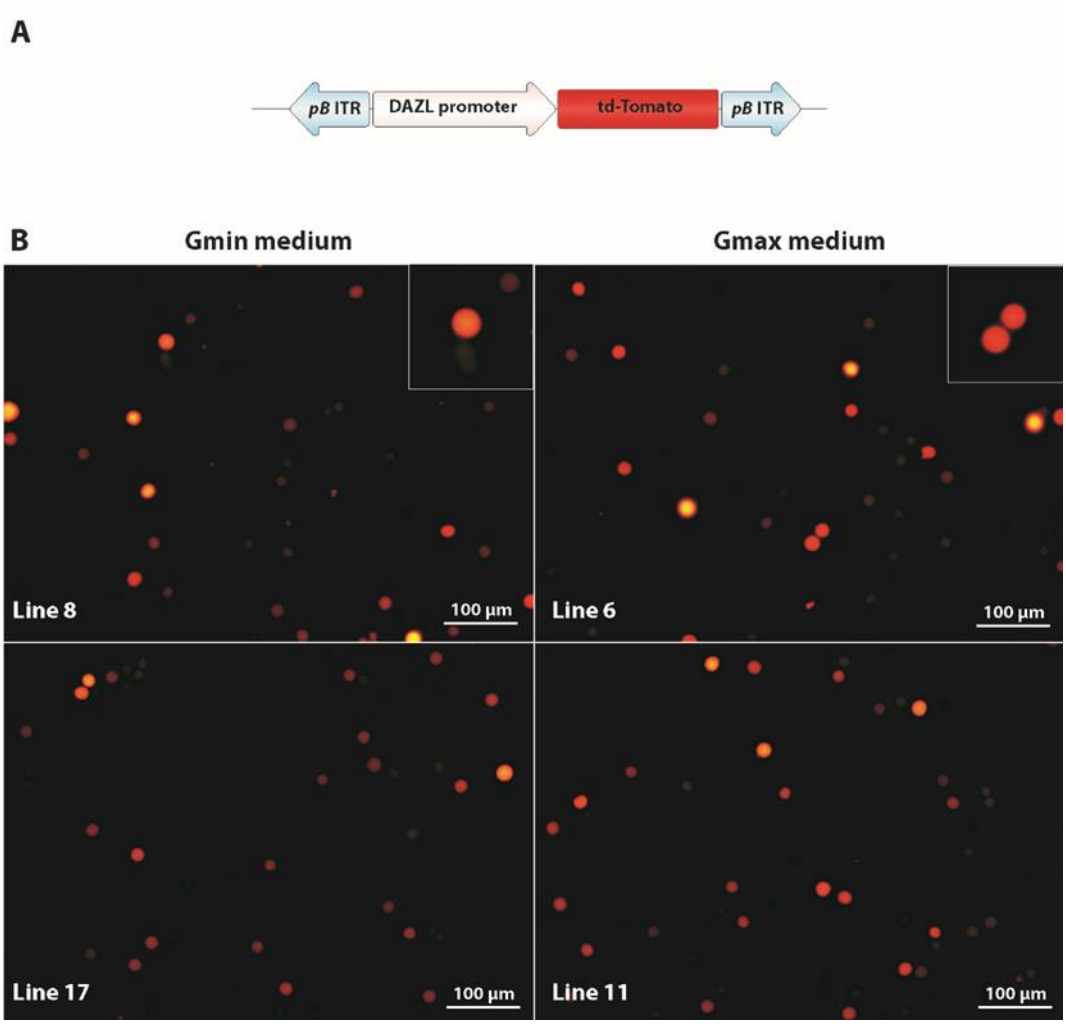

Figure 6. Promoter activity assay in cPGCs after long-term culture in the Gmin and Gmax media. (A) Schematics of the *piggyBac* transposon vector used in this study. The DAZL promoter drives the expression of tdTomato. The *piggyBac* transposon vector contains two ITRs of 206 bp. (B) cPGCs after long-term culture in the Gmin and Gmax media were transfected with the transposon construct and imaged by fluorescence microscopy. The insets in the top-left and top-right panels show digitally magnified cPGCs expressing tdTomato. Scale bar = 100 µm. Magnification = ×100

Discussion

Considering the importance of glutamine metabolism for cell survival and growth, we have evaluated the effect of glutamine stability on the long-term culture and establishment of chicken PGC lines. Despite considerable progress in the field of cPGC transgenesis, a thoroughly defined culture medium for the culture of chicken PGCs has not yet been developed. It has been reported that extrinsic factors including the feeder layer, growth factors, and the micro-environment in accordance with the intrinsic state of the cPGCs can affect the *in vitro* culture of cPGCs (Chen et al. 2018; Kong et al. 2018; Whyte et al. 2015). The source of energy is another factor that is essential to sustain cell survival and growth. The oxidation of glutamine and the metabolism of carbohydrates are two main energy sources for *in vitro* cell culture. It has been demonstrated that in the presence of both glutamine and glucose, 30-50% energy requirement is provided by glutamine. The contribution of glutamine oxidation to energy is determined by the presence of glucose. When glucose is decreased or is replaced by other carbohydrates, glutamine becomes the only source of energy in the *in vitro* cell culture (Zielke, Zielke, and Ozand 1984). Furthermore, glutamine plays an important role in cell signaling, amino acid

production, nucleotide synthesis, and redox state (Chen and Cui 2015; Gwangwa, Joubert, and Visagie 2019).

In this study, we successfully obtained cPGCs from the circulating embryonic blood. After the isolation, we cultured cPGCs using two selective media, one containing glutamine and the other containing Glutamax. As the culture progressed, along with the destruction of red blood cells, doublets became visible in both culture media. This observation confirmed the appropriate culture conditions for cPGCs and ongoing derivation of cPGCs, and also non-appropriate culture conditions for blood cells (Figure 2 B). After ~ 2 weeks of culture, we reached high cPGCs derivation efficiencies of 65% and 80% in the Gmin and Gmax media, respectively. Even though the derivation was observed in both media, our results showed higher derivation efficiency in the presence of GlutaMax. Glutamine is very labile in the culture media and spontaneously degrades over time. The rate of decomposition of glutamine is temperature-dependent, as only 2%–3% of the glutamine is available in the medium at 37 °C (Arii, Kai, and Kokuba 1999; Heeneman, Deutz, and Buurman 1993; Jagušić et al. 2016; Tritsch and Moore 1962). It has been demonstrated that restriction of glutamine metabolism through glutamine deprivation can induce autophagy and, or apoptosis both *in vivo* and *in vitro* (Chen and Cui 2015). The presence of apoptotic cells among cPGCs cultured in the Gmin medium during the derivation stage might be partly due to the depletion of the glutamine source. It has been reported that glutamine has anti-apoptotic activity independent from its application as an energy source, suggesting that glutamine plays an essential role in signaling pathways relating to cell survival (Fuchs and Bode 2006; Gwangwa, Joubert, and Visagie 2019; Harnett et al. 2013). Furthermore, the chemical degradation of glutamine generates pyroglutamate and ammonia as by-products which can negatively affect cell viability, protein glycosylation, and protein production (Ozturk and Palsson 1990).

Primary cells such as cPGCs should be gradually adapted to *in vitro* culture; otherwise, cells may encounter growth defects (ATCC Primary Cell Culture Guide, 2012). Thus, from the initial culture to the derivation stage, the medium should be refreshed in half every two days. Aggregation of ammonia in culture is toxic to the cells, especially for cells sensitive to ammonia toxicity (Bort, Stern, and Borth 2010). A diminished energy source and aggregation of ammonia resulting from the degradation of glutamine in the Gmin medium may have had a detrimental effect on cPGCs, a condition that was not observed in the Gmax medium. This could explain the presence of more apoptotic cells in cultures containing the Gmin medium (Figure 2). The viability and proliferation of cPGCs cultured in the presence of GlutaMax were more optimal (Figures 3 and 5), which can be explained by the higher stability of the Glutamx.

Although both media could successfully support the long-term culture and transfectability of cPGCs, and transfected cells retained their germline features according to the promoter assay (Figure 6), the GlutaMax medium provided better culture conditions, leading to shorter doubling time and more efficient derivation of cPGC lines. In the long-term culture of cPGCs, we didn't observe any apoptotic cells and morphological alterations in cPGC cultured both in the Gmin and Gmax media. This observation can be explained by the complete exchange of the media every two days and proper feeding. However, the proliferation rate of cPGCs cultured in the Gmax medium was higher than that in the Gmin medium. Although both Gmin and Gmax media can support the growth performance of cPGCs *in vitro*, it is reasonable to use the Gmax media for proliferation, expansion, and long-term culture of cPGCs.

In conclusion, isolation, cultivation, derivation, and establishment of chicken PGC lines are time-consuming and complicated. Therefore, using a stabilized form of glutamine such as GlutaMax could be a more reasonable and cost-effective option for the long-term culture of genetically manipulatable chicken PGCs.

Acknowledgments

The authors would like to thank the Research Institute of Biotechnology, Ferdowsi University of Mashhad, Mashhad, Iran, and Université Lyon 1, INSERM, Stem Cell and Brain Research Institute, Lyon, France for providing facilities to perform this study. This study was financially supported by Ferdowsi University of Mashhad. We dedicate this work to our deceased colleague, Dr. Mohammad Reza Bassami, for his help as the adviser of the S.Y. Ph.D. thesis research project.

Conflict of Interest

The authors declare that they have no conflict of interest.

References

Arii K., Kai T. and Kokuba Y. (1999) Degradation Kinetics of L-Alanyl-L-Glutamine and Its Derivatives in Aqueous Solution. European journal of pharmaceutical sciences : official journal of the European Federation for Pharmaceutical Sciences 7(2): 107–12.

ATCC, ATCC Primary Cell Culture Guide, ATCC, Manassas, VA, 2012, https://www.atcc.org/resources/culture-guides/primary-cell-culture-guide.

Hernández Bort J. A., Stern B. and Borth N. (2010) CHO-K1 Host Cells Adapted to Growth in Glutamine-Free Medium by FACS-Assisted Evolution. Biotechnology Journal 5(10): 1090–97.

Chen L. and Cui H. (2015) Targeting glutamine induces apoptosis: a cancer therapy approach. International Journal of Molecular Sciences 16: 22830–22855.

Chen Y. C., Chang W. C., Lin S.P., Minami M., Jean C., Hayashi H., et al. (2018) Three-Dimensional Culture of Chicken Primordial Germ Cells (CPGCs) in Defined Media Containing the Functional Polymer FP003. PLOS ONE 13(9): e0200515.

Eagle H. (1959) Amino Acid Metabolism in Mammalian Cell Cultures. Science 130(3373): 432–37.

Fridolfsson A. K. and Hans E. (1999) A Simple and Universal Method for Molecular Sexing of Non-Ratite Birds. Journal of Avian Biology 30(1): 116–21.

Fuchs B. C. and Barrie P B. (2006) Stressing out over Survival: Glutamine as an Apoptotic Modulator. The Journal of Surgical Research 131(1): 26–40.

Gwangwa M.V., Joubert A.M. and Visagie M.H. (2019) Effects of Glutamine Deprivation on Oxidative Stress and Cell Survival in Breast Cell Lines. Biological Research 52(1): 15.

Hamburger V. and Hamilton H. L. (1992) A Series of Normal Stages in the Development of the Chick Embryo. 1951. Developmental dynamics : an official publication of the American Association of Anatomists 195(4): 231–72.

Harnett C.C., Guerin P.J., Furtak T. and Gauthier E.R. (2013) Control of Late Apoptotic Events by the P38 Stress Kinase in L-Glutamine-Deprived Mouse Hybridoma Cells. Cell Biochemistry and Function 31(5): 417–26.

Heeneman S., Deutz D.E. and Buurman W. A. (1993) The Concentrations of Glutamine and Ammonia in Commercially Available Cell Culture Media. Journal of Immunological Methods 166(1): 85–91.

Jagušić M., Forčić D., Brgles M., Kutle L,. Šantak M., Jergović M., et al. (2016) Stability of Minimum Essential Medium Functionality despite L-Glutamine Decomposition. Cytotechnology 68(4): 1171–83.

Kong L., Qiu L., Guo Q., Chen Y., Zhang X., Chen B., et al. (2018) Long-Term in Vitro Culture and Preliminary Establishment of Chicken Primordial Germ Cell Lines. PLOS ONE 13(4): e0196459.

van de Lavoir M.C., Diamond J.H., Leighton P.A., Mather-Love C., Heyer B.S., Bradshaw R., et al. (2006) Germline Transmission of Genetically Modified Primordial Germ Cells. Nature 441(7094): 766–69.

Macdonald J., Glover J.D., Taylor L., Sang H.M. and McGrew M.J. (2010) Characterisation and Germline Transmission of Cultured Avian Primordial Germ Cells. PLOS ONE 5(11): e15518.

Meyer D. B. (1964) The migration of amphibian primordial germ cells in the chick embryo. Developmental Biology 10: 154–90.

Naito M., Harumi T. and Kuwana T. (2015) Long-Term Culture of Chicken Primordial Germ Cells Isolated from Embryonic Blood and Production of Germline Chimaeric Chickens. Animal Reproduction Science 153: 50–61.

Ozturk S. S. and Palsson B.O (1990) Chemical Decomposition of Glutamine in Cell Culture Media: Effect of Media Type, PH, and Serum Concentration. Biotechnology Progress 6(2): 121–28.

Tritsch G.L. and Moore G.E. (1962) Spontaneous Decomposition of Glutamine in Cell Culture Media. Experimental cell research 28: 360–64.

Whyte J., Glover J.D., Woodcock M., Brzeszczynska J., Taylor L., Sherman A., et al. (2015) FGF, Insulin, and SMAD Signaling Cooperate for Avian Primordial Germ Cell Self-Renewal. Stem Cell Reports 5(6): 1171–82.

Zielke H. R, Zielke C. L. and Ozand P.T. (1984) Glutamine: A Major Energy Source for Cultured

Mammalian Cells. Federation Proceedings 43(1): 121–25.

Journal of Cell and Molecular Research (2021) 13 (1), 54-64 DOI: 10.22067/jcmr.2021.68651.1001

Research Article

Exploring the Anticancer Efficacy of a Mixture of Local Probiotics on MDA-MB-231 and MCF-7 Breast Cancer Cell Lines

Mohadese Abdoli [1, 2], Parisa Fathi Rezaei [1*], Kamran Mansouri [2]

[1] *Biology department, Faculty of Science, University of Maragheh, Maragheh, Iran*
[2] *Medical Biology Research Center, Health Technology Institute, Kermanshah University of Medical Sciences, Kermanshah, Iran*

Received 31 January 2021 Accepted 27 April 2021

Abstract

This study aimed to investigate the cytotoxicity of a probiotic mixture on human breast cancer cell lines. To prepare the mixture, local probiotic bacteria were cultured, and the lyophilized supernatant was applied for downstream experiments. The antioxidant activity, total phenol content (TPC), and fatty acid composition of the bacterial supernatant (BS) were also measured. The possible cytotoxic/anti-proliferative effect of the probiotic mixture was accessed on both breast cancer cell lines at different concentrations using MTT assay. Furthermore, the apoptosis-inducing effects of the same mixture was studied by DAPI staining. The highest level of antioxidant activity and total phenol content (TPC) were detected for the BS at 3200 µg/ml. According to the GC–MS analysis, linoleic acid (37.40 %) and oleic acid (26.93 %) were identified as the major fatty acids of the BS. The MTT assay showed that the BS has anti-proliferative effects on MDA-MB-231 and MCF-7 cells in a time- and dose-dependent manner (IC_{50}: 3200 µg/ml). The apoptosis-inducing effects of the mixture was confirmed in both cell lines through morphological analyses of the cells' nucleoli, and the formation of apoptotic bodies. According to these experiments, cytotoxic effects and apoptosis-inducing potential were confirmed for the BS against two human breast cancer cell lines, including MDA-MB-231, and MCF-7. Hence, it could be considered as a suitable anti-cancer agent.

***Keywords*:** Breast cancer, Probiotics, Cytotoxicity, Apoptosis, Antioxidant activity

Introduction

The International Agency for Research on Cancer (IARC) reported that around 18.1 million new cancer cases and 9.6 million cancer-caused deaths occurred in 2018. Among females, breast cancer is the most commonly diagnosed cancer and is the leading cause of cancer death, followed by colorectal and lung cancers (Bray et al., 2018).

Lactic acid bacteria (LAB) are among the most important types of probiotic bacteria producing acid lactic as the final product during carbohydrates fermentation. Lactobacillus and bifidobacteria are gram-positive lactic acid bacteria, which constitute the bulk of the natural intestinal flora of humans. These microorganisms can fight with cancer by ***i***) metabolizing carcinogens, ***ii***) enhancing immune responses, ***iii***) producing anti-mutation and anti-cancer compounds, antioxidants, and anti-angiogenic factors, and ***iv***) the regulation of apoptosis and cell differentiation processes (Malik et al., 2018). The probiotic properties of lactobacillus and bifidobacteria are varied among different species. In addition, these effects are also probiotic strain-dependent (Irecta-Nájera et al., 2017).

Nowadays, probiotics because of high health potential can be used for prevention and adjuvant therapy of many chronic diseases, including cancer (Sli´zewska et al., 2021).

Different studies have shown that probiotics are effective in preventing, treating, and reducing the progression of several types of cancers such as colorectal, liver, breast, bladder, colon, lung, and cervical cancers (Biffi et al., 1997; Hassan et al., 2016; Kadirareddy et al., 2016; Lee et al., 2015; Malik et al., 2018; Maroof et al., 2012; Modarressi et al., 2014; Nami et al., 2014; Nami et al., 2015; Nouri et al., 2018; Yu and Li, 2016). Chemotherapeutics and synthetic drugs are extensively used as the standard treatment for breast cancer. These drugs are usually accompanied by life-threatening side effects and poor patients outcomes (Di Francia et al., 2013). Probiotics are less harmful and more cost-effective than various pharmacological compounds which are utilized to prevent or treat cancers (Malik et al., 2018).

The previously established cancer prevention

*Corresponding author's e-mail address: *parisafathirezaei@gmail.com*

mechanisms based on the application of probiotics include: ***i***) regulation of gut microbiota, ***ii***) improvement of gut barrier functions, ***iii***) elimination of procarcinogens, ***iv***) protection of the intestinal epithelium, and **v**) improvement of the immune and inflammatory systems. Moreover, other than cancers, probiotics reduce the risk of multiple chronic diseases, such as high serum cholesterol-related diseases, allergic diseases, and HIV (Nazir et al., 2018).

In literature, probiotics have been shown to inhibit the proliferation of several cancer cells types; but, the effect(s) of the mixture of probiotics on human breast cancer cell lines have rarely been investigated. Therefore, the purpose of this study was to investigate these effects as an alternative treatment strategy of breast cancers.

Materials and Methods

Chemicals

The chemicals, including $AlCl_3$, ethanol, ethyl acetate, the Folin-Ciocalteu reagent, $FeCl_3$, $FeSO_4$, gallic acid, glacial acetic acid, hexane, methanol, and TPTZ (tripyeridyl-s-triazine) were obtained from Merck (Germany). The mixture of local probiotic bacteria was purchased from Takgene Zist Company (Iran).

Bacterial strains

A mixture of three local probiotic bacteria from Iran (including; *Lactobacillus acidophilus*, *Bifidobacterium bifidum*, and *Lactobacillus casei*) were pre-cultured under sterile conditions on de Man, Rogosa and Sharpe (MRS) broth at 37°C overnight. Afterward, 10% of this stock was inoculated into the main culture medium, and incubated for 24h. Subsequently, the bacterial cultures (concentration: 1.5×10^{10} CFU/ml) were centrifuged at 1100*g* for 15min. Then, the pH was adjusted to 7.2 with NaOH (1N), and lyophilized. The lyophilized cell-free supernatant (CFS) was re-suspended in DMEM medium, filter sterilized, and stored at 4°C for further experiments.

Determination of antioxidant activity

The antioxidant power of the bacterial supernatant was determined by the ferric reducing ability of plasma, the FRAP assay (Benzie and Strain, 1996). Briefly, 50µL of each sample was added to 1450µL of the FRAP solution, and incubated for 30min at 37ºC. The samples' absorbances were read at 593nm, and the antioxidant activity was reported as mmol Fe^{2+}/g of each sample.

Determination of total polyphenol content

The total polyphenol content (TPC) of the bacterial supernatant was estimated in terms of the Folin–Ciocalteu (F-C) method, using gallic acid as the standard (Singleton et al., 1999). Briefly, 200µl of the extract was mixed with 1.3ml of Folin-Ciocalteu solution for 5min. Then, 1.5ml of the sodium carbonate (6%, w/v) was added, and incubated at room temperature for 30min. In addition, the absorbance of the sample was measured at 725nm. The TPC content was reported as gallic acid equivalent (GAE) (mg/l)/g of sample.

Fatty acid (FA) identification and quantification

Free fatty acids (FFAs) were analyzed using the method introduced by Torella et al. (Torella et al., 2013). Briefly, 200µL of the bacterial supernatant was extracted by the addition of 50µL of NaCl (10%, w/v), 50µL glacial acetic acid, and 200µL ethyl acetate, and then the solution vortexed for 20s. The mixture was centrifuged at 16000g for 10min, and then ethyl esters were generated by mixing 50µL of the organic phase with 450µL of a 30:1 mixture of EtOH and HCl (37%, v/v); they were incubated for 1h at 55°C. Then the mixture was cooled to the room temperature, and dH_2O (250µL) and hexane (250 µL) were added to this mixture. The mixture was vortexed for 10s, and 75µL was taken from the hexane layer for the GC-MS analysis. Extracts were run on the Agilent 5977A MSD GC-MS system (Agilent Technologies, USA) using the HP-5MS column (length: 30m; diameter: either 0.25 or 0.50mm; film: 0.25µm); the temperature was increased from 75 to 290°C (10°C/minute). Different compounds were determined via GC retention times compared to normal alkanes and verified by mass spectra. To calculate the retention indices (RI), n-Alkanes (C8-C40) were used as reference points (Babushok et al., 2011). The fatty acids were identified by computer matching with the Wiley Registry of Mass Spectral Data, 7th Edition (WILEY7 MS library), and confirmed by comparing their retention indices.

Cell culture

Dulbecco's Modified Eagle Medium (DMEM), fetal bovine serum (FBS), Penicillin-Streptomycin, and Trypsin-EDTA were purchased from Gibco (UK). Cell culture vessels were obtained from the Greiner Bio-One and Falcon. DAPI (4', 6-diamidino-2-phenylindole) was purchased from Roche (Germany).

The breast carcinoma cell lines MDA-MB-231 (ATCC HTB-26) and MCF-7 (ATCC HTB-22) were seeded in DMEM medium containing 10% FBS, and incubated in a 5% CO_2 incubator at 37°C.

Cell viability assay

The 3-(4,5-dimethylthiazol-2-yl)-2,5-diphenyltetrazolium bromide (MTT) assay was used to study the cytotoxic effects of the bacterial supernatant on MDA-MB-231 and MCF-7 cells (Rezaei et al., 2012). Briefly, 5000 cells/well were seeded in 96-well plates. After 24h the cells were exposed to different concentrations of the bacterial supernatant (100, 200, 400, 800, 1600, and 3200µg/ml) for 24, 48, and 72 h. At each time point, the MTT reagent (4 mg/ml in PBS) was added to the wells, samples were incubated at 37°C for 4h, and absorbances were determined using a microplate reader (Stat Fax 2100 Microplate ELISA Reader, Awareness Technologies) at 570nm. The IC_{50} value was defined as the concentration leading to a 50% inhibition of cell growth in comparison to the control cells.

Microscopic analysis of apoptotic cells

The apoptosis-inducing effect of the bacterial supernatant was confirmed by DAPI (4′,6-diamidino-2-phenylindole) staining (Rezaei et al., 2011). Briefly, the cells (3×10^5 cell/well) were seeded in 6-well plates, and then treated by the IC_{50} concentration of the bacterial supernatant for 24, 48, and 72h. The methanol-fixed cells were stained with 0.02% DAPI solution. Also, the plates were observed, and pictures taken using the Cytation5 Cell Imaging Multi-Mode Reader (BioTeK instruments).

Statistical analyses

The results were expressed as mean of three independent experiments±standard deviation (STDEV). Moreover, the obtained data were statistically compared by IBM SPSS Statistics22.0 using one-way analysis of variance (ANOVA). The $P<0.05$ was considered as statistically significant, and correlations among pairs of variables were determined using the Excel software.

Results

The BS content analysis

The antioxidant potential of the bacterial supernatant was calculated using a standard curve ($y=0.00289X+0.03340$, $R^2=0.99$) of the ferrous sulfate ($FeSO_4$) solution. As it was demonstrated by the results, the antioxidant activity increases along with the increase in the concentration. Also, the highest antioxidant activity (123.5 mmol Fe^{2+}/g) of the samples was measured at the concentration of 3200 µg/ml of the bacterial supernatant (Table 1).

The total phenolic content of the extract was calculated using a standard curve ($y=0.00221X + 0.04578$, $R^2=0.93$) of gallic acid. As shown in Table 1, total polyphenol content is increases in accordance with the increasing concentrations. The highest amount of 30.9 mg GAE/g was observed at 3200 µg/ml of the bacterial supernatant.

As described in the Table 2, in the bacterial supernatant, linoleic acid has the highest percentage (37%) among other investigated fatty acids, which is followed by oleic acid (27%). It is while, palmitic acid (3.42%) showed the lowest percentage.

Table 1. Antioxidant activity and TPC of the bacterial supernatant.

Bacterial supernatant concentrations (µg/ml)	TPC (mg GAE/g of sample)	Antioxidant activity (mmol Fe^{2+}/g of sample)
100	3.78±0.001	28.201±0.03
200	5±0.02	32. 83±0.05
400	7.24±0.024	45.15±0.062
800	8.91±0.035	50.77±0.051
1600	16±0.051	63.05±0.01
3200	20±0.021	100.52±0.1

Values are expressed as mean±standard deviation.
Abbreviations: TPC, total phenol content; GAE, galic acid equation.

Table 2. Fatty acid composition of the bacterial supernatant.

C number: double band number	FA	RI	Fatty acid (%)
14:0	Tetradecanoic acid	1558	6.11
16:0	Palmitic acid	1882	3.42
18:2	Linoleic acid	1974	37.40
18:1	Oleic acid	1440	26.93
20:0	Eicosanoic acid	2856	13.42
22:0	Docosanoic acid	1520	12.03

RI indices on HP-5MS column, experimentally determined using the homologue series of n-alkanes.
Abbreviations: C, carbon; FA, fatty acid; RI, linear retention.

Cytotoxic effects of the probiotic mixture

The effects of the bacterial supernatant on the viabilities of two human breast cancer cell lines MDA-MB-231 (Figure 1) and MCF-7 (Figure 2) were assessed using MTT assay at similar concentrations for 3 consecutive days. The bacterial supernatant showed a significant growth inhibitory effect in a dose- and time-dependent manner on both cell lines. The IC_{50} value on both cell lines was determined as 3200µg/ml in 72h following the exposure. The IC_{50} concentration was then used for performing further studies.

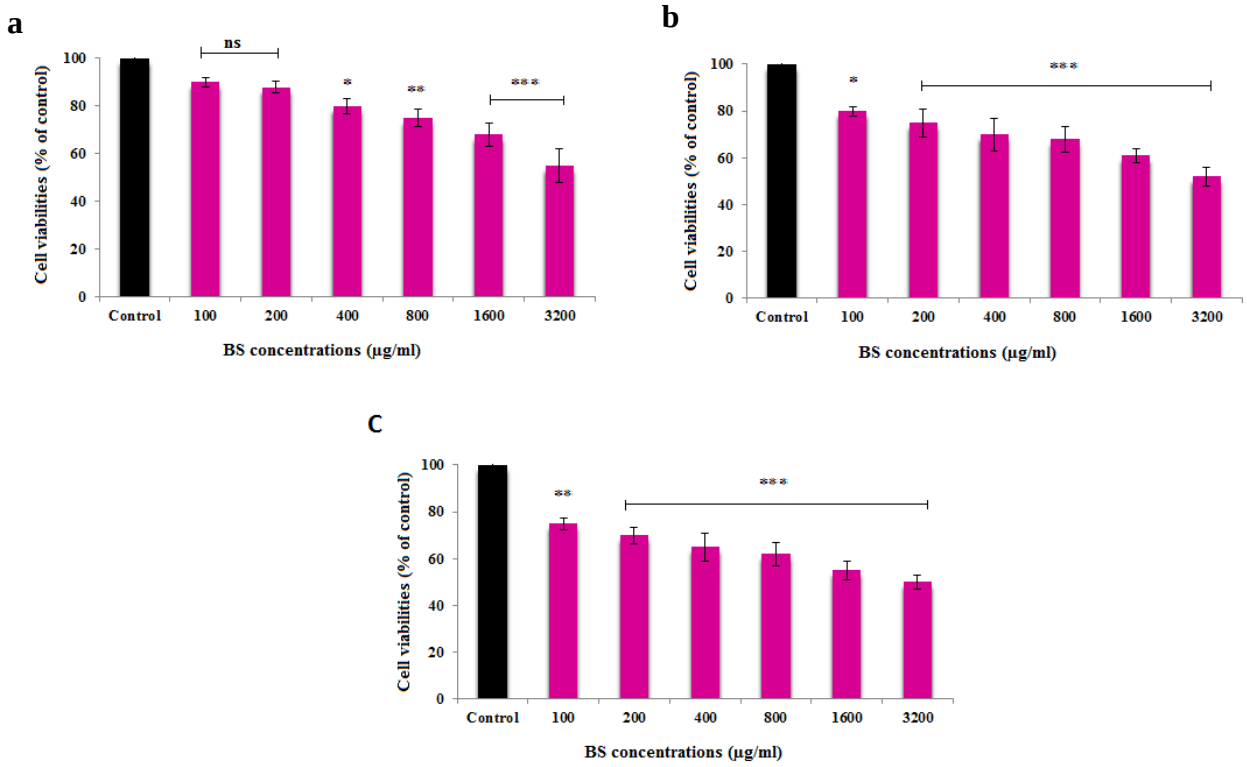

Figure 1. The cytotoxic effects of the bacterial supernatant on MDA-MB-231 cells as it was obtained by MTT assay. The MDA-MB-231 cells were exposed to different concentrations of the bacterial supernatant (100, 200, 400, 800, 1600, and 3200µg/ml) for 24 (a), 48 (b), and 72 h (c). The $p<0.05$ was considered as statistically significant in comparison to the control cells (*$p<0.05$, **$p<0.01$, ***$p<0.001$, and "ns" showed no significant difference was observed between treated and untreated groups).

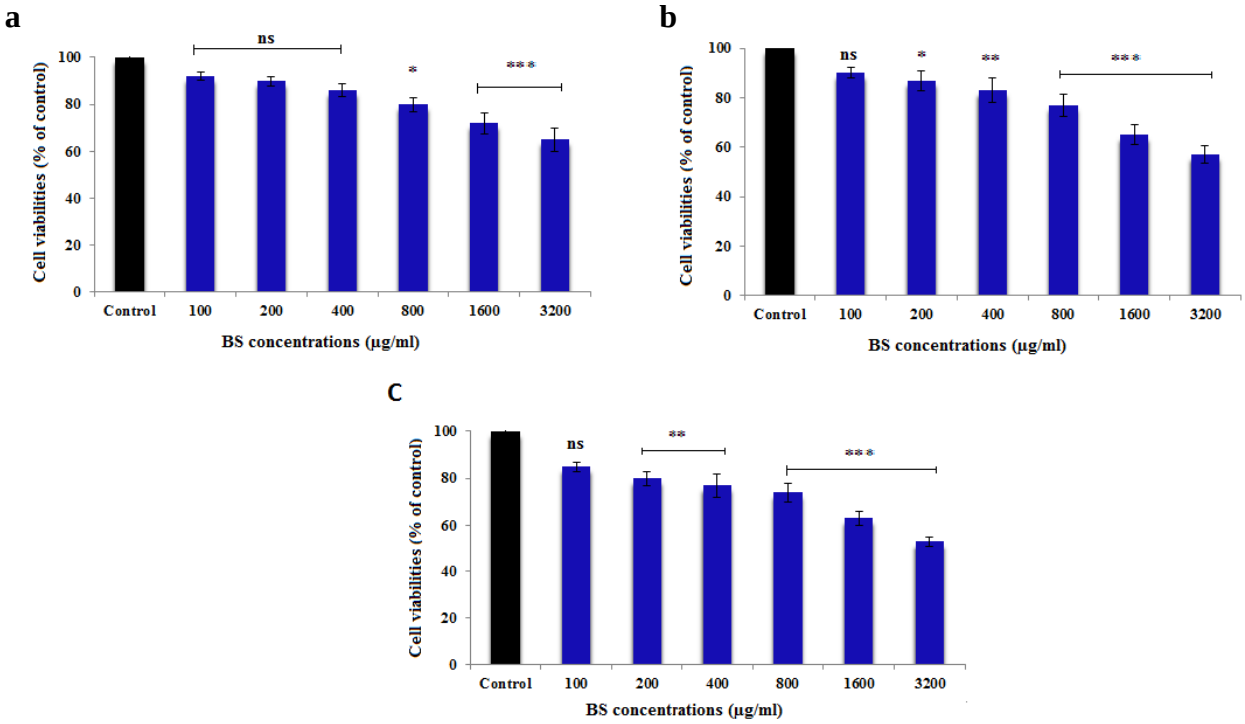

Figure 2. The cytotoxic effects of the bacterial supernatant on MCF-7 cells as it was obtained by MTT assay. The MCF-7 cells were exposed to different concentrations of the bacterial supernatant (100, 200, 400, 800, 1600, and 3200 µg /ml) for 24 (a), 48 (b), and 72 h (c). The $p<0.05$ was considered as statistically significant in comparison to the control cells (*$p<0.05$, **$p<0.01$, ***$p<0.001$, and "ns" showed no significant difference was observed between treated and untreated groups).

Correlation among total phenolic content and antioxidant capacity of BS with the cells' viability

The correlations between total phenolic contents and cell viabilities are shown in Figure 3a. The correlation coefficients of linear regression (R^2) were calculated as 0.90 and 0.82 for MCF-7 and MDA-MB-231 cells, respectively. There is a positive and high correlation between TPC values and the viabilities of MCF-7 cells.

The correlations between the antioxidant capacities and cell viabilities are shown in Figure 3b. The R^2 were calculated as 0.89 and 0.94 for MCF-7 and MDA-MB-231 cells, respectively. There is a positive and high correlation between antioxidant capacities and MDA-MB-231 cells viability.

The correlation between the TPC and the antioxidant capacity (FRAP) of the bacterial supernatant is presented in Figure 3c (R^2=0.97). Hence, there is a positive and high correlation between TPC values and antioxidant capacities of the bacterial supernatant.

In addition, significant correlations were found between antioxidant capacities and cell viabilities of MDA-MB-231 (R^2=0.94, Figure 3b); and between MCF-7 cells viabilities and TPCs (R^2=0.90, Figure 3a). Moreover, the lowest correlation was found between the antioxidant capacities and MCF-7 cell viabilities (R^2=0.89, Figure 3b; R^2=0.82, Figure 3a) with the TPC and MDA-MB-231 cell viabilities, respectively. Data are shown in Table 3.

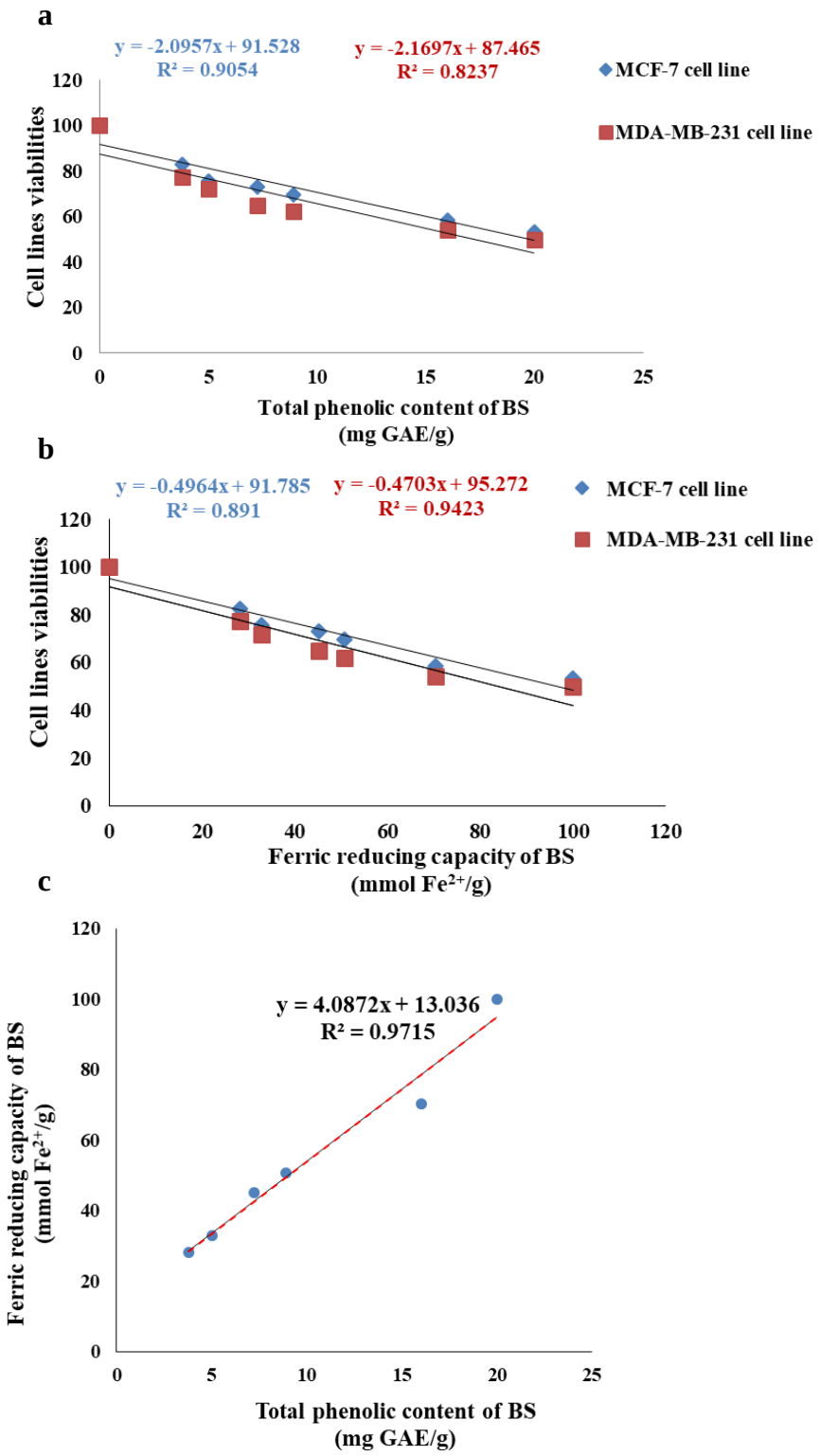

Figure 3. Linear regression among FRAP, TPC and cell lines viabilities. a) Total phenolic contents (mg gallic acid/g DW) and cell viabilities (%); b) Antioxidant capacity as it was evidenced by the FRAP assay (momol Fe^{2+}/g DW) and cell viabilities (%); c) total phenolic contents and antioxidant capacities.

Table 3. Correlation coefficient matrix between data.

	[probiotic]	TPC	FRAP	MDA-MB-231	MCF-7
[probiotic]	1				
TPC	0.948682	1			
FRAP	0.931299	0.983209	1		
MDA-MB-231	-0.76253	-0.90759	-0.9439	1	
MCF-7	-0.83134	-0.95154	-0.9707	0.989193	1

Abbreviations: [probiotic], probiotic concentration; TPC, total phenolic content; FRAP, ferric reducing ability of plasma.

Apoptosis-inducing effects of the bacterial supernatant

The apoptotic type of the cell death was confirmed through morphological analyses. The nuclear morphological changes of MDA-MB-231 cells are clearly shown in Figure 4. In BS-treated cells, nuclear morphological changes, such as nuclear condensation and fragmentation were observed 48h post treatment. As shown in Figure 5, morphological changes of the MCF-7 cells' nucleoli, including condensation in the peripheral zone of the nucleus and DNA fragmentation were observed following 24h. Dead cells were detected upon increasing the exposure time following the treatment with the bacterial supernatant.

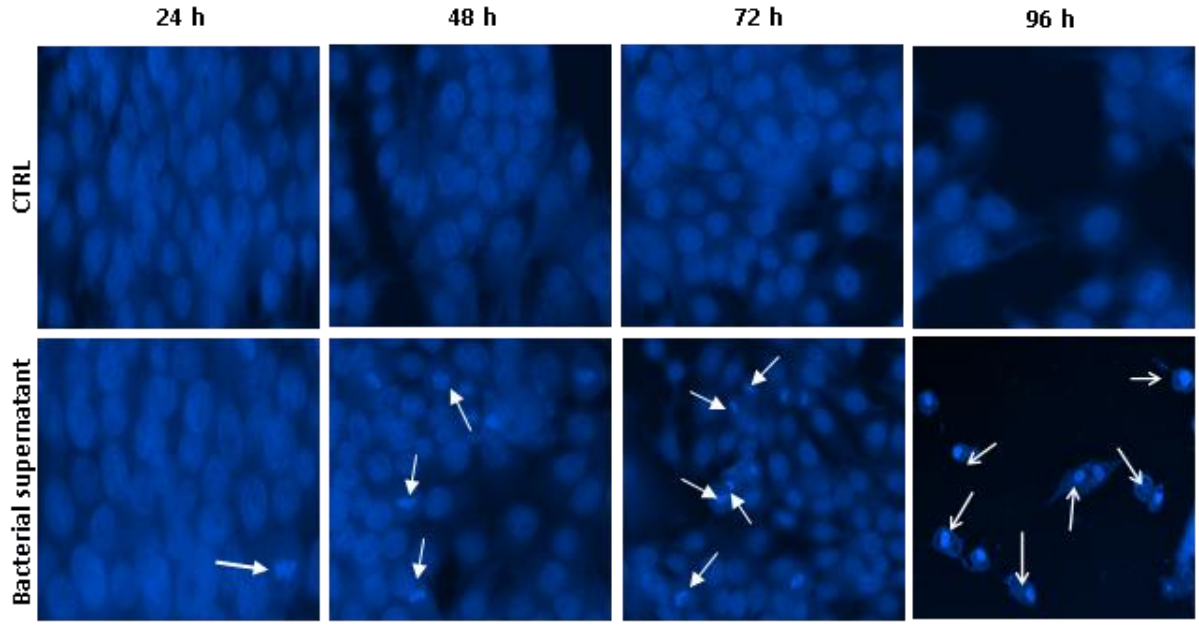

Figure 4. Effects of bacterial supernatant on nuclear morphology of MDA-MB-231 cells. MDA-MB-231 cells were cultured and exposed to the bacterial supernatant (3200 µg/ml) or left untreated (CTRL). DAPI staining was performed at different time points (24-96h) to detect apoptosis-inducing effects of the BS. The images were taken using the Cytation5 Cell Imaging Multi-Mode Reader. White arrows indicate apoptotic cells with condensed nucleoli (10X).

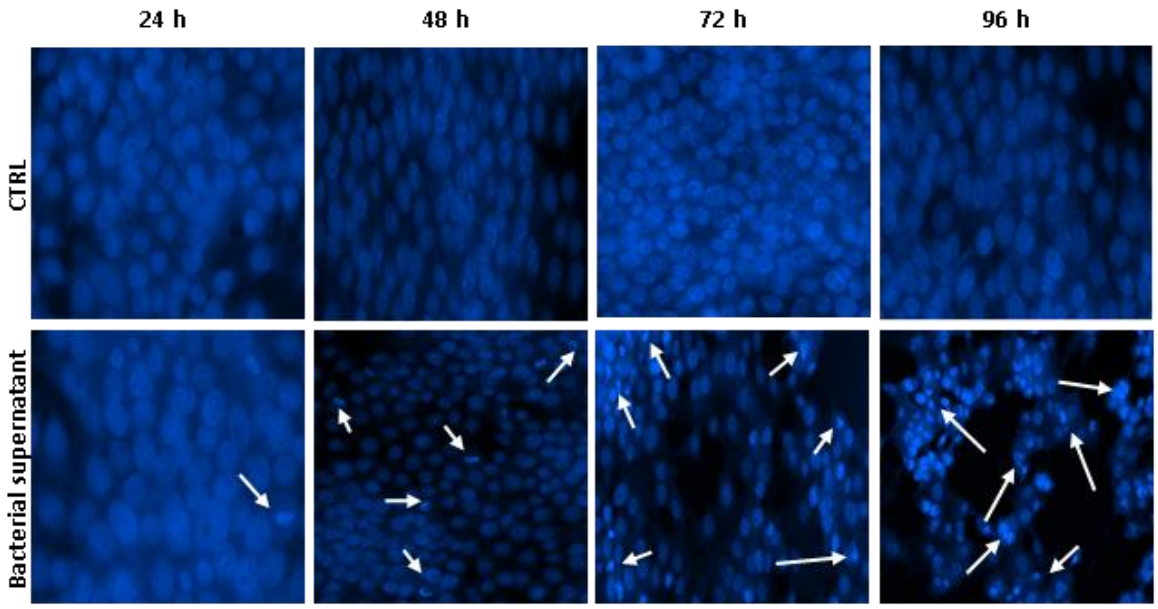

Figure 5. Effects of bacterial supernatant on nuclear morphology of MCF-7 cells. MCF-7 cells were cultured and exposed to the bacterial supernatant (3200 µg/ml), and DMEM (CTRL) for 24-96 h. The images were taken using the Cytation5 Cell Imaging Multi-Mode Reader. The white arrows indicate apoptotic cells (10 X).

Discussion

Probiotics and their metabolites can regulate key cellular processes, including proliferation, differentiation, apoptosis, and angiogenesis (Motevaseli et al., 2017). In some cases, synbiotics and a combination of two or more probiotics are more efficient than a single probiotic compound (Yu and Li, 2016). It is believed that, many commercially available probiotics are safe and have some beneficial health effects for the host. Also, probiotics could act against breast cancer progression, as it was evidenced by several *in vitro* cell-based studies, pre-clinical experiments, and large-scale clinical trials (Malik et al., 2018).

Several significant studies have illustrated that probiotics have pro-apoptotic or anti-proliferative effects on various human cancer cell lines. The induction of apoptosis is the best mode of cell proliferation inhibition or suppression. Apoptosis is an evolutionarily conserved pathway of cell death which is responsible for the programmed elimination of the cells during homeostasis and normal eukaryotic development (Singh et al., 2019). Apoptosis of eukaryotic cells is associated with specific morphological changes in their cell membranes and nuclear DNA. These morphological changes could be observed during microscopic studies (Elmore, 2007). The anti-carcinogenic effects of different probiotics are attributed to a combination of events and mechanisms. Their mechanism of function is similar to the tumor suppressor protein p53, which induces cell apoptosis and high levels of DNA damage (Yu and Li, 2016).

It was shown in a previous publication that the proteinaceous postbiotic metabolites (PPM) of *L. plantarum* I-UL4 are cytotoxic against MFC7 cells in a dose- and time-dependent manner (IC_{50}: 10.83µg/µl, 72h). In addition, they demonstrated that 48h following the treatment apoptosis is detectable in 80.87% of the cells (Tan, 2015). Also, treatment of human cancerous cell lines (HeLa, MCF-7, AGS, HT-29, Caco-2) with the *Enterococcus lactis* IW5 supernatant at concentrations less than 50µg/ml confirmed its cytotoxic effects in all investigated cell lines, and indicated its apoptosis-inducing capacity in HeLa cells (Nami et al., 2015). Lee and coworkers reported that *L. lactis* KC24 isolated from kimchi exerted antimicrobial, anti-inflammatory, antioxidant, and anti-cancer effects. Its anti-cancer effect were shown against AGS, HT-29, LoVo, MCF-7, and SK-MES-1 cells (>50% cytotoxicity) (Lee et al., 2015).

The cell free supernatant (CFS) of *B. bifidum* has the ability to inhibit the growth of SW742, Caco-2 and HT-29 colon cancer cells (Bahmani et al., 2019).

Kadirareddy et al. reported the inhibition of MDA-

MB-231 proliferation by *Lactobacillus plantarum*-conjugated linoleic acid (LP-CLA) from *Lactobacillus plantarum.* Cell detachment, rounding of cells, and oligo-nucleosomal fragmentation of DNA were reported as the main morphological changes observed following the treatment (Kadirareddy et al., 2016).

Metabolites of *E. durans* 39C showed anti-cancer characteristics against MCF-7, HeLa, HT29, and AGS cell lines mainly via induction of apoptosis (Haghshenas et al., 2014). The supernatants of *L. rhamnosus* strain GG (LRS) and *L. crispatus* strain SJ-3C-US (LCS) showed growth inhibitory effects on the HeLa cells (Nouri et al., 2018). Also, *L. acidophilus* and *L. crispatus* supernatants indicated antitumor activity (15%, v/v) on the MDA-MB-231 cells (Modarressi et al., 2014). Several probiotic strains, including *B. animalis*, *L. acidophilus*, *Bifidobacterium infantis*, *Lactobacillus paracasei*, *and Bifidobacterium bifidum* have been shown to reduce the MCF7 cancer cell's growth (Kim et al., 2007).

Probiotics produce compounds, such as polysaccharides and fatty acids, which are powerful in inhibiting the proliferation of cancerous cells. Short chain fatty acids (SCFA), by increasing the amount of butyrate, can affect the regulation of the balance amongst proliferation, differentiation, and apoptosis (Bougnoux et al., 2010). Probiotics can also stimulate the antioxidant system of the host cells, and efficiently elevate the activity of antioxidant enzymes (Wang et al., 2017).

According to the results, the antioxidant capacity of the BS is increased in a dose-dependent manner, and a positive and high correlation observed between its antioxidant capacity and the viability of MDA-MB-231 cells. The correlation between antioxidant activity and the viability of MCF-7 cells was positive and a little less than MDA-MB-231. Based on the results, linolenic acid is the most common fatty acid of the BS which may have growth inhibitory effects against both cell lines. The present findings suggest that the mixture of local probiotic bacteria, including *Lactobacillus acidophilus*, *Bifidobacterium bifidum*, and *Lactobacillus casei* not only has the antioxidant capacity, but also exert cytotoxic effects on MCF-7 and MDA-MB-231 cell lines, partially through the induction of apoptosis. The exact effector molecules and mechanisms which are responsible for the probiotic mixture properties should be further explored. In addition, as a natural bioactive compound, its suitability for clinical applications needs further evaluations and complementary studies.

Acknowledgment

We wish to acknowledge the management of Research and Technology and the Central laboratory of the University of Maragheh for their help in running the experiments.

References

Babushok V., Linstrom P. and Zenkevich I. (2011) Retention indices for frequently reported compounds of plant essential oils. Journal of Physical and Chemical Reference Data 40:043101.

Bahmani S., Azarpira N. and Moazamian E. (2019) Anti-colon cancer activity of Bifidobacterium metabolites on colon cancer cell line SW742. The Turkish Journal of Gastroenterology 30:835.

Benzie I. F. and Strain J. J. (1996) The ferric reducing ability of plasma (FRAP) as a measure of "antioxidant power": the FRAP assay. Analytical biochemistry 239:70-76.

Biffi A., Coradini D., Larsen R., Riva L. and Di Fronzo G. (1997) Antiproliferative effect of fermented milk on the growth of a human breast cancer cell line.

Bougnoux P., Hajjaji N., Maheo K., Couet C. and Chevalier S. (2010) Fatty acids and breast cancer: sensitization to treatments and prevention of metastatic re-growth. Progress in lipid research 49:76-86.

Bray F., Ferlay J., Soerjomataram I., Siegel R. L., Torre L. A. and Jemal A. (2018) Global cancer statistics 2018: GLOBOCAN estimates of incidence and mortality worldwide for 36 cancers in 185 countries. CA: a cancer journal for clinicians 68:394-424.

Di Francia R., Siesto R. S., Valente D., Del Buono A., Pugliese S., Cecere S., and et al. (2013) Current strategies to minimize toxicity of oxaliplatin: selection of pharmacogenomic panel tests. Anti-cancer drugs 24:1069-1078.

Elmore S. (2007) Apoptosis: a review of programmed cell death. Toxicologic pathology 35:495-516.

Haghshenas B., Nami Y., Abdullah N., Radiah D., Rosli R. and Khosroushahi A. Y. (2014) Anti-proliferative effects of Enterococcus strains isolated from fermented dairy products on different cancer cell lines. Journal of functional foods 11:363-374.

Hassan Z., Mustafa S., Rahim R. A. and Isa N. M. (2016) Anti-breast cancer effects of live, heat-killed and cytoplasmic fractions of Enterococcus faecalis and Staphylococcus hominis isolated from human breast milk. In Vitro Cellular & Developmental Biology-Animal 52:337-348.

Irecta-Nájera C. A., del Rosario Huizar-López M., Casas-Solís J., Castro-Félix P. and Santerre A. (2017) Protective effect of Lactobacillus casei on DMH-induced colon carcinogenesis in mice. Probiotics and antimicrobial proteins 9:163-171.

Kadirareddy R. H., Vemuri S. and Palempalli U. (2016) Probiotic Conjugated Linoleic Acid Mediated Apoptosis in Breast Cancer Cells by Downregulation of NFκB. Asian Pacific journal of cancer prevention: APJCP 17:3395-3403.

Lee N.-K., Han K. J., Son S.-H., Eom S. J., Lee S.-K. and Paik H.-D. (2015) Multifunctional effect of probiotic Lactococcus lactis KC24 isolated from kimchi. LWT-Food Science and Technology 64:1036-1041.

Malik S. S., Saeed A., Baig M., Asif N., Masood N. and Yasmin A. (2018) Anticarcinogenecity of microbiota and probiotics in breast cancer. International journal of food properties 21:655-666.

Maroof H., Hassan Z. M., Mobarez A. M. and Mohamadabadi M. A. (2012) Lactobacillus acidophilus could modulate the immune response against breast cancer in murine model. Journal of clinical immunology 32:1353-1359.

Modarressi R. E.-V., Daneshvar M., Beigom M. and Mobasheri E. M. (2014) Lactobacillus acidophilus and Lactobacillus crispatus culture supernatants downregulate expression of cancer-testis genes in the MDA-MB-231 cell line. Asian Pacific Journal of Cancer Prevention 15:4255-4259.

Motevaseli E., Dianatpour A. and Ghafouri-Fard S. (2017) The role of probiotics in cancer treatment: emphasis on their in vivo and in vitro anti-metastatic effects. International journal of molecular and cellular medicine 6:66.

Nami Y., Abdullah N., Haghshenas B., Radiah D., Rosli R. and Khosroushahi A. Y. (2014) Probiotic potential and biotherapeutic effects of newly isolated vaginal Lactobacillus acidophilus 36YL strain on cancer cells. Anaerobe 28:29-36.

Nami Y., Haghshenas B., Haghshenas M., Abdullah N. and Yari Khosroushahi A. (2015) The prophylactic effect of probiotic Enterococcus lactis IW5 against different human cancer cells. Frontiers in microbiology 6:1317.

Nazir Y., Hussain S. A., Abdul Hamid A. and Song Y. (2018) Probiotics and their potential preventive and therapeutic role for cancer, high serum cholesterol, and allergic and HIV diseases. BioMed research international 2018.

Nouri Z., Neyazi N., Modarressi M. H., Karami F., Abedin-Do A., Taherian-Esfahani Z., Ghafouri-Fard S. and Motevaseli E. (2018) Down-regulation of TSGA10, AURKC, OIP5 and AKAP4 genes by Lactobacillus rhamnosus GG and Lactobacillus crispatus SJ-3C-US supernatants in HeLa cell line. Klinická onkologie 31.

Rezaei P. F., Fouladdel S., Cristofanon S., Ghaffari S., Amin G. and Azizi E. (2011) Comparative cellular and molecular analysis of cytotoxicity and apoptosis induction by doxorubicin and Baneh in human breast cancer T47D cells. Cytotechnology 63:503.

Rezaei P. F., Fouladdel S., Hassani S., Yousefbeyk F., Ghaffari S. M., Amin G. and et al. (2012) Induction of apoptosis and cell cycle arrest by pericarp polyphenol-rich extract of Baneh in human colon carcinoma HT29 cells. Food and Chemical Toxicology 50:1054-1059.

Singh R., Letai A. and Sarosiek K. (2019) Regulation of apoptosis in health and disease: the balancing act of BCL-2 family proteins. Nature Reviews Molecular Cell Biology 20:175-193.

Singleton V. L., Orthofer R. and Lamuela-Raventós R. M. 1999. [14] Analysis of total phenols and other oxidation substrates and antioxidants by means of folin-ciocalteu reagent. *In* Methods in enzymology. Vol. 299. Elsevier. 152-178.

Torella J. P., Ford T. J., Kim S. N., Chen A. M., Way J. C. and Silver P. A. (2013) Tailored fatty acid synthesis via dynamic control of fatty acid elongation. Proceedings of the National Academy of Sciences 110:11290-11295.

Wang Y., Wu Y., Wang Y., Xu H., Mei X., Yu D., and et al. (2017) Antioxidant properties of probiotic bacteria. Nutrients 9:521.

Yu A.-Q. and Li L. (2016) The potential role of probiotics in cancer prevention and treatment. Nutrition and cancer 68:535-544.

Journal of Cell and Molecular Research (2021) 13 (1), 65-71 DOI: 10.22067/jcmr.2021.71395.1010

Research Article

The Effect of Androgen Deprivation on the Expression of Connexin-43 mRNA in the Heart

Mahnaz Ghowsi [1*], Nazli Khajehnasiri [2], Sajjad Sisakhtnezhad [1]

[1]*Department of Biology, Faculty of Sciences, Razi University, Kermanshah, Iran*
[2]*Department of Biological Sciences, Faculty of Basic Sciences, Higher Education Institute of Rab-Rashid, Tabriz, Iran*

Received 10 July 2021 Accepted 20 September 2021

Abstract

Connexin-43 (Cx-43) plays axial roles in the propagation of action potentials and contractile coupling in the heart. Down-regulation of Cx-43 in the heart is associated with arrhythmia, dilated cardiomyopathy, and heart failure. To date, no studies have examined the effects of androgen deprivation therapy (ADT)-induced hypogonadism on the expression of Cx-43 in the heart. This study investigated the effects of testosterone deprivation and its replacement with testosterone enanthate on the expression of Cx-43 mRNA and the muscle-specific miRNAs miR-206 and miR-1, as two potential regulators of the Cx-43 protein expression in the ventricular tissue. Accordingly, 21 male *Wistar* rats were divided into three groups: I) Normal control, II) ORX-S: castrated rats serving as animal models for ADT and receiving the sesame oil as a solvent of testosterone enanthate for ten weeks, and III) ORX-T: these animals were castrated, receiving testosterone enanthate (25 mg/kg) for ten weeks. The relative expression of Cx-43 mRNA, miR-206, and miR-1 was determined by qRT-PCR. Cx-43 mRNA was found to be decreased in the ORX-S group. The Cx-43 mRNA was up-regulated after the administration of testosterone enanthate. There were no significant changes in miR-206, and miR-1 levels in the ORX-S and ORX-T groups compared to the controls. Our results indicated that testosterone should be regarded as an important factor in the regulation of Cx-43 mRNA expression in the heart, and testosterone deprivation may down-regulate the Cx-43 mRNA expression; however, it doesn't alter miR-1 and miR-206 levels. These results suggest that ADT-induced hypogonadism may put males at risk for cardiac dysfunctions.

***Keywords*:** Connexin-43, miR-206, miR-1, Heart, Testosterone, Androgen deprivation therapy

Introduction

Intercellular gap junction proteins form a membrane-spanning channel allowing a forthright intercellular passage of small molecules and inorganic ions between cells; this then leads to electrical and metabolic coupling between two adjacent cells, regulating the ionic conduction and metabolic coupling between cells (Kamal et al., 2020). In cardiac tissue, gap junctions are involved in the formation of cell-to-cell communication pathways, helping propagation a wave of electrical stimulation between myocytes; this leads to the synchronous contraction of atria and ventricles (Kurtenbach et al., 2014). Also, they provide the fast exchange of ions and small molecules such as ATP, glutathione, cAMP, IP3, and glucose between myocytes (Michela et al., 2015). In cardiomyocytes, connexin-43 (Cx-43) is the most abundant isoform of gap junction channels (Jansen et al., 2010). New findings indicate that the canonical muscle-specific miRNAs (myomiRs) miR-1, -133, and -206 are involved in the development of skeletal and cardiac muscles and their health maintenance. They can down-regulate the targeted mRNA to degrade or inhibit translation. They also regulate the members of different cell signaling pathways in the muscle cells. Therefore, they play important role in myogenesis, muscle development, and muscle remodeling (Liu and Olson, 2010; McCarthy, 2011; Mitchelson and Qin, 2015). MiR-1, together with a few other miRs, serve a significant role in the development of embryonic stem cells and cardiomyocyte progenitor cells; it also plays important role in the expression of some cardiac transcription factors; as a result, it can change cardiac function (Kura et al., 2020). In normal cellular conditions, both miR-1/ -206 help myogenic differentiation and homeostasis (Mitchelson and Qin, 2015).

In vitro reports have shown that overexpression of miR-206 could reduce apoptosis of cardiomyocytes, and down-regulation of miR-206 could raise apoptosis of these cells(Yan et al., 2020).

* Corresponding author's e-mail address: *ghowsi.mahnaz@razi.ac.ir*

Recent findings on the irregular expression and functional significance of miR-1 have shown that miR-1 is dysregulated in some types of cardiac diseases, particularly arrhythmia and heart failure (Duan et al., 2014). There are two binding sites for the expression miR-206 and miR-1 in the 3′-untranslated region of Cx-43 mRNA; their activity is necessary for the down-regulation of Cx-43 (Oyamada et al., 2013). MiRs-1 and -206 have similar mature sequences, and their seed sequences are precisely identical. In addition, to sharing some common target genes, they have some independent target genes (Mitchelson and Qin, 2015).

The increased or decreased concentrations of androgen both raise the risk of heart failure. In this regard, testosterone abuse in athletes can significantly elevate the possibility of unexpected heart failure (Huang et al., 2016). The influence on the contractile function of the myocardium, endothelial function, and alterations in skeletal muscles are among the suggested mechanisms by which androgen may affect cardiac function (Huang et al., 2016; Malkin et al., 2009). On the other hand, various studies conducted on the men with prostate cancer who had received androgen deprivation therapy (ADT) indicated that the risk of developing heart failure and cardiovascular mortality in these subjects was high. They have concluded that androgen deprivation might promote heart failure (Keating et al., 2006; Shahani et al., 2008). Besides, there is some evidence showing that the down-regulation of Cx-43 protein is associated with arrhythmia, dilated cardiomyopathy, and heart failure (Chang et al., 2017). Thus, changes in Cx-43 expression and its distribution may be involved in developing heart failure and heart dysfunctions. ADT is one treatment for inhibiting testosterone production in the testes, and although new drugs targeting androgen receptors have been developed for many years, ADT is the mainstay of treatment for prostate cancer (Mitsuzuka and Arai, 2018). To date, no studies have examined the effect of ADT-induced hypogonadism on the expression of Cx-43 in cardiac tissue. Therefore, in the present study, the effects of hypogonadism caused by orchiectomy on an animal model for ADT and testosterone replacement on the mRNA expression of Cx-43 were evaluated. Also, the expression of miR-1 and miR-206 as two critical factors involved in the regulation of Cx-43 protein expression were determined.

Materials and Methods

Experimental Animals

Twenty-one male *Wistar* rats (190–200 g) were maintained at an animal facility (Razi University, Kermanshah, Iran). All experimental protocols were approved by the Local Animal Care and Use Committee of Razi University, Kermanshah, Iran and they were according to the research guidelines on animal experimentation (Kermanshah, Iran, permit number: IR.RAZI.REC.1399.017). Rats were kept on a 12-h light/dark cycle with free access to standard pelletized rat food and tap water. The animals were randomly divided into three groups (n=7). These included: I) the normal control group with no treatment during ten weeks (group NC). II) the castrated group (group ORX-S, to eliminate circulating testosterone, testes of these animals were removed via bilateral orchiectomy surgery). The animals belonging to this group were subcutaneously injected with sesame oil every day for ten weeks. III) the castrated group received testosterone enanthate 25 mg/kg/day by the subcutaneous injection as testosterone replacement therapy for ten weeks (group ORX-T). The sesame oil was used as a solvent for testosterone. For orchiectomy, the animals were anesthetized and maintained using a combination of ketamine and xylazine. The skin of the scrotal region was shaved and washed using the sterile technique. The orchiectomy surgery was done using the scrotal approach technique (Foley, 2005).

At the end of treatments, the rats were anesthetized and the blood samples were collected from their hearts by cardiac puncture. Also, a sample from the left ventricular tissue was snap-frozen in liquid nitrogen and stored at –80◦C. The sera samples were separated from the collected blood, and the serum total testosterone contents were determined using an enzyme-linked immunoassay (ELISA) kit (Cusabio, Wuhan, China). Both the intra-assay coefficient of variation and the inter-assay coefficient of variation (CV) for the testosterone kit were < 15%.

The RNA Isolation and Real-time PCR Analysis of CX-43 mRNA, miR-1, and miR-206 Expression in the Ventricular Tissue

Approximately 50 mg of the ventricular tissue samples were homogenized in TRIzol reagent (Life Technologies, U.S.A.); the total RNA samples were isolated according to the manufacturer's instructions. Each of the total RNA samples was quantified using a Nanodrop.

Reverse transcription into cDNA was then performed using the cDNA synthesis kit (Fermentas, California, U.S.A.) according to the manufacturer's guidelines. To eliminate the genomic DNA, RNA was treated with DNaseI (RNase-free) (Aminsan, Tehran, Iran). 2 µl cDNA, 3 µl water, 6 µl 2 X SYBR Green Master mixes (SYBR premix Ex Taq TMII (Takara Holdings Inc., Kyoto, Japan), and primer pairs at five pmol concentrations were mixed in a final volume of 12 µl; the PCR reactions were done in triplicates by using the Corbett Research RG 3000 thermal cycler (CR CORBETT, Australia). The forward and reverse primers used for gene expressions were as follows: Cx-43 forward: 5′ TGTGATGAGGAAGGAAGAGAAG 3′, reverse: 5′ AGAGGATGGTGATGATGTAGGT 3′; Glyceraldehyde-3-phosphate dehydrogenase (GAPDH) forward: 5′ AAGTTCAACGGCACAGTCAAGG3′, reverse: 5′ CATACTCAGCACCAGCATCACC33′.

Reverse transcription and quantitative expression analyses of rno-miR-1(*Rattus norvegicus*-miR-1), miR-206, and the endogenous control U6 were performed using real-time PCR, as described previously (Kramer, 2011). The primer sequences used for stem-loop RT-PCR were as follows: the mir stem-loop RT primer 5′ GTCGTATCCAGTGCAGGGTCCGAGGTATTC GCACTGGATACGACNNNN 3′; miR-1 forward primer 5′TGCTTCGGCAGCACATATAC 3′; rno-miR-206 forward primer 5′-TGGAATGTAAAGAAGTAT-3′; Universal reverse primer 5′CCAGTGCAGGGTCCGAGGTA -3′; U6 forward primer 5′TGCTTCGGCAGCACATATAC 3′; U6 reverse primer AGGGGCCATGCTAATCTTCT3′. The primers were provided by Sinaclon (Tehran, Iran). The cycling condition was one cycle of 10 min 95°C, 40 cycles of 95°C for 10 s, and 60°C for 1 min.

To calculate the relative gene expression, the comparative CT method was applied (Schmittgen and Livak, 2008). The expression of Cx-43 was normalized to *Gapdh* gene; also, the expression of miR-1 and miR-206 were normalized to that of the U6 snRNA gene.

Statistical Analysis

Statistical analyses were carried out using SPSS, version 16. The level of significance for comparison was set at $P < 0.05$. To determine the differences between groups, the data were analyzed by ANOVA, which was followed by Tukey's test. Data are presented as means with a standard error of the mean (mean ± SEM). The GraphPad Prism 5 software was then applied for plotting the figures.

Results

Castration decreased the concentration of testosterone in the ORX-S group. In the ORX-T group, testosterone replacement could not restore the testosterone levels up to normal levels of the control rats (Figure 1a). The expression levels of Cx-43 in the ORX-S group (5.118e-006 ± 2.562e-006) were significantly lower than those of the control group (3.105e-005 ± 4.571e-006) (P = 0.001). These levels in the ORX-T group (2.009e-005 ± 3.815e-006) were similar to those of the control group (P = 0.138) (Figure 1b). Meanwhile, the expression levels of Cx-43 in the ORX-T group were higher than those of the ORX-S group (P = 0.038) (Figure 1b). The miR-1 expression levels were not, however, significantly different between control group (0.004998 ± 0.001207) and the ORX-S (0.002695 ± 0.001160) and ORX-T groups (0.005500 ± 0.002538) (P =0.634 and p = 0.978, respectively). The miR-1 levels in the ORX-T and ORX-S groups were similar (P = 0.515) (Figure 1c). The expression levels of miR-206 in the ORX-S (0.005034 ± 0.002442) and ORX-T groups (0.005484 ± 0.001900) were not significantly different from those of the control group (0.007303 ± 0.0006013) (P = 0.661 and p = 0.764, respectively). Meanwhile, the miR-206 levels in the ORX-T and ORX-S groups were similar (P = 0.983) (Figure 1d).

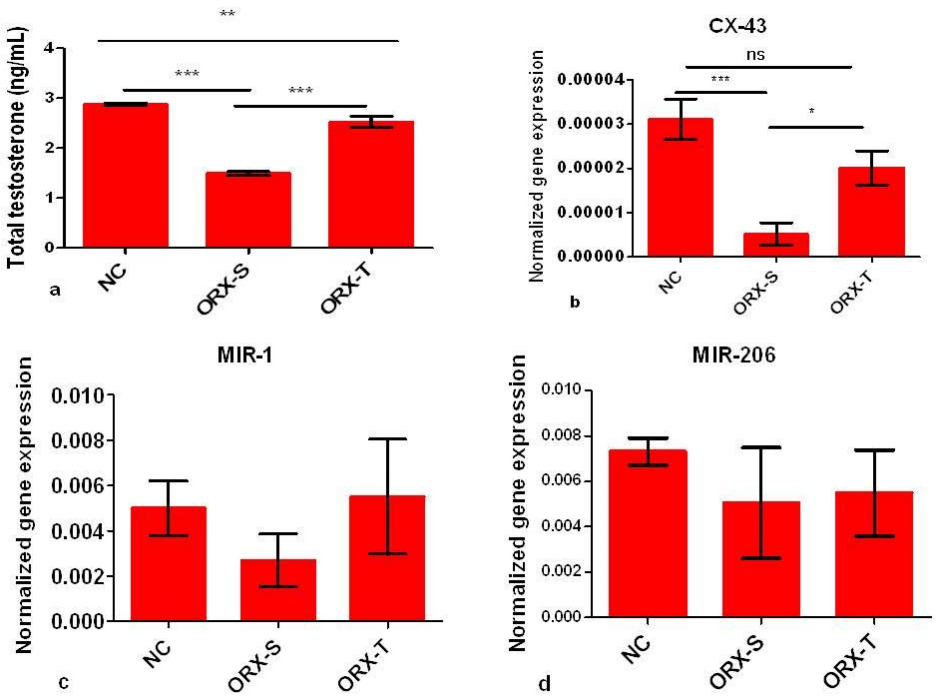

Figure 1. Total testosterone concentration (a); expression of CX-43 mRNA (b), miR-1 expression (c), and miR-206 expression (d) in the left ventricular tissue of rats. NC group, normal control rats; ORX-S group, Castrated rats; ORX-T group, castrated rats that received testosterone enanthate 25 mg/kg/day. Data are expressed as mean ± SEM; One-way ANOVA followed by Tukey's *post hoc* test. ***: $P < 0.001$;**: $P < 0.01$; *: $P < 0.05$. Abbreviations: CX-43, Connexin-43; miR-1, miRNA-1; miR-206, miRNA-206.

Discussion

In the present study, to investigate the effects of testosterone deficiency on the Cx-43 mRNA, miR-206, and miR-1 expression, a rat model of ADT, was established by following the orchiectomy surgery. Also, the expression of Cx-43, the most abundant connexin expressed in the adult working myocardium (Jansen et al., 2010), was evaluated. Our results showed the marked influence of testosterone deprivation on the expression of Cx-43; so, the expression of Cx-43 mRNA in the castrated rats was decreased in comparison to the controls. In line with our results, one study done by Zhang et al. (2016) reported that the alteration of testosterone could influence the expression of Cx-43 in Leydig cells (Zhang et al., 2016). Also, another study showed that excess androgen levels reduced Cx-43 expression and impaired the gap junction intercellular communication between human granulosa cells through androgen receptors (Wu et al., 2010). In the hormone-responsive tissues, the expression, modification, stability, and localization of connexin can be influenced by nuclear hormone receptors and their ligands (Firestone and Kapadia, 2012). In this regard, the current study showed that testosterone is involved in the expression of Cx-43 in heart. These findings were consistent with another study reporting that the treatment with flutamide, an androgen receptor blocker, changed Cx-43 expression in the pig's uterus (Wieciech et al., 2014). Animal and human studies also implicated that estrogen receptor subtypes (ERα and ERβ) and the progesterone receptor could regulate the functions of the gap junctions in the reproductive tissues through transcriptional or non-transcriptional mechanisms (Firestone and Kapadia, 2012). Considering the roles of connexin in the cell-cell interactions for carrying out different cellular and physiological processes, a disruption in the connexin expression can result in the malfunction of the intercellular communication and cardiac tissue, which may cause the onset of physiological disorders; because, it has been shown that the down-regulation of the major cardiac gap junction protein Cx-43 in many cases is associated with arrhythmia, dilated cardiomyopathy and heart failure (Chang et al., 2017). In the present study, the treatment of castrated rats with testosterone enanthate increased the Cx-43 mRNA expression. Consistent with our finding, the results of a previous study showed that the phosphorylated-Cx-43/ total-Cx-43 ratios were significantly reduced in the

castrated rats, and testosterone replacement increased this parameter in the cardiac ischemia-reperfusion injury (Pongkan et al., 2015). The pattern of alteration in the Cx-43 mRNA expression studied here suggests that the changes of serum testosterone levels may have noticeable effects on the Cx-43 expression in men. It has been reported that male hypogonadism or testosterone deficiency syndrome (TDS) is one of the frequent endocrine disorders among middle-aged to older men. Also, it has been estimated that the serum testosterone leve in nearly 37.8% of American males who are > 45 years old and visit a physician in the USA are < 300 ng/dL. Also, in men, ADT is associated with a marked decrease in testosterone levels (Xu et al., 2016). The impact of androgen imbalance was supposed to cause cardiovascular disorders (Pongkan et al., 2015) such as heart failure (Keating et al., 2006; Shahani et al., 2008). One study done by Pastor-Perez et al. showed that 28% deficiency of testosterone and less circulating testosterone concentrations in the body could be related to exercise capability in male patients with chronic heart failure (Manzano-Fernández et al., 2011). One study also reported that the arrhythmia score was significantly increased in the castrated rats, thus indicating the high susceptibility to arrhythmia and testosterone replacement markedly decreased the arrhythmia score (Pongkan et al., 2015).

Recently, some studies have shown that miRNAs play some roles in the regulation of connexin expression (Oyamada et al., 2013). MiR-1 is the most abundant miR in the adult mouse heart since embryonal development (Kura et al., 2020). It has also been revealed that the expression of MiR-1 is dysregulated during cardiac hypertrophy and heart failure (Duan et al., 2014). MiR-1, by affecting the expression of some cardiac transcription factors like myocardin, Nkx2.5, serum response factor (SRF), WNT and fibroblast growth factors (FGFs) signaling pathways, and targeting cyclin-dependent kinase-9 (Cdk9), histone deacetylase 4 (HDAC4), SRY-Box transcription factor 6 (Sox6), FZD7 (Frizzled-7) and FRS2 (fibroblast growth factor receptor substrate 2), can alter cardiac function (Kura et al., 2020). The activity of miR-1 is necessary for the down-regulation of Cx-43 (Oyamada et al., 2013). Yang et al. also showed that in the cultured myocytes, the treatment with miR-1 isolated from neonatal rats decreased Cx-43 (Anderson et al., 2006). Also, miR-206 was found to be an important factor in the regulation of Cx-43 expression, and it could negatively target Cx-43 (Anderson et al., 2006). Mature microRNAs have 22 nucleotides that can prevent the expression of the seed region of miRNA and 3′ untranslated regions of mRNA (Oyamada et al., 2013). In the normal rodent hearts, the miR-206 level is very low; during pathological conditions such as myocardial infarction, miR-206 is induced (Dong et al., 2009; Shan et al., 2009). One study on mice showed that down-regulation of both miR-133 and miR-1 was involved in cardiac hypertrophy in mice (Care et al., 2007). Also, in another study on hypertrophic rat cardiomyocytes, under both in vitro and in vivo conditions, it was shown that the down-regulation of miR-1 mediated the induction of pathologic cardiac hypertrophy (Curcio et al., 2013). MicroRNAs participated in the post-transcriptional regulation of gene expression (Huang et al., 2019).

It has also been shown that miR-1-2 by straight targeting Iroquois homeobox 5 (Irx5), which is a repressor of the potassium channel Kcnd2, could increase arrhythmias. Also, miR-1 is involved in regulating the Cx-43 expression and activity. miR-1 has remarkable effects on a range of ion channels, Ca^{2+}-handling, and contractile proteins. Also, miR-1 increases phosphorylation of L- type and ryanodine receptor 2 (RyR2) channels and enhances the immature Ca^{2+} transient amplitude and kineticsand the excitation-contraction coupling (Duan et al., 2014). Besides, it has been reported that in infarct rat hearts, the removal of miR-1 alleviates arrhythmogenesis (Yang et al., 2007).

KCNJ2 encodes the K^+ channel subunit Kir2.1, and GJA1 encodes Cx-43. Overexpression of miR-1 via post-transcriptionally repressing *KCNJ2* and *GJA1* makes slow conduction and depolarize the cytoplasmic membrane; the effects could be a cause for its arrhythmogenic potential (Duan et al., 2014). Although, there are response elements for testosterone in the promoter region of myomiRs (Nielsen et al., 2014), it seems that our hypothesis, that expression of miR-1, and miR-206 may be regulated in the cardiac tissue by the alteration of testosterone concentrations, was not true, as we observed that the relative expression of miR-206 and miR-1 in heart of rats did not change significantly by alterations in the testosterone concentration. Also, we found that the expression of miR-1 and miR-206 in the ventricular tissue of castrated rats receiving testosterone replacement was not affected, as compared to the controls. Our findings were by one study done by Oyamada (2013), showing that the ectopic expression of miR-206 decreased the expression of Cx-43 protein, but it didn't alter the expression of Cx-43 mRNA (Oyamada et al., 2013). In the present study, testosterone replacement with testosterone enanthate caused the up-regulation of

Cx-43 mRNA. Evidence obtained by in vitro and *ex vivo* studies has also shown that testosterone might have protective effects on the heart through androgen receptors (Pongkan et al., 2015).

To summarize, the current study delineated the effects of testosterone deprivation and the influence of testosterone replacement on the ventricular expression of Cx-43 mRNA and myomiRs miR-1 and miR-206 as two potential regulators of Cx-43 protein expression in the heart of rats.

Castration was associated with the down-regulation of the expression of Cx-43 mRNA in rats; however, it didn't affect miR-1 and miR-206. Our results, thus, suggest that an alteration in the Cx-43 mRNA expression may be a mechanism by which androgen deficiency may affect cardiac function.

If down-regulation of Cx-43 mRNA (induced by the low levels of circulating testosterone) contributed to cardiac function in male subjects for whom a significant decrease in serum testosterone levels was recorded, more research is needed to carefully monitor the cardiac function of the patients receiving ADT therapy. These results, suggest that ADT may put men at risk for heart dysfunction. Future clinical studies are, however, required to determine the effects of ADT on the cardiac tissue and function in ADT-recipient patients.

Conflicts of Interest

The authors declare no conflict of interest

References

Anderson C., Catoe H. and Werner R. (2006) MIR-206 regulates connexin43 expression during skeletal muscle development. Nucleic Acids Research 34: 5863-5871.

Care A., Catalucci D., Felicetti F., Bonci D., Addario A., Gallo P., et al. (2007) MicroRNA-133 controls cardiac hypertrophy. Nature Medicine 13: 613-618.

Chang K.-T., Cheng C.-F., King P.-C., Liu S.-Y. and Wang G.-S. (2017) CELF1 mediates connexin 43 mRNA degradation in dilated cardiomyopathy. Circulation Research 121: 1140-1152.

Curcio A., Torella D., Iaconetti C., Pasceri E., Sabatino J., Sorrentino S., et al. (2013) MicroRNA-1 downregulation increases connexin 43 displacement and induces ventricular tachyarrhythmias in rodent hypertrophic hearts. PloS One 8: e70158.

Dong S., Cheng Y., Yang J., Li J., Liu X., Wang X., et al. (2009) MicroRNA expression signature and the role of microRNA-21 in the early phase of acute myocardial infarction. Journal of Biological Chemistry 284: 29514-29525.

Lian D., Xiong X., Liu Y. and Wang J. (2014) miRNA-1: functional roles and dysregulation in heart disease. Molecular BioSystems 10: 2775-2782.

Firestone G. L. and Kapadia B.J. (2012) Minireview: regulation of gap junction dynamics by nuclear hormone receptors and their ligands. Molecular Endocrinology 26: 1798-1807.

Foley PL. (2005) common surgical procedures in rodents', laboratory animal medicine and management. office of animal research education and compliance, University of Virginia, Charlottesville, VA, USA: International Veterinary Information Service, Ithaca NY (www. ivis. org).

Huang C.-K., Lee S. O., Chang E., Pang H. and Chang C. (2016) Androgen receptor (AR) in cardiovascular diseases. The Journal of Endocrinology 229: R1.

Huang Y. M., Li W. W., Wu J., Han M. and Li B. H. (2019) The diagnostic value of circulating microRNAs in heart failure. Experimental and Therapeutic Medicine 17: 1985-2003.

Jansen J. A., van Veen T. A., de Bakker J. M. and van Rijen H. V. (2010) Cardiac connexins and impulse propagation. Journal of Molecular and Cellular Cardiology 48: 76-82.

Kamal D. A. M., Ibrahim S. F. and Mokhtar M. H. (2020) Effects of testosterone on the expression of Connexin 26 and Connexin 43 in the uterus of rats during early pregnancy. In Vivo 34: 1863-1870.

Keating N. L., O'Malley A. J. and Smith M. R. (2006) Diabetes and cardiovascular disease during androgen deprivation therapy for prostate cancer. Journal of clinical oncology 24: 4448-4456.

Kramer M. F. (2011) Stem-loop RT-qPCR for miRNAs. Current Protocols in Molecular Biology. 95: 15.10. 1-15.10. 15.

Kura B., Kalocayova B., Devaux Y. and Bartekova M. (2020) Potential clinical implications of miR-1 and miR-21 in heart disease and cardioprotection. International Journal of Molecular Sciences 21: 700.

Kurtenbach S., Kurtenbach S. and Zoidl G. (2014) Gap junction modulation and its implications for heart function. Frontiers in Physiology 5: 82.

Liu N. and Olson E. N. (2010) MicroRNA regulatory networks in cardiovascular development. Developmental Cell 18: 510-525.

Malkin C.J. and Channer K. (2009) Testosterone in chronic heart failure. Advances in the Management of Testosterone Deficiency 37: 183-196.

Manzano-Fernández S., Pastor-Pérez F. J., Barquero-Pérez Ó, Pascual-Figal DA, Goya-Esteban R, Rojo-Álvarez J. L., et al. (2011) Short-term variability of heart rate turbulence in chronic heart failure. Journal of Cardiac Failure 17: 735-741.

McCarthy J. J. (2011) The MyomiR network in skeletal muscle plasticity. Exercise and Sport Sciences Reviews 39: 150.

Michela P., Velia V., Aldo P. and Ada P. (2015) Role of connexin 43 in cardiovascular diseases. European Journal of Pharmacology 768: 71-76.

Mitchelson K. R. and Qin W.-Y. (2015) Roles of the canonical myomiRs miR-1,-133 and-206 in cell development and disease. World Journal of Biological Chemistry 6: 162.

Mitsuzuka K. and Arai Y. (2018) Metabolic changes in patients with prostate cancer during androgen deprivation therapy. International Journal of Urology 25: 45-53.

Nielsen S., Hvid T., Kelly M., Lindegaard B., Dethlefsen C., Winding K., et al. (2014) Muscle specific miRNAs are induced by testosterone and independently upregulated by age. Frontiers in Physiology 4: 394.

Oyamada M., Takebe K. and Oyamada Y. (2013) Regulation of connexin expression by transcription factors and epigenetic mechanisms. Biochimica et Biophysica Acta (BBA)-Biomembranes 1828: 118-133.

Pongkan W., Chattipakorn S. C. and Chattipakorn N. (2015) Chronic testosterone replacement exerts cardioprotection against cardiac ischemia-reperfusion injury by attenuating mitochondrial dysfunction in testosterone-deprived rats. PloS One 10: e0122503.

Schmittgen T. D. and Livak K.J. (2008) Analyzing real-time PCR data by the comparative CT method. Nature Protocols 3: 1101-1108.

Shahani S., Braga-Basaria M. and Basaria S. (2008) Androgen deprivation therapy in prostate cancer and metabolic risk for atherosclerosis. The Journal of Clinical Endocrinology & Metabolism 93: 2042-2049.

Shan Z.-X., Lin Q.-X., Fu Y.-H., Deng C.-Y., Zhou Z.-L., Zhu. J.-N., et al. (2009) Upregulated expression of miR-1/miR-206 in a rat model of myocardial infarction. Biochemical and Biophysical Research Communications 381: 597-601.

Wieciech I, Grzesiak M., Knapczyk-Stwora K., Pytlik A. and Słomczyńska M. (2014) Influence of the antiandrogen flutamide on connexin 43 (Cx43) gene and protein expression in the porcine placenta and uterus during pregnancy. Folia Biologica (Kraków) 62: 367-375.

Wu C.-H., Yang J.-G., Yang J-J., Lin Y.-M., Tsai H.-D., Lin C.-Y., et al. (2010) Androgen excess down-regulates connexin43 in a human granulosa cell line. Fertility and Sterility 94: 2938-2941.

Xu M., Hu C., Khan H.-h., Shi F.-h., Cong X.-d., Li Q., et al. (2016) Argirein alleviates stress-induced and diabetic hypogonadism in rats via normalizing testis endothelin receptor A and connexin 43. Acta Pharmacologica Sinica 37: 246-254.

Yan Y., Dang H., Zhang X., Wang, X., and Liu, X. (2020) The protective role of MiR-206 in regulating cardiomyocytes apoptosis induced by ischemic injury by targeting PTP1B. Bioscience Reports 40: BSR20191000.

Yang B., Lin H., Xiao J., Lu Y., Luo X., Li B., et al. (2007) The muscle-specific microRNA miR-1 regulates cardiac arrhythmogenic potential by targeting GJA1 and KCNJ2. Nature Medicine 13: 486-491.

Zhang J., Jin S., Zhao J. and Li H. (2016) Effect of dibutyl phthalate on expression of connexin 43 and testosterone production of leydig cells in adult rats. Environmental Toxicology and Pharmacology 47: 131-135.

Journal of Cell and Molecular Research (2021) 13 (1), 72-80 DOI: 10.22067/JCMR.2021.71513.1012

Review / Mini-Review

Understanding the Effect of Natural Products on Breast Cancer via P53-MDM 2 Signal Pathway

Zahra Ghavidel, Madjid Momeni Moghaddam*, Toktam Hajjar, Eisa Kohan-Baghkheirati

Department of Biology, Faculty of Sciences, Hakim Sabzevari University, Iran

Received 17 July 2021 Accepted 14 September 2021

Abstract

The use of medicinal plants in the treatment of diseases has a long history dating back to the presence of humans on earth. Cancer has almost been an incurable disease, and among the various cancers, breast cancer is the most common type of cancer among women and imposes an enormous burden on patients. Although medical and surgical solutions have been proposed for the disease, it has not been successful enough to treat the disease in many patients. In recent years, more studies have been done on the effects of medicinal plants on breast cancer, and scientists are trying to find the exact mechanisms of action for these plants to find effective ways for controlling cancer cell growth. This article focuses on *P53* and *MDM2*, two very important genes involved in regulation of cell growth and proliferation both in cancer and normal tissue, and we also gathered the list of natural compounds targeting the MDM2-p53 pathway. Our results provide a list of plant families that can influence this pathway and have great potential in designing treatments against cancers that encompass deregulation of the MDM2-p53 pathway.

***Keywords*:** Breast Cancer, Herbal, MDM2, p53, Medicinal Plants

Introduction

Cancer is one of the leading causes of death worldwide, and WHO expects that by 2030, 25% of people worldwide will have at least one type of cancer(Parker, Tong et al. 1997). Breast cancer is the leading cause of cancer death among women worldwide(Key, Verkasalo et al. 2001). Lack of understanding of the basic mechanisms involved in the development and progression of breast cancer (recurrence, metastasis, and resistance to treatment) is one of the most important problems in the treatment and prevention of this disease. Genetic changes in human breast cancer are divided into two groups: gain of function mutations in proto-oncogenes, which promote cell growth, division, and loss of function mutations in tumor suppressor genes that normally prevent uncontrolled cell growth(Lee and Muller 2010). Mutations in known tumor suppressor genes such as *BRCA1* and *BRCA2*, *TP53*, *PTEN*, *ATM*, *CHK2*, *NBS1*, *RAD50*, *PALB2*, and *BRIP* are associated with inherited breast cancer. Pieces of Evidence suggest that the overexpression of oncogenes such as *MDM2*, *ERBB2*, *PI3KCA*, *MYC*, and *CCND1* play an important role in the progression of breast cancer (Lee, To et al. 1988, Lee and Muller 2010, Qin, Wang et al. 2015). The knowledge about oncogenes and tumor suppressors is helping to provide new insights for the development of anti-cancer treatments. Our main focus is to review the relationship between the *TP53*-MDM2 pathway and herbal treatment of cancer with an emphasis on breast cancer. At first, we describe the contribution of *TP53* and *MDM2* in cancer initiation and progression, and then we explain herbal medicines that can affect these two genes in breast cancer.

Herbal plants are primary medicines used for alleviating symptoms of various disorders. By meeting prerequisites such as controlled planting conditions, quality control, and supervision of professional herbal medicine specialists on prescriptions, medicinal plants are safe and non-toxic. Herbal medicines are used due to their antioxidant and anti-inflammatory properties, and they regulate the immune system and have the ability to induce anti-proliferative effects on cancer cells(McGrowder, Miller et al. 2020).

TP53

One of the most important factors in the development of breast cancer is the inactivation of *TP53* tumor suppressor gene, which leads to a lack of protein expression(Wang, Ma et al. 2011). It is well established that *P53* is the guardian of the

*Corresponding author's e-mail address:
m.momeni@hsu.ac.ir, *iranbioman@yahoo.com*

genome (Qin, Wang et al. 2015) and plays its role as a transcription factor that participates in cell cycle checkpoint control and apoptosis (Sjöström, Blomqvist et al. 2000). It modulates the expression of a large group of genes regulating cell cycle progression, cell death, metabolic homeostasis, genomic integrity, differentiation, *etc*. (Brekman, Singh et al. 2011). Rare germline mutations of *TP53* gene lead to Li-Fraumeni familial cancer syndrome. On the other hand, somatic mutations of *TP53* occur in the majority of sporadic cases of cancers (Lane 1992). MDM2 and MDMX are the most important regulators of p53 (de Oca Luna, Wagner et al. 1995). MDM2 heterodimerization with its homologous MDMX protein increases ubiquitination and p53 degradation. Unlike MDM2, MDMX does not degrade p53 but reduces its transcriptional activity by binding to this protein (de Oca Luna, Wagner et al. 1995). In normal cells, the wild type of p53 is in the standby mode, and it is maintained at low concentration via inhibition of MDM2 protein (Brown, Lain et al. 2009). Under stressful conditions such as DNA damage, post-translational changes in MDM2 lead to dissociating of this protein from p53 and its activation. This process prevents abnormal cell proliferation (G1 or G2 arrest or apoptosis) (Sjöström, Blomqvist et al. 2000, Brown, Lain et al. 2009, Raza, Ohm et al. 2015). Wild-type p53 breast tumors often have high levels of the MDM2 protein, indicating an inhibitory function of MDM2 on p53 (Brekman, Singh et al. 2011). Inactivation of p53, in addition to tumorigenesis and cancer progression, increases resistance to common standard treatments available for breast cancer (Park, Woo et al. 2016). While mutations in the *TP53* gene are prevalent in all types of cancer, in the breast cancer occurs in only in 20% of the cases (Brekman, Singh et al. 2011). It has been shown that the most cancer-related alterations in *TP53* are missense mutations in the DNA binding domain of the protein (Xu 2008). Loss of p53 in the breast cancer stem cells (CSCs) leads to asymmetric cell division that leads to maintenance of the CSC population (Cicalese, Bonizzi et al. 2009). Nowadays, editing DNA repair pathways, inhibiting CSCs, and also reactivating of p53 are applied for cancer treatment(Lee and Muller 2010).

MDM2

MDM2 protein consists of 489 amino acids that contain a binding domain for the protein (Saji, Nakashima et al. 1999). This oncogene is involved in breast cancer, and its major oncogenic activity is established through inhibition of p53 and, as a result, cell apoptosis (Li, Liu et al. 2015). *MDM2* amplification is uncommon in breast cancers, but its mRNA and, or protein level is upregulated in about 40% of breast cancer samples (Saji, Nakashima et al. 1999). The *MDM2* gene was first identified as a highly amplified gene on double minute chromosomes (McCann, Kirley et al. 1995). It inactivates p53 in two ways: protein degradation via the polyubiquitin-proteasome pathway (or mono-ubiquitination: inhibition of transcription activity) or direct blockage of the activation domain of p53 (de Oca Luna, Wagner et al. 1995, Park, Woo et al. 2016). These two proteins build a negative-feedback loop, in which p53 induces the expression of MDM2, but MDM2 enhances the degradation of p53. MDM2 has interaction with many other molecules such as retinoblastoma protein (pRB), E2F (transcription factor), ribosomal protein (L5), cell fate regulator (Numb), and cell cycle inhibitor p19 (Xiong, Li et al. 2017). MDM2 responses to a variety of carcinogenic and tumor inhibitory pathways, which are regulated at the transcriptional level. *In vitro* study suggests that MDM2 expression causes breast cancer cells to proliferate and inhibit apoptosis, and *in vivo* experiments on mice showed that high expression of *MDM2* gene causes the development of breast cancer (Li, Liu et al. 2015).

The MDM2–p53 feedback loop

Transcription of *MDM2* is controlled by two distinct promoters including, P1 and P2. Reports suggest that the p53 protein acts as a transcription factor that can regulate *MDM2* gene through P2 promoter (Li, Liu et al. 2015). MDM2 and p53 form a compact complex that ubiquitinates P53via E3 ligase, resulting in recognition of p53 by proteasome and degradation (Qin, Wang et al. 2017). MDM2 could probably bind to the activation domain of p53 and inhibit its transcriptional activity (Saji, Nakashima et al. 1999). MDM2 also enhances the interaction of PIASy (a nuclear matrix-associated SUMO E3 ligase) with p53 and activates its nuclear export, and finally, it inhibits the binding of p53 to transcriptional coactivators and reduces expression of downstream target genes, including *MDM2*. The MDM2-p53 feedback loop is important for controlling p53 levels in normal cells because high levels of p53 expression inhibit normal cell growth and differentiationMdm4 can bind to the transactivation domain of p53 and inhibit its transcriptional activity by inhibiting its interaction

with components of the transcriptional machinery (Chandler, Singh et al. 2006, Brekman, Singh et al. 2011, Li, Liu et al. 2015). In total, overexpression of *MDM2* and *MDM4* is normal in more than 25% of breast cancer cases(Wang and Yan 2011). The upregulation of MDM2 and MDM4 genes or aberrant expression of their regulators, including Wip1, Akt, and ATM promote inhibition of p53 in breast cancer cells (de Oca Luna, Wagner et al. 1995). In vivo studies have shown that small molecules (such as RITA, Nutlin-3a MI-219) can disrupt the MDM2-p53 interaction and activate p53, leading to tumor regression (Vassilev, Vu et al. 2004, Shangary, Qin et al. 2008, Wang and Yan 2011, Vu, Wovkulich et al. 2013).

MDM2-p53 signal pathway: a promising therapeutic target for breast cancer

Targeting the MDM2-p53 pathway can be an effective strategy for breast cancer prevention and treatment. Here we collected the studies on natural compounds that affect the p53-MDM2 pathway in breast cancer (the detailed data is shown in **Error! Reference source not found.**). These compounds were inhibiting the expression of *MDM2*, and the interaction of P53 with this gene, and as a result, p53 would be activated. In previous studies, curcumin was effective in blocking progress of breast cancer by up-regulating pro-apoptotic genes such as *TP53* and *BAX* and down-regulating anti-apoptotic genes like *MDM2* and *BCL2* (Talib, Al-Hadid et al. 2018). Qin et al. showed that in breast cancer cell lines and also in cancer tissues, NFAT1 activates MDM2 independent of p53, and it was considered as a new target for the development of anticancer drugs. (Li, Zhang et al. 2005). Another study looked at the function of MDM2 in the proliferation of estrogen-induced breast cancer cells, which could be targeted for treatment (Brekman, Singh et al. 2011). It was shown that tumors with normal p53 and deregulation of MDM2 are more responsive to MDM2. (Tovar, Rosinski et al. 2006, Shangary and Wang 2009, Wiley, Schaum et al. 2018). The alternatively spliced forms of *MDM2* gene without the p53 binding domain were reported among cancer patients (Evans, Viswanathan et al. 2001). Pellegrino et al. developed a peptide that targets the heterodimeric interaction of MDM2 and MDM4 to prevent the inhibition of p53 in cancer cells (Evans, Viswanathan et al. 2001).

Natural products that target the MDM2-p53 pathway

Up to now, many studies have shown that secondary metabolites or active compounds of medicinal plants have anti-cancer effects (Syed Najmuddin, Romli et al. 2016). Natural plant compounds such as flavonoids, alkaloids, terpenoids, coumarins are known for their antioxidant and anti-inflammatory properties. They activate lymphocytes and regulate the immune system. (Baraya, Wong et al. 2017). In Sub-Saharan Africa, the leaves and roots of *Vernonia amygdalina* (bitter leaf) are used traditionally to improve digestion, reduce fever, and protect against intestinal parasites and nematodes.

The extract of *Pfaffia paniculate*, used for stress reduction in traditional medicine, has an anti-cancer effect on MCF-7 cell line. (Nagamine, da Silva et al. 2009). The presence of naturally occurring compounds such as curcumin, genistein, lycopene, shikonin, sulforaphane in herbal medicines is effective in priventing of breast cancer (Mitra and Dash 2018). Phytochemical studies on *Falcaria vulgaris* have shown that it contains tannins, saponins, vitamin C, and phytosterols (Soudamani, Yuvaraj et al. 2005, Khazaei, Yadegari et al. 2006) and various compounds such as antioxidants, anti-microbial compounds (Choobkar, Kakoolaki et al. 2017). In another study, the results of HPLC analysis showed that the antioxidant and anti-microbial compounds *F. vulgaris* has the highest concentrations of carvacrol and fumaric acid at 119 mg/kg and 966 mg/kg plant weight, respectively (Shafaghat 2010, Salahshoor, Mohammadi et al. 2018). Samadi et al. mentioned that *Falcaria vulgaris* effectively reduces the growth of breast tumor cells in vivo and in vitro.

Cinnamomum verum and reduced the volume of 4T1 tumors by 44%, and *Thymus vulgaris* can reduce tumor volume in mouse models (Kubatka, Uramova et al. 2019, Kubatka, Kello et al. 2020). Application of Tetrandrine could also reduce tumor size significantly (Wang, Yang et al. 2020).

Kubatka et al. reported an anti-cancer effect of *Rhus coriaria* on breast cancer in 4T1 cell line and in vivo. Studying tumor tissues extracted from the mouse model showed the anti-cancer effect of *Rhus coriaria* depends on the tissue type and dose. Higher doses of sumac significantly reduced the volume of 4T1 tumors by about 27%. The results showed a dose-dependent decrease in mitotic activity index in the treated groups compared with cancer samples (36.5% and 51%) (Kubatka, Kello et al. 2020).

TP53 is an important tumor suppressor gene that regulates various stress signals by regulating specific cellular responses (such as cell cycle arrest, cellular aging, apoptosis, Bcl-2, and p53, *etc*.) (Bellazzo, Sicari et al. 2018). Examining *TP53* gene expression in different degrees of breast cancer by real-time PCR showed abnormal expression of the *TP53* gene at almost all stages of many types of breast cancer in samples with deregulation of this gene.

Phoenix dactylifera L. extract has been reported to inhibit breast adenocarcinoma cells by inducing apoptosis and stopping the cell cycle. The expression levels of Bax, Bcl-2, and p53 were analyzed using flow cytometry. A dose-dependent increase in p53 and Bax expression was observed in MCF7-treated cells compared with controls (more than 4-fold and 10-fold increase in cells treated with 15 and 20 mg/ml *Phoenix dactylifera L*. methanolic extract, compared with control)(Khan, Ahmed et al. 2016). MDM2 overexpression is associated with metastases and chemotherapy resistance (Cordon-Cardo, Latres et al. 1994).

Gossypol (a natural phenol compound) could also reduce the expression level of *MDM2* and *VEGF* in breast cancer cells (Xiong, Li et al. 2017). Another study showed that proliferation, migration, and invasion of negative triple breast cancer cells were suppressed by berbamine through a reduction in *MDM2* and induction of *TP53* (Liu, Yan et al. 2021).

The crude extract of *Annona muricata* has anticancer properties and reduces the size and weight of the tumorvia induction of apoptosis (Najmuddin, Romli et al. 2016). In another study, treatment of breast cancer cells with *Astragalus membranaceus* extract at doses of 25 and 50 µg / ml increased the rate of apoptosis compared to the control group (Zhou, Chen et al. 2018). Lang et al., applied *Artemisia annua* extract, which showed strong anticancer activity against triple-negative breast cancer (Lang, Schmiech et al. 2020). Table1 shows a List of natural products that target the MDM2-p53 signal pathway.

Table 1. List of natural products that target MDM2-p53 pathway.

Natural compounds	in vitro study results	in vivo study results	Mechanism of action	References
Genistein	Inhibits cell proliferation, arrests cells at G2/M phase, and induces cell apoptosis	Inhibits tumor growth in PC3 xenograft model and sensitizes tumors to gemcitabine	Inhibits NFAT1-mediated MDM2 transcription and promotes MDM2 autoubiquitination and degradation	(Li, Zhang et al. 2005)
Ginsenosides and saponins 25-OCH3-PPD	Inhibits cell migration	Inhibits tumor growth in MCF7 and MDA-MB-469 xenograft models and inhibits lung metastasis in MDA-MB-231 metastatic model	Inhibits MDM2 transcription and promotes MDM2 ubiquitination and degradation	(Wang, Wang et al. 2008, Wang, Rayburn et al. 2009, Wang, Rayburn et al. 2009)
Diterpenes	Induces apoptosis through the mitochondrial pathway	Not reported	Regulates the expression of *P53* and *MDM2*	(Subash-Babu, Alshammari et al. 2017)
Melatonin	Not reported	Not reported	Inhibits transcription of *MDM2* and	(Proietti, Cucina et al. 2014)
Xanthones, naphthoquinones, and polyphenols Gambogic acid	Inhibits cell growth in MCF7 and H1299, arrests	Inhibits tumor growth in H1299 xenograft model	Inhibits transcription of *MDM2* and promotes ubiquitination	(Rong, Hu et al. 2009)

	cells at G2/M phase, and induces cell apoptosis		and degradation of *MDM2*	
Chalcone Derivatives (LQFM064)	Induces apoptosis	Not reported	Cell cycle arrest in G0 / G1 stage, induces expression of p53 and p21 Inhibits the interaction of MDM2 with p53	(Cabral, da Silva et al. 2017)
Gossypol	Induces apoptosis in MCF7 and MDA-MB-468	Suppresses the tumor growth in MCF7 and MDA-MB-468 xenograft models	Inhibits binding of MDM2 to VEGF and induces MDM2 self-ubiquitination and protein degradation	(Xiong, Li et al. 2017)
Japonicone A	Inhibits cell growth, proliferation, and colony formation Induces cell cycle arrest at G2/M phase and apoptosis	Inhibits tumor growth in MCF7 and MDA-MB-231 xenograft models	Inhibits NFAT1-mediated *MDM2* transcription and promotes MDM2 ubiquitination and degradation	(Qin, Wang et al. 2015, Qin, Wang et al. 2015)
Parthenolide	Not reported	Not reported	Induces MDM2 ubiquitination and proteasomal degradation, activating p53 and other MDM2-regulated tumor suppressors	(Gopal, Chanchorn et al. 2009)
Inulanolide A	Inhibits cell growth proliferation, and colony formation, induces cell cycle arrest at G2/M phase and apoptosis, and prevents cell migration and invasion, regardless of p53	Inhibits tumor growth in MDAMB-231 orthotopic model	Inhibits NFAT1-mediated MDM2 transcription and promotes MDM2 ubiquitination and degradation	(Qin, Wang et al. 2016)
Berberine	Not reported	Not reported	induces transcription of *TP53* and inhibits its degradation	(Kim, Han et al. 2012)
Tricetin	Inhibits MCF7 cell growth and colony formation, and induces cell cycle arrest at G2/M phase and apoptosis	Not reported	Inhibits MDM2-p53 binding and induces p53 phosphorylation at Ser15 and Ser392	(Hsu, Uen et al. 2009))
Lineariifolianoid A	Inhibits cell growth (IC50 Z 4.4 e9.1 mM), proliferation, and colony formation, induces cell	Not reported	Inhibits NFAT1-mediated MDM2 transcription and promotes MDM2 ubiquitination and	(Qin, Sarkar et al. 2016)

	cycle arrest at G2/M phase and apoptosis, and prevents cell migration and invasion, regardless of p53		degradation	
Triptolide	Inhibition of proliferation, induction of apoptosis, and G1 phase cell cycle arrest.	Inhibition of tumor growth	Regulates Akt activation via MDM2 / REST pathway	(Xiong, Su et al. 2016)

Conclusion

The MDMX-p53 pathway plays a vital role in suppressing tumors in human cancers (Brekman, Singh et al. 2011). The interaction between *TP53* tumor suppressor gene and its negative regulator MDM2 has been under investigation for nearly a decade since the discovery of chemotherapeutic drugs (Klein and Vassilev 2004). Accordingly, in various studies, re-expression of *TP53* by inhibiting MDM2 or MDM4 has been considered an appropriate strategy for the treatment of at least some types of breast cancer with deregulation of this pathway (Wang and Yan 2011, Zawacka-Pankau and Selivanova 2015, Gupta, Shah et al. 2019, Portman, Milioli et al. 2020). Increasingly there has been a broad consensus that these two genes might be used as an important target for drug development. Herbal medicines with an influence on the MDM2-p53 pathway have the potential for designing treatments against many cancer types, including breast tumors.

References

Baraya. Y. S., K. K. Wong and N. S. Yaacob (2017). The Immunomodulatory Potential of Selected Bioactive Plant-Based Compounds in Breast Cancer: A Review. Anticancer Agents Med Chem 17(6): 770-783.

Bellazzo. A., D. Sicari, E. Valentino, G. Del Sal and L. Collavin (2018). Complexes formed by mutant p53 and their roles in breast cancer. Breast Cancer (Dove Med Press) 10: 101-112.

Brekman. A., K. E. Singh, A. Polotskaia, N. Kundu and J. Bargonetti (2011). A p53-independent role of Mdm2 in estrogen-mediated activation of breast cancer cell proliferation. Breast Cancer Research 13(1): 1-14.

Brown. C. J., S. Lain, C. S. Verma, A. R. Fersht and D. P. Lane (2009). Awakening guardian angels: drugging the p53 pathway. Nature Reviews Cancer 9(12): 862-873.

Cabral. B. L. S., A. C. G. da Silva, R. I. de Avila, A. P. Cortez, R. M. Luzin, et al. (2017). A novel chalcone derivative, LQFM064, induces breast cancer cells death via p53, p21, KIT and PDGFRA. European Journal of Pharmaceutical Sciences 107: 1-15.

Chandler. D. S., R. K. Singh, L. C. Caldwell, J. L. Bitler and G. Lozano (2006). Genotoxic stress induces coordinately regulated alternative splicing of the p53 modulators MDM2 and MDM4. Cancer research 66(19): 9502-9508.

Choobkar. N., S. Kakoolaki and F. Mohammadi (2017). The biological effects of herbal medicine, Falcaria vulgaris: An article review. Iranian Journal of Aquatic Animal Health 3(1): 74-81.

Cicalese. A., G. Bonizzi, C. E. Pasi, M. Faretta, S. Ronzoni, B. Giulini, et al. (2009). The tumor suppressor p53 regulates polarity of self-renewing divisions in mammary stem cells. Cell 138(6): 1083-1095.

Cordon-Cardo. C., E. Latres, M. Drobnjak, M. R. Oliva, D. Pollack, J. M. Woodruff, et al. (1994). Molecular abnormalities of mdm2 and p53 genes in adult soft tissue sarcomas. Cancer research 54(3): 794-799.

de Oca Luna. R. M., D. S. Wagner and G. Lozano (1995). Rescue of early embryonic lethality in mdm2-deficient mice by deletion of p53. Nature 378(6553): 203-206.

Evans. S. C., M. Viswanathan, J. D. Grier, M. Narayana, A. K. El-Naggar and G. Lozano (2001). An alternatively spliced HDM2 product increases

p53 activity by inhibiting HDM2. Oncogene 20(30): 4041-4049.

Gopal. Y. V., E. Chanchorn and M. W. Van Dyke (2009). Parthenolide promotes the ubiquitination of MDM2 and activates p53 cellular functions. Molecular cancer therapeutics 8(3): 552-562.

Gupta. A., K. Shah, M. J. Oza and T. Behl (2019). Reactivation of p53 gene by MDM2 inhibitors: A novel therapy for cancer treatment. Biomedicine & Pharmacotherapy 109: 484-492.

Hsu. Y.-L., Y.-H. Uen, Y. Chen, H.-L. Liang and P.-L. Kuo (2009). Tricetin, a dietary flavonoid, inhibits proliferation of human breast adenocarcinoma mcf-7 cells by blocking cell cycle progression and inducing apoptosis. Journal of agricultural and food chemistry 57(18): 8688-8695.

Key. T. J., P. K. Verkasalo and E. Banks (2001). Epidemiology of breast cancer. The lancet oncology 2(3): 133-140.

Khan. F., F. Ahmed, P. N. Pushparaj, A. Abuzenadah, T. Kumosani, E. Barbour, et al. (2016). Ajwa Date (Phoenix dactylifera L.) Extract Inhibits Human Breast Adenocarcinoma (MCF7) Cells In Vitro by Inducing Apoptosis and Cell Cycle Arrest. PLoS One 11(7): e0158963.

Khazaei. M., M. Yadegari and R. Ghorbani (2006). SURVEY OF PROTECTIVE EFFECT OF HYDRO ALCOHOLIC EXTRACT OF FALCARIA VULGARIS ON ASPIRIN-INDUCED GASTRIC ULCER IN RAT.

Kim. S., J. Han, N.-Y. Kim, S. K. Lee, D. H. Cho, M.-Y. Choi, et al. (2012). Effect of berberine on p53 expression by TPA in breast cancer cells. Oncology reports 27(1): 210-215.

Klei. C. and L. Vassilev (2004). Targeting the p53–MDM2 interaction to treat cancer. British journal of cancer 91(8): 1415-1419.

Kubatka. P., M. Kello, K. Kajo, M. Samec, K. Jasek, D. Vybohova, et al. (2020). Chemopreventive and Therapeutic Efficacy of Cinnamomum zeylanicum L. Bark in Experimental Breast Carcinoma: Mechanistic In Vivo and In Vitro Analyses. Molecules 25(6).

Kubatka. P., M. Kello, K. Kajo, M. Samec, A. Liskova, K. Jasek, et al. (2020). Rhus coriaria L. (Sumac) Demonstrates Oncostatic Activity in the Therapeutic and Preventive Model of Breast Carcinoma. Int J Mol Sci 22(1).

Kubatka. P., S. Uramova, M. Kello, K. Kajo, M. Samec, K. Jasek, et al. (2019). Anticancer Activities of Thymus vulgaris L. in Experimental Breast Carcinoma in Vivo and in Vitro. Int J Mol Sci 20(7).

Lane. D. P. (1992). p53, guardian of the genome. Nature 358(6381): 15-16.

Lang. S. J., M. Schmiech, S. Hafner, C. Paetz, K. Werner, M. El Gaafary, et al. (2020). Chrysosplenol d, a Flavonol from Artemisia annua, Induces ERK1/2-Mediated Apoptosis in Triple Negative Human Breast Cancer Cells. Int J Mol Sci 21(11).

Lee. E., H. To, J.-Y. Shew, R. Bookstein, P. Scully and W.-H. Lee (1988). Inactivation of the retinoblastoma susceptibility gene in human breast cancers. Science 241(4862): 218-221.

Lee. E. Y. and W. J. Muller (2010). Oncogenes and tumor suppressor genes. Cold Spring Harbor perspectives in biology 2(10): a003236.

Li. H., Q. Liu, Z. Wang, R. Fang, Y. Shen, X. Cai, Y. Gao, Y. Li, et al. (2015). The oncoprotein HBXIP modulates the feedback loop of MDM2/p53 to enhance the growth of breast cancer. Journal of Biological Chemistry 290(37): 22649-22661.

Li. M., Z. Zhang, D. L. Hill, X. Chen, H. Wang and R. Zhang (2005). Genistein, a dietary isoflavone, down-regulates the MDM2 oncogene at both transcriptional and posttranslational levels. Cancer Research 65(18): 8200-8208.

Liu. L., J. Yan, Y. Cao, Y. Yan, X. Shen, B. Yu, et al. (2021). Proliferation, migration and invasion of triple negative breast cancer cells are suppressed by berbamine via the PI3K/Akt/MDM2/p53 and PI3K/Akt/mTOR signaling pathways. Oncol Lett 21(1): 70.

McCann. A., A. Kirley, D. Carney, N. Corbally, H. Magee, G. Keating et al. (1995). Amplification of the MDM 2 gene in human breast cancer and its association with MDM2 and p53 protein status. British journal of cancer 71(5): 981-985.

McGrowder. D. A., F. G. Miller, C. R. Nwokocha, M. S. Anderson, C. Wilson-Clarke, K. Vaz, et al. (2020). Medicinal Herbs Used in Traditional Management of Breast Cancer: Mechanisms of Action." Medicines 7(8): 47.

Mitra. S. and R. Dash (2018). Natural Products for the Management and Prevention of Breast Cancer. Evidence-based Complementary and Alternative Medicine 2018: 23.

Nagamine. M. K., T. C. da Silva, P. Matsuzaki, K. C. Pinello, B. Cogliati, C. R. Pizzo, et al. (2009). Cytotoxic effects of butanolic extract from Pfaffia paniculata (Brazilian Ginseng) on cultured human breast cancer cell line MCF-7. Experimental and toxicologic pathology 61(1): 75-82.

Najmuddin. S. U. F. S., M. F. Romli, M. Hamid, N. B. Alitheen and N. M. A. N. Abd Rahman (2016). Anti-cancer effect of Annona Muricata Linn Leaves Crude Extract (AMCE) on breast cancer cell line. BMC complementary and alternative medicine 16(1): 1-20.

Park. E. Y., Y. Woo, S. J. Kim, D. H. Kim, E. K. Lee, U. De, K. S. Kim, et al. (2016). Anticancer effects of a new SIRT inhibitor, MHY2256, against human breast cancer MCF-7 cells via regulation of MDM2-p53 binding. International journal of biological sciences 12(12): 1555.

Parker. S. L., T. Tong, S. Bolden and P. A. Wingo (1997). Cancer statistics, 1997. CA: A cancer journal for clinicians 47(1): 5-27.

Portman. N., H. H. Milioli, S. Alexandrou, R. Coulson, A. Yong, K. J. Fernandez, et al. (2020). MDM2 inhibition in combination with endocrine therapy and CDK4/6 inhibition for the treatment of ER-positive breast cancer. Breast Cancer Research 22(1): 1-17.

Proietti. S., A. Cucina, G. Dobrowolny, F. D'Anselmi, S. Dinicola, M. G. Masiello, et al. (2014). Melatonin down-regulates MDM 2 gene expression and enhances p53 acetylation in MCF-7 cells. Journal of pineal research 57(1): 120-129.

Qin. J.-J., S. Sarkar, S. Voruganti, R. Agarwal, W. Wang and R. Zhang (2016). Identification of lineariifolianoid A as a novel dual NFAT1 and MDM2 inhibitor for human cancer therapy. Journal of biomedical research 30(4): 322.

Qin. J.-J., W. Wang, S. Sarkar, S. Voruganti, R. Agarwal and R. Zhang (2016). Inulanolide A as a new dual inhibitor of NFAT1-MDM2 pathway for breast cancer therapy. Oncotarget 7(22): 32566.

Qin. J.-J., W. Wang, S. Voruganti, H. Wang, W.-D. Zhang and R. Zhang (2015). Identification of a new class of natural product MDM2 inhibitor: In vitro and in vivo anti-breast cancer activities and target validation. Oncotarget 6(5): 2623.

Qin. J.-J., W. Wang, S. Voruganti, H. Wang, W.-D. Zhang and R. Zhang (2015). Inhibiting NFAT1 for breast cancer therapy: new insights into the mechanism of action of MDM2 inhibitor JapA. Oncotarget 6(32): 33106.

Qin. J.-J., W. Wang and R. Zhang (2017). Experimental therapy of advanced breast cancer: targeting NFAT1–MDM2–p53 pathway. Progress in molecular biology and translational science 151: 195-216.

Raza. S., J. E. Ohm, A. Dhasarathy, J. Schommer, C. Roche, K. D. Hammer et al. (2015). The cholesterol metabolite 27-hydroxycholesterol regulates p53 activity and increases cell proliferation via MDM2 in breast cancer cells. Molecular and cellular biochemistry 410(1): 187-195.

Rong. J.-J., R. Hu, Q. Qi, H.-Y. Gu, Q. Zhao, J. Wang, et al. (2009). Gambogic acid down-regulates MDM2 oncogene and induces p21Waf1/CIP1 expression independent of p53. Cancer letters 284(1): 102-112.

Saji. S., S. Nakashima, S. i. Hayashi, M. Toi, S. Saji and Y. Nozawa (1999). Overexpression of MDM2 in MCF-7 promotes both growth advantage and p53 accumulation in response to estradiol. Japanese journal of cancer research 90(2): 210-218.

Salahshoor. M. R., M. M. Mohammadi, S. Roshankhah and C. Jalili (2018). Effect of Falcaria Vulgaris on Milk Production Parameters in Female Rats' Mammary Glands. J Family Reprod Health 12(4): 177-183.

Shafaghat. A. (2010). Free radical scavenging and antibacterial activities, and GC/MS analysis of essential oils from different parts of Falcaria vulgaris from two regions. Nat Prod Commun 5(6): 981-984.

Shangary. S., D. Qin, D. McEachern, M. Liu, R. S. Miller, S. Qiu, Z. Nikolovska-Coleska, et al. (2008). Temporal activation of p53 by a specific MDM2 inhibitor is selectively toxic to tumors and leads to complete tumor growth inhibition. Proceedings of the National Academy of Sciences 105(10): 3933-3938.

Shangary. S. and S. Wang (2009). Small-molecule inhibitors of the MDM2-p53 protein-protein interaction to reactivate p53 function: a novel approach for cancer therapy. Annual review of pharmacology and toxicology 49: 223-241.

Sjöström. J., C. Blomqvist, P. Heikkilä, K. Von Boguslawski, A. Räisänen-Sokolowski, N.-O. Bengtsson, I. Mjaaland, et al. (2000). Predictive value of p53, mdm-2, p21, and mib-1 for chemotherapy response in advanced breast cancer. Clinical cancer research 6(8): 3103-3110.

Soudamani. S., S. Yuvaraj, T. Malini and K. Balasubramanian (2005). Experimental diabetes has adverse effects on the differentiation of ventral prostate during sexual maturation of rats. Anat Rec A Discov Mol Cell Evol Biol 287(2): 1281-1289.

Subash-Babu. P., G. M. Alshammari, S. Ignacimuthu and A. A. Alshatwi (2017). Epoxy clerodane diterpene inhibits MCF-7 human breast cancer cell growth by regulating the expression of the functional apoptotic genes Cdkn2A, Rb1, mdm2 and p53. Biomedicine & Pharmacotherapy 87: 388-396.

Syed Najmuddin. S. U., M. F. Romli, M. Hamid, N. B. Alitheen and N. M. Nik Abd Rahman (2016). Anti-cancer effect of Annona Muricata Linn Leaves Crude Extract (AMCE) on breast cancer cell line. BMC Complement Altern Med 16(1): 311.

Talib. W. H., S. A. Al-Hadid, M. B. W. Ali, I. H. Al-Yasari and M. R. Abd Ali (2018). Role of curcumin in regulating p53 in breast cancer: An overview of the mechanism of action. Breast Cancer: Targets and Therapy 10: 207.

Tovar. C., J. Rosinski, Z. Filipovic, B. Higgins, K. Kolinsky, H. Hilton, et al. (2006). Small-molecule MDM2 antagonists reveal aberrant p53 signaling in cancer: implications for therapy. Proceedings of the National Academy of Sciences 103(6): 1888-1893.

Vassilev. L. T., B. T. Vu, B. Graves, D. Carvajal, F. Podlaski, Z. Filipovic, N. Kong, U. Kammlott, et al. (2004). In vivo activation of the p53 pathway by small-molecule antagonists of MDM2. Science 303(5659): 844-848.

Vu. B., P. Wovkulich, G. Pizzolato, A. Lovey, Q. Ding, N. Jiang, J.-J. Liu, et al. (2013). Discovery of RG7112: a small-molecule MDM2 inhibitor in clinical development. ACS medicinal chemistry letters 4(5): 466-469.

Wang. C. H., J. M. Yang, Y. B. Guo, J. Shen and X. H. Pei (2020). Anticancer Activity of Tetrandrine by Inducing Apoptosis in Human Breast Cancer Cell Line MDA-MB-231 In Vivo. Evid Based Complement Alternat Med 2020: 6823520.

Wang. H., X. Ma, S. Ren, J. K. Buolamwini and C. Yan (2011). A small-molecule inhibitor of MDMX activates p53 and induces apoptosis. Molecular cancer therapeutics 10(1): 69-79.

Wang. H. and C. Yan (2011). A small-molecule p53 activator induces apoptosis through inhibiting MDMX expression in breast cancer cells. Neoplasia 13(7): 611-IN616.

Wang. W., E. R. Rayburn, J. Hang, Y. Zhao, H. Wang and R. Zhang (2009). Anti-lung cancer effects of novel ginsenoside 25-OCH3-PPD. Lung Cancer 65(3): 306-311.

Wang. W., E. R. Rayburn, Y. Zhao, H. Wang and R. Zhang (2009). Novel ginsenosides 25-OH-PPD and 25-OCH3-PPD as experimental therapy for pancreatic cancer: anticancer activity and mechanisms of action. Cancer letters 278(2): 241-248.

Wang. W., H. Wang, E. Rayburn, Y. Zhao, D. Hill and R. Zhang (2008). 20 (S)-25-methoxyl-dammarane-3 β, 12 β, 20-triol, a novel natural product for prostate cancer therapy: activity in vitro and in vivo and mechanisms of action. British journal of cancer 98(4): 792-802.

Wiley. C. D., N. Schaum, F. Alimirah, J. A. Lopez-Dominguez, A. V. Orjalo, G. Scott, et al. (2018). Small-molecule MDM2 antagonists attenuate the senescence-associated secretory phenotype. Scientific reports 8(1): 1-9.

Xiong. J., J. Li, Q. Yang, J. Wang, T. Su and S. Zhou (2017). Gossypol has anti-cancer effects by dual-targeting MDM2 and VEGF in human breast cancer. Breast Cancer Research 19(1): 1-10.

Xiong. J., T. Su, Z. Qu, Q. Yang, Y. Wang, J. Li and S. Zhou (2016). Triptolide has anticancer and chemosensitization effects by down-regulating Akt activation through the MDM2/REST pathway in human breast cancer. Oncotarget 7(17): 23933.

Xu. Y. (2008). Induction of genetic instability by gain-of-function p53 cancer mutants. Oncogene 27(25): 3501-3507.

Zawacka-Pankau. J. and G. Selivanova (2015). Pharmacological reactivation of p53 as a strategy to treat cancer. Journal of internal medicine 277(2): 248-259.

Zhou. R., H. Chen, J. Chen, X. Chen, Y. Wen and L. Xu (2018). Extract from Astragalus membranaceus inhibit breast cancer cells proliferation via PI3K/AKT/mTOR signaling pathway. BMC complementary and alternative medicine 18(1): 1-8.

Journal of Cell and Molecular Research (2021) 13 (1), 81-91 DOI: 10.22067/jcmr.2021.70313.1006

Research Article

Isolation and Characterization of Lytic Bacteriophages Infecting *Escherichia coli* Antibiotic-Resistant Isolates from Urinary Tract Infections in North-west of Iran

Raheleh Majdani*

Department of Biology, Faculty of Basic Sciences, University of Maragheh, Maragheh, Iran

Received 8 May 2021 Accepted 15 August 2021

Abstract

One of the most prevalent bacterial infections, urinary tract infection (UTI), affects millions of people yearly worldwide. To control the increasing antibiotic-resistant infections, it is essential to introduce alternative approaches such as phage therapy. In this study, isolation, purification, and enrichment of eight lytic bacteriophages, which are active against antibiotic-resistant *Escherichia coli* strains from human urinary tract infections, were carried out. Molecular analysis of the bacteriophages was performed using two endonuclease enzymes (*Eco*RV and *Xba*I). Then, two of eight isolated bacteriophages with the highest host range were further characterized to determine their morphology, one-step growth, latent period, burst size, and stability under different environmental conditions. Allbacteriophage isolates (n=8) showed genome variation as it was evidenced by the enzyme digestion process (*Eco*RV). Both phages with the broadest host ranges (PEcMa2/17 and PEcMa3/17) showed an efficient lytic activity against five bacterial isolates. Electron microscopy confirmed that selected phages belong to S*iphoviridae* and *Myoviridae* families. The latent period of both propagated phages was determined as 15min. The burst size was estimated to be 100pfu/ml and 120pfu/ml in PEcMa2/17 and PEcMa3/17, respectively. Both phages showed more than 50% stability at 37ºC and lower investigated temperatures, and they were survived efficiently in pH=7. It was while their genome properties were different. The introduced bacteriophages showed high stability and strong antibacterial potential against *Escherichia coli* strains from UTIs. As candidates for phage therapy, more characterization steps, such as molecular analysis and experimental assays are needed before the therapeutic application.

***Keywords*:** Bacteriophage; Urinary tract infection; *Escherichia coli*; Antibiotic resistance; Phage therapy

Introduction

Urinary tract infection (UTI), as one of the most prevalent bacterial infections, affects millions of people yearly worldwide (Stamm and Norrby, 2001). Due to the notable role of UTIs in the morbidity of all aged adults, significant economic and public health problems have resulted. As a result of these problems, the quality of life in afflicted individuals is changing consequently (Flores-Mireles et al., 2015; Kostakioti et al., 2012). Some complex situations such as frequent recurrences and high-levels of antibiotic resistance are reported as severe challenges in UTIs (Flores-Mireles et al., 2015). The most common causative agent for uncomplicated and complicated UTIs is uropathogenic *Escherichia coli* (UPEC) (Flores-Mireles et al., 2015). Antibiotic resistance in uropathogenic bacteria such as *Escherichia coli* (*E.coli*) could be explained as the major cause of community and nosocomially acquired UTIs. The incidence of multi- drug resistant strains of *E. coli*, especially those producing extended-spectrum beta-lactamases (ESBL) such as CTX-M-type enzymes, may cause more challenges for the prognosis of urinary tract infections (Pouillot et al., 2012).

Bacteriophages (phages), viruses that infect bacteria, are the most abundant entities on the earth. They are non-hazardous and self-replicating natural agents which increase in number with the lysis of their bacterial targets. Also, virulent phages could be effective agents in removing bacterial biofilms (Jassim., 2012). Phage therapy could be a more appropriate approach to treat urinary tract infections. Comparing with the last generation of antibiotics, using bacteriophages is not expensive, and it can be used with a catheter under the control of medical personnel several times a day. Also, systemic therapy is not required, and bacteriphages will be applied locally. The efficiency of phage therapy

* Corresponding author's e-mail address: *rahelehmajdani@yahoo.com*

combatting UTIs increases because of no physical and metabolic barriers in this kind of therapeutics, and also the occurrence of adverse effects will be reduced (Sybesma et al., 2016). Some previous studies also investigated the phage therapy potential to treat UTIs. The effect of oral and topical application of a phage cocktail was evaluated on patients with UTI. The study confirmed the lytic effects of phages on reducing the biofilms of uropathogenic *E.coli* (Chibeu et al., 2012). In addition, the effectiveness of commercial phages targeting an *E.coli* isolate from UTI patients was reported (Sybesma et al., 2016). Interestingly, the antibiotic resistance pattern of *E.coli* and its specific phages were variable in different regions (Tuem et al., 2018). Considering the advantages of phages over antibiotics, the lower rate of discovering effective antibiotics against antibiotic-resistant bacterial strains, and the high prevalence of UTIs, phages could be explained as a promising and highly potentiated alternative to antibiotics to control the urinary tract infections.

In this study, isolation, purification, and enrichment of eight lytic bacteriophages against antibiotic-resistant *E.coli* strains from human urinary tract infections were performed. Also, to suggest effective phages for phage therapy procedures of UTIs, their antibacterial efficacies and host ranges were determined. After analyzing the variety of genomes using endonuclease enzymes, two phages with thebroadest host ranges were selected for more characterizations as proper candidates for future phage therapy eperiments.

Materials and Methods

Bacterial strains and characterization

A number of 55 *E.coli* isolates of human urinary tract infections were obtained from clinical diagnostic centers in theEast Azerbaijan province of Iran between January- August 2017. Confirmation of all isolates as *E.coli* was performed in the microbiology laboratory of the University of Maragheh by applying biochemical standard tests (Quinn et al., 1994). Afterward, preservation and storage of *E. coli* isolates were done at the temperature of -20°C.

Antibiotic susceptibility and bacterial selection

Evaluation of antibiotics sensitivity of identified *E. coli* isolates was conducted using the disk diffusion method (Bauer et al., 1966). 13 different common antibiotic discs were applied in the present study, including nitrofurantoin (300 micrograms), tetracycline (30 micrograms), amoxicillin (25 micrograms), ciprofloxacin (5 micrograms), nalidixic acid (30 micrograms), trimethoprim/sulfamethoxazole (1.25/23.75 micrograms) gentamicin (10 micrograms), ceftriaxone (30 micrograms), amikacin (30 micrograms), ceftazidime (30 micrograms), cefpime (30 micrograms), cefotime), chloramphenicol (30 micrograms) (Padan Teb, Iran). *E coli* ATCC 25922 and *E.coli* ATCC 35218 were used as quality controls. According to the National Committee for Clinical Laboratory Standards (NCCLS) guidelines the isolates were reported as resistant, intermediate, or sensitive to different antibiotics . Finally, eight multi-drug resistant bacterial isolates were subjected to phage isolation assay, and stored at -20°C.

Isolation and purification of phages

Samples To isolate bacteriophages against eight multi-drug resistant human *E.coli* bacteria samples were collected from rivers and an urban sewage treatment center in Maragheh (The East Azerbaijan province, north-west of Iran). Samples were immediately transported to the microbiology laboratory of the University of Maragheh under cold conditions (4ºC). They were centrifuged and then filtered using a 0.45µm millipore membrane filter. Concentrated sterile trypticase soy broth (TSB) and antibiotic-resistant bacterial suspension (host-bacteria) were added to sterile water samples. After adding 1% $MgSO_4$ (v/w), the mixture was shaked (130rpm) overnight at 37ºC. Then, 3 ml chloroform was added, and the mixture was shaked for another 24h at 37ºC. After 2h at room temperature, it was centrifuged (25min, 1500*g*), and the supernatant was filtered with a 0.45µm membrane. Phage activity of the filtrate against 10 *E. coli* isolates was determined using the double-layer agar overlay technique (Adams, 1959) and the spot test (Chang et al., 2005). Purifying the isolated phages was performed according to the previous study (Jun et al., 2013). Moreover, single plaque isolation steps were repeated three times.

Titration and precipitation of bacteriophages

The double-layer agar overlay method was carried out to evaluate the titre of the bacteriophage suspensions (Adams, 1959). Also, 10X dilutions in TSB containing tubes were used, and the plates were incubated at 37°C for 24h. The bacteriophage titer of each solution is expressed as pfu/ml. One-step filtration of phages was done, and the solution was further concentrated and purified using polyethylene glycol (PEG) precipitation (Ahmadpour et al., 2016).

Determination of host range of bacteriophages

In this study, we used eight isolates of multi-drug-resistant *E. coli* originated from the human urinary tract infections. To determine the host range of the phages, spotting 10µl of phage suspension (10^9pfu/ml) was carried out onto the bacterial isolate lawn cultures. All tests were repeated three times. According to the host range, two isolated bacteriophages were suggested for effective phage therapy to combat antibiotic-resistant *E.coli* bacteria from human urinary tract infections (East Azerbaijan, Iran). Then, characteristics of selected phages were further studied.

Morphological characterization of bacteriophages

Two selected phages with the highest host range were used for morphological examination via transmission electron microscopy (TEM) following the negative staining. Briefly, a drop of purified phages (10^{10}pfu/ml) was loaded on the surface of a formvar coated grid (copper grid size 200 mesh), and after staining with 2% uranyl-acetate, it was examined using a Zeiss Leo 906 TEM instrument operating at 100kV (Carl Zeiss Company, Germany).

The efficiency of bacteriophage adsorption

Bacteria were grown in the TSB medium at 37ºC and the OD was adjusted to 0.3 (Wavelenght 600nm). Samples were then centrifuged, and the resultant pelletswere washed with 1ml of 0.85% NaCl . Then, the pellet was re-suspended in 1.5ml of TSB medium, and incubated at 37ºC for 15min. Bacteriophages were added to the bacterial suspension with the lysate multiplicity of infection (MOI) of 0.1. Samples were withdrawn periodically through out the incubation time with 5min intervals to be titrated. The first sample collected immediately following the addition of the phage lysate to the bacterial suspension (zero time point) was considered as the reference with 100% of nonadsorbed phages.

One-step growth experiment

Determination of the latent period and burst size of selected phages (PEcMa2/17 and PEcMa3/17) was carried out using one-step growth curve experiment, as it was described previousely with some modifications (Pajunen et al., 2000). The bacteriophages at MOI of 0.01 were added to *E.coli* cultures (10^8pfu/ml). Then, the mixtures were incubated for 15min at 37ºC, which allows the bacteria to adsorb phages. After incubation, the mixture was centrifuged for one min at 4ºC to remove any nonabsorbed phages. Pellets were resuspended in the fresh TSB medium, and incubated at 37ºC. Then, the samples were obtained at 5-min intervals, and the phage titer (pfu/ml) was evaluated using the double-layer agar method, and one-step growth curves were plotted. All experiments were performed at least in triplicate.

Stability studies

The thermal stability of phages was tested in 10^9pfu/ml of phage lysate that was subjected to different temperatures, including -20, 4, 22, 37, 60, and 90˚C for 1 and 24h. After incubation in a temperature-controlled water bath, the phage activity was determined using the agar overlay method. Investigated pH ranges were from 3 to 11. To determine the stability the phage lysates were incubated at a pH-controlled environment for 1 and 24h. Also, the phages were exposed to U.V. radiation according to the method of Ramirez et al. (Ramirez et al., 2018). Briefly, phages were placed in sterile plates and irradiated for 15 and 30min with a U.V. lamp in a laminar flow cabinet (λ=254 nm) at a distance of 0.6m, and phage survival was calculated in each case. The stability results were represented as viability percentages at different pH ranges. All experiments were repeated in triplicates.

DNA extraction and enzymatic digestion

Isolated phage suspensions (n=8) were treated with DNase I (1U/µl; Jena Bioscience, Germany) and RNase A (5ug/µl; Jena Bioscience, Germany) to degrade bacterial nucleic acids, and the mixtures were incubated for 40min at 37ºC. After inactivation of the enzymes, purified phage genomic DNA was prepared using QIAamp DNA Mini Kit (Qiagene, Germany) with some modifications. Briefly, after mixing the solution with the lysis buffer, it was vortexed, and placed at 65ºC for 30min. Then, ethanol was added, and the resultant mixture was transferred to a particular column, and centrifuged. After twice washing, DNAs were eluted. In the next step, obtained genomic DNA solutions of bacteriophages were subjected to a round of nuclease treatment using *Xba*I (Jena Bioscience, Germany) and *Eco*RV (Jena Bioscience, Germany) enzymes according to the manufacturer's instructions. Fragments were visualized on 2% agarose gel using an ultraviolet transilluminator (ECX-20-M, Syngen, USA).

Results

Antibiotic sensitivity test

In the current study, 55 bacteria (from 63 samples) were confirmed as *E.coli* based on

standard biochemical tests. The antibiotic susceptibility test was conducted for all samples. According to the results, the highest antibiotic resistance rate among the isolates was related to amoxicillin (51.2%). 64.6% of bacteria were resistant to three or more investigated antibiotics, among which 18.2% of isolates showed resistance to five or more antibiotics.

Eight multi–drug (5 or more) resistant bacteria were selected as bacterial references to isolate bacteriophages which were active against these bacteria as the host cells. Obtained results, including the titre of bacteriophages are shown in Table 1.

Isolation of lytic bacteriophages

Table 1. Titration results obtained forphage isolates which are active against 8 multi-drug resistant *E.coli* isolates.

Phages	*E.coli* isolates (resistant to five or more antibiotics)	Phage titer (pfu/ml)
P1	Isolate 1	1.2×10^{8}
P2 (PEcMa2/17)	Isolate 2	3.2×10^{9}
P3	Isolate 3	10^{10}
P4	Isolate 4	1.8×10^{7}
P5	Isolate 5	5.6×10^{7}
P6	Isolate 6	1.1×10^{8}
P7	Isolate 7	2.8×10^{9}
P8 (PEcMa3/17)	Isolate 8	10^{8}

Based on the results, 2 of 8 phages indicated the most lytic effects against bacterial isolates. They effectively lysed five *E.coli* bacterial strains. Although, the bacterial isolates that each of the two bacteriophages lysed were not identical. These bacteriophages were selected for studying their morphology and other biological characteristics. Selected phages with the highest hostrange value were named PEcMa2/17 and PEcMa3/17. Resultant plagues of PEcMa2/17 and PEcMa3/17 using double-layer agar method are shown in Figure 1a and b (Figure 1). They showed clear plaques with 2.5-3 and 1.5-2 mm in diameter on lawn cultures of bacteria, respectively. All isolated phages (n=8) were purified and enriched. Precipitated phages (n=8) were stored at 4ºC for further experiments.

The morphology of the bacteriophages PEcMa2/17 and PEcMa3/17 was examined by TEM (Figure 2a and b). PEcMa2/17 had a head with a diameter of 70±5nm, a hexagonal outline, a long noncontractile tail of 10nm in diameter, and a length of 120±5nm which belongs to order *Caudovirales*, family *Siphoviridae* (Figure 2a). PEcMa3/17 has a head of about 80±5nm in diameter, a hexagonal outline, contractile tail with a diameter of 10nm, and length of 100±5 nm that was classified as a member of order *Caudovirales*, family *Myoviridae* (Figure 2b).

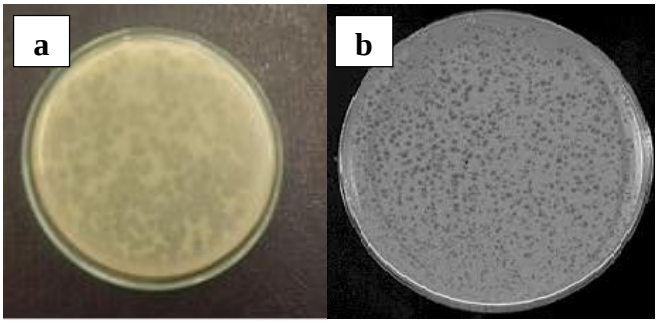

Figure 1. Plaque morphology of selected bacteriophages, PEc2-Ma17 (a) and PEc3-Ma17 (b), in bilayer agar method.

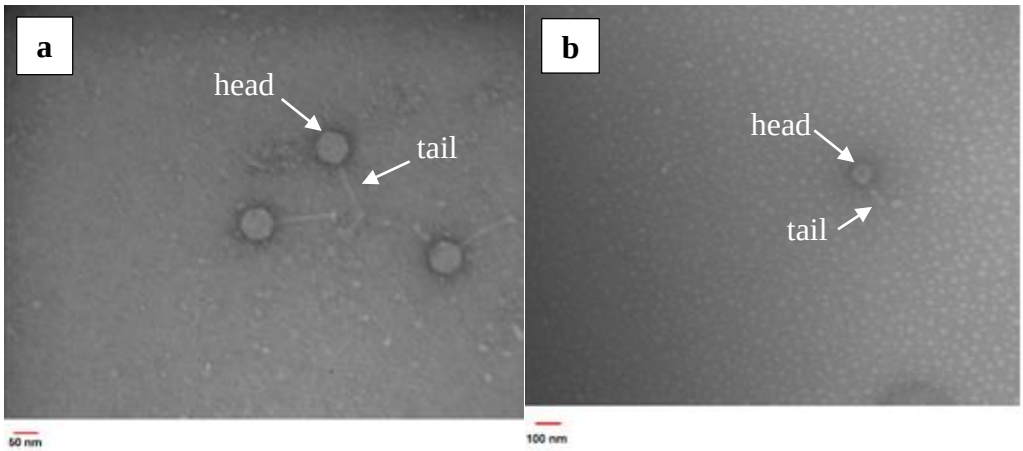

Figure 2. Transmission electron microscopy images of the bacteriophages PEcMa2/17 and PEcMa3/17 following the negative staining with uranyl acetate. Electron micrographs of PEcMa2/17 virions showthe typical morphology of phages within the family *Siphoviridae* with a head (diameter 70±5nm) and a hexagonal outline, a long noncontractile tail of 10nm,and the length of 120±5nm. (a). PEcMa3/17 virions showed the typical morphology of phages within the family *Myoviridae* with a head of about 80±5nm in diameter, a hexagonal outline, and a contractile tail with a diameter of 10nm and length of 100±5nm (b).

One-step growth experiment

According to the one-step growth experiment, the latent period, which is defined as the time intervals between the absorption and the beginning of the first burst, was 15min for both of the propagated phages. The burst size was estimated to be 100pfu/ml after 40min and 120pfu/ml after 45min in PEcMa2/17 and PEcMa3/17, respectively (Figure 3).

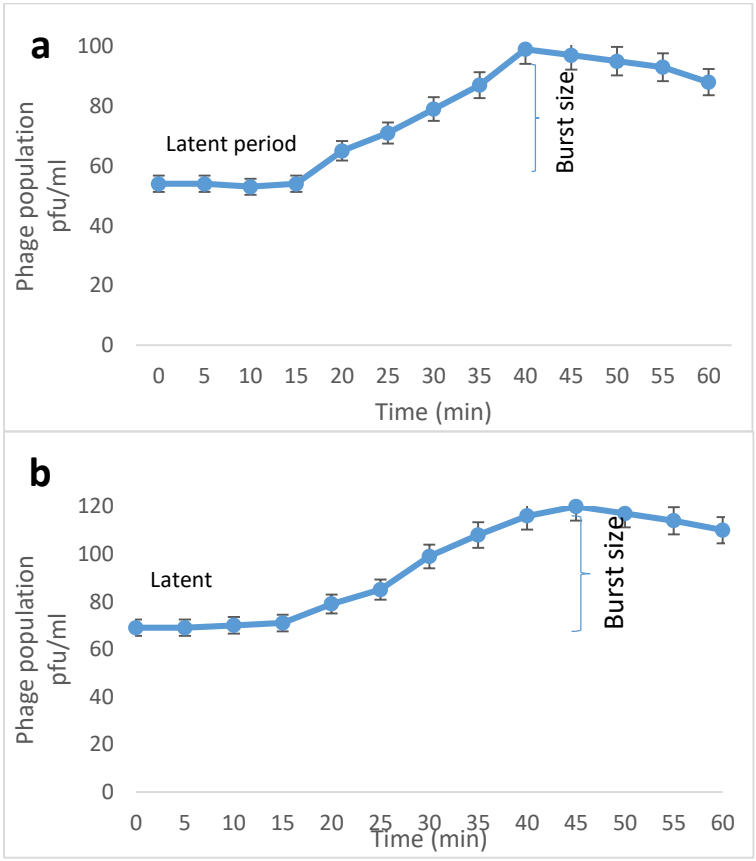

Figure 3. One-step growth curves of the PEcMa2/17 (a) and PEcMa3/17 (b) phages. The vertical axis showspfu per infected cell in the cultures at different time points. Each data point represents the mean from three independent experiments, and the error bars indicate standard deviations. (a) The latent period of PEcMa2/17 is 15min, and burst

size was estimated to be 100pfu/ml. (b) The latent period of PEcMa3/17 is 15min, and burst size was estimated to be 120pfu/ml.

Stability results

The sensitivity of virions of PEcMa2/17 and PEcMa3/17 bacteriophages was tested under different environmental conditions, including temperature, pH, and U.V. radiation. Results are shown in Table 2, Table 3, and Table 4, respectively.

Table 2. Resistance of two phage virions to different temperatures (percent of surviving phages under certain conditions is shown).

Phage name	-20°C		4°C		22°C		37°C		60°C		90°C	
	1h	24h	1h	24h	1h	24h	1h	24h	1h	24h	1h	24h
PEcMa2/17	96	95.4	65	60	68.4	56.7	75	70.7	22.1	3.6	17.3	0
PEcMa3/17	97	86.5	84.6	61.9	76.3	52.5	76	56.3	31.7	7.9	18.6	0

Table 3. Resistance of two phage virions to different pH rates (percent of surviving phages under certain conditions are shown).

Phage name	pH=3		pH=5		pH=7		pH=9		pH=11	
	1h	24h	1h	24h	1h	24h	1h	24h	1h	24h
PEcMa2/17	23.4	10	47.6	34.1	97	88	53.5	42	32.9	13.4
PEcMa3/17	16.7	10.5	84.1	74.5	99	91.2	57.8	37.1	40.5	34.3

Table 4. Resistance of two phage virions to U.V. radiation (percent of surviving phages under certain conditions are shown).

Phage name	U.V. radiation	
	15min	30min
PEcMa2/17	35	0
PEcMa3/17	11	0

DNA extraction and enzymatic digestion

Extracted genomic DNAs of all phage isolates, including PEcMa2/17 and PEcMa3/17, are shown in Figure 4 (a). Eight different RFLP (restriction fragment length polymorphism) patterns were determined in isolated bacteriophages through the digestion of their genomic DNA using the *EcoR*V enzyme (Figure 4b). The resultant fragments of genomic digestion was distinct for PEcMa2/17 and PEcMa3/17. One of the bacteriophage genomes (in lane 7) was not digested with the *EcoR*V enzyme, and eight obtained patterns were different. The digestion results of the eight bacteriophage genomes using *XbaI* are shown in the Figure 4 4c). As it was mentionedno phage genomes were digested. The genomes of two bacteriophages PEcMa2/17 and PEcMa3/17 were not digested with *Xba*I. Molecular analysis of two selected bacteriophages using *EcoR*V enzyme determined the genome size of about 33,600bp for PEcMa2/17, and more than 36,200bp for PEcMa3/17, respectively.

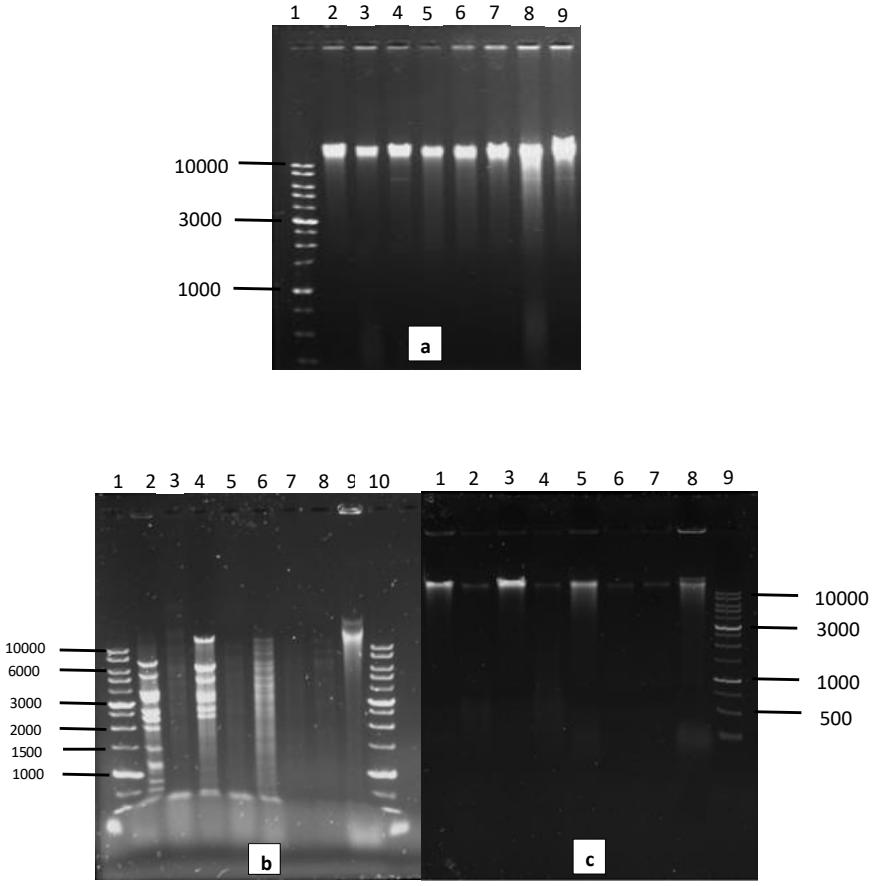

Figure 4. Genomic DNAs of 8 phage isolates were run onagarose gel 1%. (a) lane1: 1Kb DNA Ladder (Cinaclon, Iran), lane 2: bacteriophage PEcMa2/17, lane 3: bacteriophage PEcMa3/17, lanes 4-9: extracted genomic DNAs from other isolated bacteriophages, (b) Phage genomes digested with *Eco*RV; Lane 1: 1Kb DNA Ladder (Cinaclon, Iran), lane 2: bacteriophage PEcMa2/17, lane 4: bacteriophage PEcMa3/17, lanes 3 and 5-9: extracted genomic DNAs from other isolated bacteriophages, lane 10: 1Kb DNA Ladder (Cinaclon, Iran). (c) Phage genomes digested with *Xba*I; lane 1: bacteriophage PEcMa2/17, lane 2: bacteriophage PEcMa3/17, lanes 3-8: extracted genomic DNAs from other isolated bacteriophages, Lane 10: 1Kb DNA Ladder (Cinaclon, Iran). The molecular size of the DNA marker is shown (bp) in a, b and c.

Discussion

The emergence of antibiotic-resistant strains of bacteria has become a severe concern over recent decades, and it can be a significant threat to human healthcare in the future years. Then appropriate alternative therapies should be founded to fill the gap of infections treatment. Phage therapy as an effective and biological approach is highly regarded by researchers today.

In the current study, the antibiotic sensitivity of *E.coli* isolates from urinary tract infections was determined. The highest rate of antibiotic resistance was observed to amoxicillin, and 64.6% of isolates were resistant to three and more used antibiotics, and also 18.2% of isolates showed resistance to five and more antibiotics. In a previous study, the highest rate of antibiotic resistance of urinary *E.coli* bacteria was shown to ampicillin (50%), according to our results (Rfalskiy et al., 2020). Also, in a survey in Tabriz (north-west of Iran), the rate of resistance to tetracycline, SXT, nalidixic acid, gentamycin, ceftriaxone, ciprofloxacin, and nitrofurantoin was 80.9%, 63.9%, 43.98%, 43.11%, 33.01%, 26.96%, and 10.98% respectively (Molaabaszadeh et al., 2013). In other recent studies, more antibiotic resistance of urinary *E.coli* isolates was reported as Yazdi et al. revealed that 78.8% of *E.coli* isolates were MDR (multi-drug resistant), and the most resistance was observed to ampicillin and ciprofloxacin with the rate of 92.3% and 61.9% respectively (Yazdi et al., 2020). Also, 40% of *E.coli* bacteria isolated from urinary infections in Sari (north of Iran) were resistant to nalidixic acid and

ceftriaxone while were sensitive to amikacin, gentamycin, and nitrofurantoin (Rahimzadeh et al., 2020).

Our results showed a wide host range of selected bacteriophages about 62%. Also, using two isolated bacteriophages together could be more efficient against uropathogenic *E.coli* bacteria. In a survey on lytic effectiveness of 29 phage suspensions and four commercial phage cocktails on different *E.coli* isolates from urinary cultures of patients with UTIs, the highest lytic activity of the phage cocktails were 66%-93%, while used phage suspensions had the highest lysis on 42%, 39% and 24% of *E.coli* isolates respectively (Sybesma et al., 2016). Necel and colleagues evaluated the host range of phages vB_Eco4M-7 and ECML-117 against 97 *E.coli* strains. They reported that the phages had a lytic effect on 34 and 39 strains, respectively The majority of the *E.coli* strains were lysed by these bacteriophages belonged - to the O157 serotype (Necel et al., 2020). Phage VB_EcoS-Golestan, isolated from Iran, showed lytic activity against 56% of *E.coli* from urinary infections. Also, the phage had a lytic effect on 15 of 25 isolates resistant to ten used antibiotics, and it could lyse four of six *E.coli* bacteria resistant to all (n=17) used antibiotics (Yazdi et al., 2020). In another study, one bacteriophage isolated from Sari, Iran, had a lytic effect on all of nine used *E.coli* isolates from urinary infections (Rahimzadeh et al., 2020). In China, the ability of one isolated bacteriophage, vB_EcoS-B2, was tested against some MDR strains of *E.coli* that could lyse only seven of 35 clinical MDR strains. Despite a relatively narrow host spectrum of the bacteriophage, authors suggested it as a biocontrol agent against *E.coli* due to its strong lytic effect (Xu et al., 2018).

In the current study, selected bacteriophages against *E.coli* from urinary tract infections belonged to *Caudovirales, Siphoviridae,* and *Caudovirales, Myoviridae* that was by other studies (Yazdi et al., 2020; Rahimzadeh et al., 2020). Three other coliphages from the human gut (ϕAPCEc01, ϕAPCEc02 and ϕAPCEc03) were also classified in *Caudovirales*, family *Myoviridae* and *Siphoviridae* (Dalmasso et al., 2016). Reports of some other works refer to locate the phage with lytic activity against urinary *E.coli* bacteria (myPSH) in *Caudovirales*, family *Podoviridae* (Manohar et al., 2018). Also, in another study, lytic phage vB_EcoS-B2 with an isometric head with a mean diameter of 48 nm and the long noncontractile tail targeted *E.coli* clinical strains belonged to the family of *Siphoviridae* (Xu et al., 2018). Two isolated bacteriophages against pathogenic *E.coli* strains with 66 nm diameter heads and contractile tails belonged to the *Myoviridae* family (Necel et al., 2020).

Two important characteristics for phage therapy candidate bacteriophages are large burst size and short latency period. The burst size is closely related to phage propagation (Amarrillas., 2017). Then a phage with a large burst size may have a selective advantage as an antibacterial agent since phages with a large burst size can increase the initial dose of phages several 100-fold in short periods. Bacteriophages with these desirable features are more appropriate candidates for therapeutic purposes. Therefore, high burst size (100 and 120 pfu/ml) and short latent period (15 min) of both isolated phages, PEc2-Ma/17 and PEc3Ma/17, would indicate their strong potential application for phage therapy after more characterization. Bacteriophages vB_Eco4M-7 and ECML-117 had a strong lytic effect on O157 *E.coli* strains, showed a latent period of 10 min, with a burst size of approximately 100 phages per cell (Necel et al., 2020). The burst size and latent period of coliphages in other studies were determined 40 min and 100 pfu/ml (Yazdi et al., 2020), 20 min and 1200 pfu/ml (Rahimzadeh et al., 2020), and 10 min and about 90 pfu/ml (Dalmasso et al., 2016). Also, another phage isolated against MDR (multi-drug resistant) clinical strains of *E.coli* had a latent period of 15min and a burst size of approximately 224.1±10.7 (Xu et al., 2018).

Our results showed that the most viability of both bacteriophages (PEcMa2/17 and PEcMa3/17) was observed at a temperature of -20°C after 1 h. The bacteriophages were totally deactivated after 24h at 90ºC. Their stability was more than 50% at the temperature range of -20 to 37°C. In these temperatures, the survival rate of the bacteriophages was not strongly affected by the length of incubation time, especially about PEcMa2/17. In a study, the biological activity of phage vB_EcoS-B2 had no difference in the temperature ranging from 4 to 50ºC, but increasing the temperature above 55ºC decreased the activity sharply (Xu et al., 2018). Both phages were shown the most survival rate in pH value of 7 with the rate of more than 87% after 1 and 24 h incubation. Both of the bacteriophages showed lytic effects at pH 3 and 11. The lowest stability rate of the bacteriophages was in pH value of 3 after 24h incubation. Survivability of two bacteriophages was similar in pH values of 3, 7, 9, but not in pH value of 5 that survival rate of PEcMa3/17 was more than PEcMa2/17 after 1 and 24h incubation. In a previous study, a coliphage against *E.coli* originated from UTIs showed maximum activity at pH values of 7 and 8, according to our results. The bacteriophage

showed a high lytic effect in the pH values from 5 to 10 after 1 h incubation. However, the bacteriophage stability was decreased significantly at pH values of 3 and 11 after 1 and 24h incubation. In our study, both bacteriophages were deactivated after 30min exposure to U.V. radiation, and after 15min, stability of PEcMa2/17 was more than PEcMa3/17.

Environmental conditions such as temperature and pH level can affect the applications of bacteriophages to combat pathogenic bacteria (Ly-Chatain, 2014). Declining phage titer in lower pH values could have been happened due to high concentration of H+ and hydroxyl ions and consequently denaturation of capsid proteins (Feng et al., 2003). In addition, the concentration of hydrogen ions in an acidic solution can result in a decrease in bacteriophage concentration because of the aggregation process. High temperatures cause irreversible damage or denaturation of the virus particles (Wang tan et al., 2021). Some works suggested the possibility of a relationship between the structure of bacteriophages and their stability under adverse environmental conditions (Lasobras et al., 1997). Tailed phages suffer adverse conditions better than other phages (Ackermann et al., 2004). They generally show a higher ability to adapt to adverse conditions, leading to the applicable phage therapy. Also, other studies reported that strong ultraviolet light and large temperature fluctuations cause phages belonging to *Myoviridae* to protect themselves in biofilms or pseudo-lysogens formed by their bacterial hosts (Jonczyk et al., 2011). Extreme resistance of *Podoviridae* family bacteriophages to dry environments and large temperature fluctuations also was reported (Prigent et al., 2005). Generally, more stability of a bacteriophage in a wide range of environmental conditions is an important advantage to a phage therapy candidate (Jamal et al., 2015). For using phages in phage cocktails of phage therapy, it is essential to consider the stability of each bacteriophage at different environmental conditions. Based on our data, phages PEcMa2/17 and PEcMa3/17 with high stability in a wide range of temperatures and pH conditions could be used as the candidate for phage therapy at different environmental settings. Both phages had approximately similar pH values and temperatures stability, which could be used together in a phage cocktail.

Results of molecular analysis confirmed differences among eight isolated bacteriophages, also in two selected bacteriophages, with the digestion by one of the enzymes (*Eco*RV). Based on resultant fragments from enzyme digestion, the genome size of PEcMa2/17 (approximately 33,200 bp) was shorter than PEcMa3/17. Comparing to other studies, Pacifico and colleagues reported that the genome size of phages against *E.coli* from clinical samples classified to *Myoviridae* was between 33,688 to 33,807bp and isolated *Siphoviridae* phages in the study had more than 44,000 bp length that was following our results (Pacifico et al., 2019). The genome size of other bacteriophages (e VB_EcoS-Golestan) isolated against *E.coli* from urinary tract infection belonged to the *Siphoviridae* family, was 44,829bp in length (Yazdi et al., 2020). Different RFLP patterns of all eight bacteriophages using *Eco*RV suggested the presence of some variations in their genetic characteristics. Unfortunately, no reports were found about enzyme digestion of *Escherichia coli* bacteriophages, but in a study in Poland, 51 genomes of phages isolated against uropathogenic strains of *Proteus mirabilis* showed 34 different RFLP patterns using *Eco*RV enzyme (Maszewska et al., 2016). In another study, six isolated bacteriophages against *Vibrio parahaemolyticus* that belonged to *Siphoviridae* and *Podoviridae* families showed some variations in their RFLP patterns (Wang tan et al., 2021). Variations in the genome of isolated bacteriophages from the same origin can be helpful to access more phages to design effective bacteriophage packages, which can be useful to control antibiotic-resistant urinary tract infections.

Conclusion

PEcMa2/17 and PEcMa3/17 are virulent phages against UTIs *E.coli* bacteria. The large burst size and short latent period of both isolated phages in addition to their high stability could indicate their strong potential as the candidates for phage therapy of UTIs caused by *E.coli*. Further molecular analyses and sequencing of the entire genome are required to characterize the introduced bacteriophages. It is worth mentioning that we need more advanced experimental studies to evaluate their potential for the therapeutic applications.

Acknowledgment

This paper is published as part of a research project supported by the University of Maragheh Research Affairs Office.

References

Adams, M.H., 1959. Bacteriophages, Interscience Publishers, New York.

Ahmadpour, S., Mardani, K., Tukmechi, A. (2016). Culture and molecular characterization of phages

isolated from rainbow trout farms and sewage treatment plants and investigation of their effects on Yersinia ruckeri. Iranian Journal of Fishery Sciences 15: 267-280.

Ackermann, H.W., Tremblay, D., Moineau, S. (2004). Long-term bateriophage preservation. WFCC Newslett 38: 35-40.

Amarillas, L., Rubi-Raangel, L., Chaidez, C., Robles, A., Rojas, Felix, J. L. (2017). Isolation and characterization of phiLLS, a novel phage with potential biocontrol agent against multidrugresistant *Escherichia coli*. Frontiers in Microbiology 8: article 1355.

Bauer, A.W., Kirby, W.M.M., Sherris, J.C., Turck, M. (1966). Antibiotic susceptibility testing by a standardized single disk method. American Journal of Clinical Pathology 45(4): 493-496.

Chibeu, A., Lingohr, E. J., Masson, L., Manges, A., Harel, J., Ackermann, H. W. (2012). Bacteriophages with the ability to degrade uropathogenic *Escherichia coli* biofilms. Viruses 4(4): 471-487.

Dalmasso, M., Strain, R., Neve, H., Charles, M. A., Franz, P., Fabien J. and et al. (2016). Three new *Escherichia coli* phages from the human gut show promising potential for phage therapy. PLoS One 9: 0156773.

Feng, Y. Y., Ong, S. L., Hu, J. Y., Tan, X. L., Ng, W. J. (2003). Effects of pH and temperature on the survival of coliphages MS2 and Qβ. Journal of Industrial Microbiology and Biotechnology 30(9): 549-52.

Flores-Mireles, A.L., Walker, J.N., Caparon, M., Hultgren, S.J. (2015). Urinary tract infections: epidemiology, mechanisms of infection and treatment options. Nature Reviews Microbiology 13 (5): 269-84.

Jamal, M., Hussain, T., Das, C.R., Andleeb, S. (2015). Characterization of *Siphoviridae* phage Z and studying its efficacy against multidrugresistant *Klebsiella pneumoniae* planktonic cells and bioflm. Journal of Medical Microbiology 64: 454-462.

Jassim, S., Abdulamir, A.S., Bakar, F.A. (2012). Novel phage-based bio-processing of pathogenic *Escherichia coli* and its biofilms. World Journal of Microbiology and Biotechnology 28(1): 47-60.

Jonczyk, E., Klak, M., Miedzybrodzki, R., Gorski, A. (2011). The influence of external factors on bacteriophages-review. Folia Microbiologica 56: 191-200.

Jun, J.W., Kim, J.H., Shin, S.P., Han, J.E., Chai, J.Y., Park, S.C. (2013). Characterization and complete genome sequence of the *Shigella* bacteriophage pSf-1. Research in Microbiology 164: 979-986.

Kostakioti, M., Hultgren, S.J., Hadjifrangiskou, M. (2012). Molecular blueprint of uropathogenic Escherichia coli virulence provides clues toward the development of anti-virulence therapeutics. Virulence 3(7): 592-3.

Lasobras, J., Muniesa, M., Frias, J., Lucena, F., Jofre, J. (1997). Relationship between the morphology of bacteriophages and their persistence in the environment. Water Science and Technology 35: 129-132.

Ly-Chatain, M. H. (2014). The factors affecting effectiveness of treatment in phages therapy. Frontiers in Microbiology 5: article 51.

Manohar, P.T., Tamhankar A.J., Lundborg C.S., Ramesh, N. (2018). Isolation, characterization and *in vivo* efficacy of *Escherichia coli* phage myPSH1131. PLoS one 13(10): e0206278.

Maszewska, A., Wójcik, E., Ciurzyńska, A., Wojtasik, A., Piątkowska, I., Dastych, J., Różalski, A. (2016). Differentiation of polyvalent bacteriophages specific to uropathogenic *Proteus mirabilis* strains based on the host range pattern and RFLP. Acta Biochimica Plonica (63): 303-310.

Merabishvili, M., Vandenheuvel, D., Kropinski, A.M., Mast, J., De Vos, D., Verbeken, G. et al. (2014). Characterization of newly isolated lytic bacteriophages active against *Acinetobacter baumannii*. PloS One 9(8): e104853.

Mohamed, M.A., Abdifetah, O., Hussein, F.A. (2020). Antibiotic resistance pattern of *Escherichia coli* isolates from outpatient with urinary tract infections in Somalia. Journal of Infection in Developing Countries 14(3): 284-289.

Molaabaszadeh, H., Hajisheikhzadeh, B., Mollazadeh, M, Eslami, K., Mohammadzadeh Gheshlaghi, N. (2013). The study of sensibility and antimicrobial resistance in *Escherichia coli* isolated from urinary tract infection in Tabriz City. Journal of *Fasa* University of Medical Sciences 3(2): 149-154.

Necel, A., Bloch, S., Nejman-Faleńczyk, B., Grabski, M., Topka, G., Dydecka, A., Kosznik-Kwaśnicka, K., Grabowski, L., Jurczak-Kurek, A., Wołkowicz, T., Węgrzyn, G., Węgrzyn, A. (2020).

Characterization of a bacteriophage, vB_Eco4M-7, that efectively infects many *Escherichia coli* O157 strains. Scientific Reports 10: 3743.

Pacifico, C., Hilbert, M., Sofka, D., Dinhopl, N., Pap, I. J., Aspöck, C., Carriço, J. A., Hilbert, F. (2019). Natural occurance of *Escherichia coli*-infecting bacteriophages in clinical samples. Frontiers in Microbiology 10: article 2484.

Pajunen, M., Kiljunen, S., Skurnik, M. (2000). Bacteriophage φYeO3-12, Specific for *Yersinia enterocolitica* Serotype O:3, Is Related to Coliphages T3 and T7. Journal of Bacteriology 182(18): 5114-5120.

Pouillot, F., Chomton, M., Blois, H., Courroux, C., Noelig, J., Bidet, P., et al. (2012). Efficacy of bacteriophage therapy in experimental sepsis and meningitis caused by a clone O25b: H4-ST131 *Escherichia coli* strain producing CTX-M-15. Antimicrobial Agents and Chemotherapy 56(7): 3568-75.

Prigent, M., Leroy, M., Confalonieri, F., Dutertre, M., DuBow, M. S. (2005). A diversity of bacteriophage forms and genomes can be isolated from the surface sands of the Sahara Desert. Extremophiles 9: 289-296.

Quinn, P.J., Carter, M.E., Markey, B.K., Cartel, G.R. (1994). Clinical Veterinary Microbiology, Mosby-Year book Europe Limited, Wolfe publishing Ltd. London, England.

Rafalskiy, V., Pushkar, A., Yakovlev, S., Epstein, O., Putilovskiv, M. (2020). Distribution and antibiotic resistance profile of key gram-negative bacteria that cause community-onset urinary tract infections in the Russian Federation. Journal of Global Antimicrobial Resistance 21: 188-194.

Rahimzadeh, G., Resch, G., Rezai1, M. S., Nemati Hevelaee, E. (2020). Characterization and lytic activity of isolated *Escherichia coli* bacteriophages against *Escherichia Coli in Vitro*. Iranian Journal of Medical Sciences 45(4): 298-303.

Ramirez, K., Cazarez-Montoya, C., Lopez Moreno, H. S., Castro-del Campo, N. (2018). Bacteriophage cocktail for biocontrol of Escherichia coli O157:H7: Stability and potential allergenicity study. PLoS One 13(5):1-19.

Sabouri Ghannad, M., Mohammadi, A. (2012). Bacteriophage: time to re-rvaluate the potential of phage therapy as a promising agent to control multidrug-resistant bacteria. Iranian Journal of Basic Medical Sciences 15(2): 693-701.

Stamm, W.E., Norrby, S.R. (2001). Urinary tract infections: disease panorama and challenges. The Journal of Infectious Diseases 183(1): S1-S4.

Sybesma, W., Zbinden, R., Chanishvili, N., Kutateladze, M., Chkhotua, A., Ujmajuridze, A. (2016). Bacteriophages as potential treatment for urinary tract infections. Frontiers in Microbiology 7: article 465.

Tuem, K. B., Gebre, A. K., Atey, T. M., Bitew, H., Yimer, E. M., Berhe, D. F. (2018). Drug resistance patterns of *Escherichia coli* in Ethiopia: A Meta-Analysis. BioMed Research International 4536905.

Tan, C. W., Rukayadi, Y., Hasan, H., Abdul-Mutalib, N. A., Jambari, N. N., Hara, H., Thung, T. y., Lee, E., Radu, S. (2021). Isolation and characterization of six *Vibrio parahaemolyticus* lytic bacteriophages from seafood samples. Frontiers in Microbiology 12: article 616548.

Xu, Y., Yu, X., Gu, Y., Huang, X, Liu, G., Liu, X. (2018). Characterization and Genomic Study of Phage vB_EcoS-B2 Infecting Multidrug-Resistant *Escherichia coli*, Frontiers in Microbiology 9: article 793.

Yazdi, M., Bouzari, M., Ghaemi, E., Shahin, Kh. (2020). Isolation, characterization and genomic analysis of a novel bacteriophage VB_EcoS-Golestan infecting multidrug-resistant *Escherichia coli* isolated from urinary tract infection. Scientific Reports 10: 7690.

Journal of Cell and Molecular Research (2021) 13 (1), 92-97 DOI: 10.22067/JCMR.2021.71443.1011

Research Article

Vitamin C-Loaded Albumin Nanoparticles Treatment and Its effect on Collagen I and III and miR-133 Gene Expression in Mice

Hamid Reza Shojania[1], Madjid Momeni-Moghaddam[2 *], Seyed Ebrahim Hosseini[3]

[1]*Department of Genetics, Marvdasht Branch, Islamic Azad University, Marvdasht, Iran*
[2]*Department of Biology, Faculty of science, Hakim Sabzevari University, Sabzevar, Iran*
[3]*Department of Biology, Faculty of Sciences, Zand Institute of Higher Education, Shiraz, Iran*

Received 13 July 2021 Accepted 6 August 2021

Abstract

Wound healing is a complex biological process in which many molecules, including microRNA molecules, play an essential role in its regulation. It is well-established that reducing miR-155 expression can accelerate wound healing. This study investigated the effect of using nanoparticles loaded with vitamin C on miR-133, collagen I, and III expressions. In this study, first, nanoparticles of albumin protein were produced and then loaded with vitamin C. 3T3 mouse fibroblast cells were affected by these nanoparticles, and cell behavior was investigated to evaluate the toxicity and appropriate doses. In addition, the expression of collagen I and III genes was studied. The results showed that nanoparticles containing vitamin C in 20 µg/ml concentration had a positive effect on collagen I and III expressions compared to the control group. Moreover, we observed a decrease in the expression of miR-133 in comparison to the control group. Therefore, according to the results of this study, it can be argued that nanoparticles containing vitamin C can significantly decrease the expression of the miR-133 gene and lead to collagen I and III gene overexpression in fibroblasts cells, which is directly effective in wound healing.

***Keywords*:** Wound Healing, Collagen I, Collagen III, MiR-133, Vitamin C

Introduction

Wound healing, in which the skin repairs itself in response to damage, is a complex process. It involved several stages: homeostasis, inflammation, proliferation, and finally, the regenerative phase (Rezaie et al., 2019). These stages occur in continuous biochemical events and eventually leads to the repair of damaged tissue. The speed of wound healing depends on several local and systemic factors, the state of inflammation and the levels of growth factors. Therefore, regulation of inflammation factors and candidate gene expression in wound healing is essential (Kirsner and Eaglstein, 1993).

Fibroblasts are one of the most important cells involved in wound healing. They are one of the active cells in almost all stages and advancement of this process. Fibroblasts can invade the fibrin clot, destroy it and pave the way for the other repair cells to migrate to the wound space (Xie et al., 2008). They produce and secrete extracellular matrix components and interact with them (Frantz et al., 2010).

The extracellular matrix is another critical factor in the proper advancement of wound healing and provides a scaffold and physical support for the formation of new tissues and acts as a storage repository for restorative cytokines (Frantz et al., 2010). Therefore, the proliferation and activity of fibroblast cells regulate the production and secretion of extracellular matrix components, such as collagen I and III, for the proper and timely healing of wounds. The role of collagen I and III in optimizing wound healing is well-known, so it is essential to know how they are expressed and formed and the related substrates or drugs involved with them (Klinge et al., 2000).

Vitamin C can be found in its large amounts in healthy skin, responsible for stimulating collagen synthesis and protection against light damage caused by UV radiation. During the proliferative phase of wound healing, fibroblasts produce collagen fibers using divalent ions such as iron and copper and vitamins such as vitamin C (Lanman and Ingalls, 1937).

MicroRNAs (miRNAs or miRs) are a subset of non-coding RNAs containing 18-22 nucleotides (Teymoori et al., 2017) that are evolutionarily conserved and have pivotal roles in the progression

* Corresponding author's e-mail address:
m.momeni@hsu.ac.ir, *Iranbioman@yahoo.com*

of the various biological process, including wound healing (Sanjari et al., 2015). The TGFb1 gene is considered as one of the principal targets of miR-133a (Roderburg et al., 2013).

Nanotechnology is a multidisciplinary science including various aspects of research and technology. Nanoparticles are some kinds of metal substances with a size range of 1-100 nm and are in the form of blocks made of nanotechnology. Metal nanoparticles such as gold, silver, and platinum have gained considerable attention in recent years due to their helpful basis and technology. These nanoparticles have the unique catalytic, electronic and optical properties of metal particles. Many methods have been developed for the synthesis of nanoparticles in recent years, such as physical, chemical, and biological methods (Saxena et al., 2020).

In this study, vitamin C-loaded human serum albumin (HAS) nanoparticles were made, fibroblast cells were affected in different group treatments, and then the expression of various genes, including miR-133 and collagen I and III had been examined.

Materials and Methods

Nanoparticle Production

As fully explained in the previous study (Shojania et al., 2019): HSA nanoparticles (Octalbin 20%) are a sterile protein solution containing at least 96% human albumin. In order to make albumin nanoparticles, the following steps were performed: 250 µl of Octalbin solution (equivalent to 50 mg of HSA) was added to 750 µl of distilled water, and adjusted the pH of the solution to 7.4. Then Tween 80 (2% v / v) was added to the solution and stirred for 30 minutes at 500 rpm (round per minute), followed by adding 4 ml of ethanol (dropwise) to the stirring suspension. Then 12 µl of 8% aqueous glutaraldehyde solution was added to the suspension to concentrate the nanoparticles. In the next step, nanoparticle suspension was stirred for another 500 rpm for 24 hours at room temperature. Finally, nanoparticle suspension was centrifuged at 500 rpm for 15 minutes at 4 °C to remove any impurities. Vitamin C-loaded albumin nanoparticles were prepared by the nanoprecipitation method. Briefly, 250 µl of Octalbin solution (50 mg of HSA) was added to 750 µl of distilled water, and pH was adjusted to 7.4. Tween 80 (2% v/v) was added to the solution and stirred at 500 rpm for 30 min. Then, 25 mg of vitamin C was added to the solution, and 4 ml of ethanol was gradually dropped into it. After the desolvation process, 20 µl of 8% glutaraldehyde aqueous solution was added to promote particle condensation under 500 rpm for 5 h. Nano suspension was centrifuged at 5000 rpm for 15 min at 4°C and washed with PBS for further analysis (All chemicals were purchased from Sigma-Aldrich) Further purification of nanoparticles was performed by the dialysis method. For nanoparticle characterization particle size and zeta potential were measured using the size and zeta analyzer (Beckman Coulter) also Nanoparticles morphology was investigated by using an EM3200 scanning electron microscope. Freeze dried samples were prepared and used for electron microscopy.

Cell

In this study, 3T3 fibroblast cells were provided from Sabzevar University of Medical Sciences and were cultured in T25 flasks (1.2×10^6). They were grown in DMEM medium (Gibco) with high glucose supplemented with 10% fetal bovine serum (Gibco) and 1% penicillin/Streptomycin antibiotic (Sigma-Aldrich). The cells were maintained at 37 ° C with 5% CO2 and 95% air (memmert incubator). They were passaged after thawing and followed in appropriate confluency.

Cell Viability Assay

Cells were cultured in 96-well plates for 24- and 48-hours incubation periods for cell cytotoxicity assessment. After 24 hours, the previous medium was exchanged, and 5, 10, 20, 30, 40 µg/ml of nanoparticle concentrations were added in 5 replications. The control group was considered separately for each group of concentrations, and PBS was used instead of the same amount of nanoparticle solutions. MTT assay (3-(4,5-dimethylthiazol-2-yl)-2,5-diphenyl-2H-tetrazolium bromide) according to the kit (Biotium) instructions was performed after 24- and 48-hours treatments; the supernatant was removed, and 100 µl of RPMI 1640 solution containing 10 µl of 0.5 mg/ml MTT solution was added to each well. The plate was incubated at 37 ° C for 4 h. After formazan crystals formation, the previous medium was removed, and 100 µl of DMSO solution was added. After several pipetting, the plates were incubated for 10 minutes, and then the light absorption at 570 nm was read by the plate reader.

Trypan Blue Staining

Trypan blue was used to study the ratio of living cells to dead cells in cell cultures. Since living cells are resistant to the penetration of this substance into the cell membrane, dead cells were shown in blue

color. All concentrations and replications were performed as MTT assay and following the protocol.

Real-time PCR

Exiqon provided the primers applied in this study. RNA extraction and cDNA synthesis, by oligo dT primers, were carried out according to the company's protocols and kits (TRIpure reagents and TaKaRa cDNA synthesis kit, respectively). SYBR Green was used to perform real-time PCR (Rotor- Gene 3000). The primer efficiency was calculated, and then real-time PCR analysis was performed for the samples (Takapozist SYBRgreen). All primers and sequences used are listed in Table 1.

Table 1. The list of primers used for real-time PCR.

primer	Sequence	NCBI Reference Sequence
Col I	F: ACATGTTCAGCTTTGTGGACC R: GGTTTCCACGTCTCACCATT	NM_007742.4
Col III	F: CTGTAACATGGAAACTGGGGAAA R: CCATAGCTGAACTGAAAACCACC	NM_009930
b-actin	F: TTCTTTGCAGCTCCTTCGTT R: ATGGAGGGGAATACAGCCC	BC138614.1

Results

Nanoparticle Synthesis

In this study, the exact synthesized nanoparticles for the previous article were used, and all confirmations (including measurement of zeta potential and defining size using electron microscope photography) are available in the previous report (Shojania et al., 2019).

Cell Viability Assays

In this study, two methods (MTT assay and trypan blue staining) were used to study cell survival and growth behavior. The effect of HSA nanoparticles carrying vitamin C on viability, growth, and proliferation of 3T3 fibroblast cells at 24- and 48-hours treatments was evaluated by MTT assay. The results showed that vitamin C-carrying HSA nanoparticles in 20 µg/ml concentration had the most significant stimulatory effect on the growth of 3T3 fibroblast cells compared to the control group both in 24 and 48 hours after treatments ($P < 0.05$) (Figure 1). In addition, the trypan blue staining method also provided similar results (Figure 2).

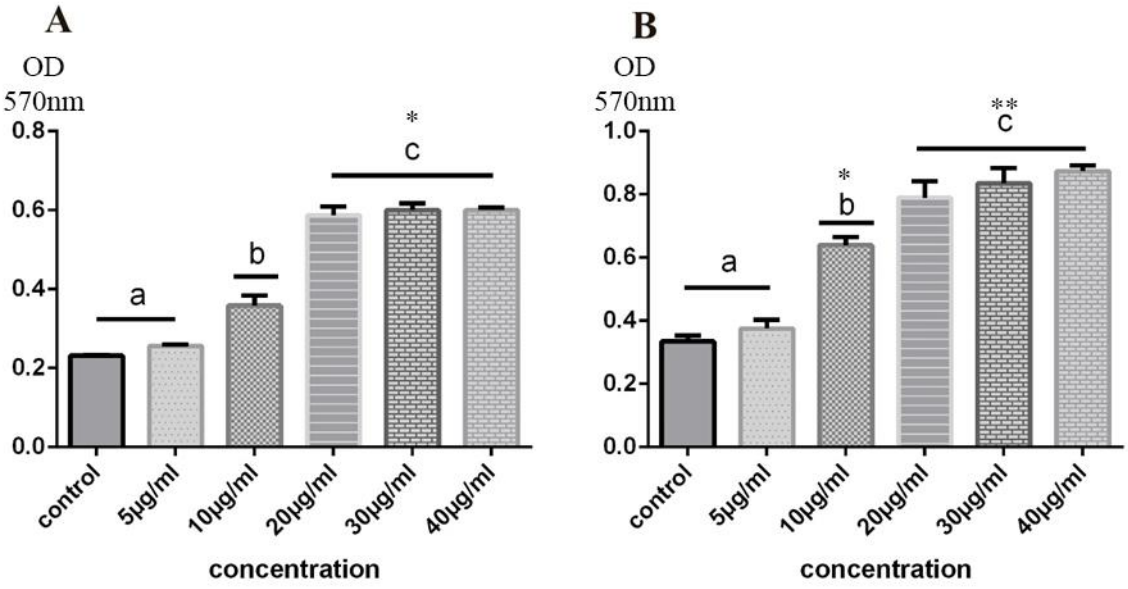

Figure 1. MTT assay test of vitamin C-loaded HSA nanoparticles on 3T3 fibroblast cells after 24 (A) and 48 h (B). 20 µg/ml of vitamin C-loaded HSA nanoparticles induced 3T3 fibroblast cells growth and proliferation after 24 and 48 h ($P \leq 0.05$).The vertical axis represents the optical density (570 nm), and the horizontal axis represents the nanoparticle concentration.

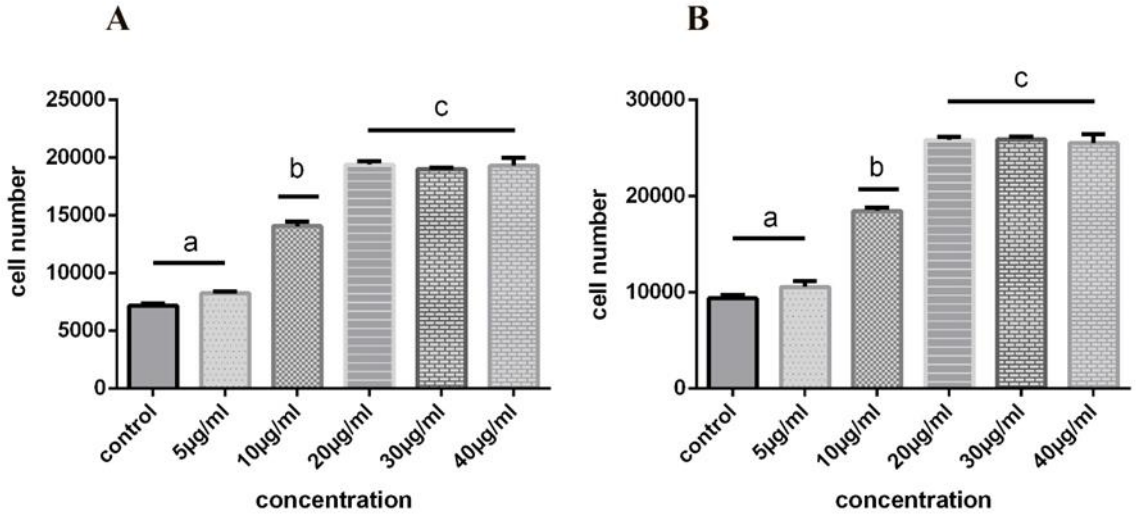

Figure 2. Trypan blue staining test of cell viability of vitamin C-loaded HSA nanoparticles on 3T3 fibroblast cells after 24 (A) and 48 h (B). 20 µg/ml of vitamin C-loaded HSA nanoparticles induced 3T3 fibroblast cells growth and proliferation after 24 and 48 h ($P \leq 0.05$). The vertical axis represents the number of cells, and the horizontal axis represents the concentration of nanoparticles.

Gene Expression

RNA extraction and cDNA synthesis were performed from the treated and untreated fibroblast cells. The expression of *miR-133*, type I and type III collagen genes were assessed. As shown in Figure 3, a decrease in the expression of miR-133 and an increase in expression of type I and III collagen were observed in cells treated with vitamin C–loaded HSA nanoparticles.

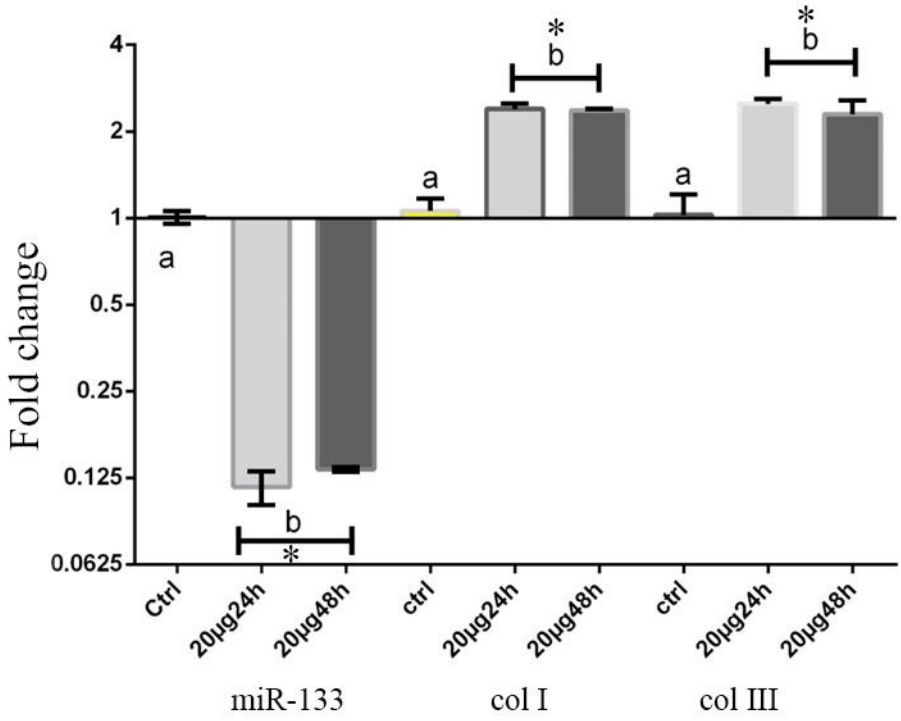

Figure 3. miR-133, type I and type III collagen expression in control and vitamin C-loaded human serum albumin (HSA) nanoparticles treated groups. The level of miR-133 in vitamin C-loaded nanoparticles treated groups was significantly decreased after 24 and 48 h compared with control groups. On the other hand, types I and III collagen level was significantly increased ($P < 0.05$) compared to the control group.

Discussion

Many factors are involved in wound healing. One of these factors is the proper formation of collagen fibers in damaged tissue, which is done by fibroblast cells. While any defect in collagen synthesis can cause problems, finding ways to properly manage collagen production in the wound bed can accelerate the wound healing process. Today, with the significant growth of nanotechnology, producing efficient nanoparticles in the field of wound healing can be introduced as a promising option (Saxena et al., 2020).

This study sought to investigate the effect of human serum albumin (HSA) nanoparticles containing vitamin C on collagen expression in fibroblast cells. For this purpose, we first studied the effective concentration of this nanoparticle on cells and then we examined expression changes of col I, col III, and miR-133, using the real-time PCR method.

Collagen synthesis by fibroblast cells is directly involved in wound healing. This extracellular matrix can be introduced as a suitable substrate for the placement of other cells, so any factor that enhances collagen gene expression can be considered in this process (Clore et al., 1979).

Based on the literature, vitamin C plays a major role in collagen synthesis by inhibiting the production of proline hydroxyl in treating of skin wounds (Lanman and Ingalls, 1937). This study examined the toxicity of nanoparticles and their biocompatibility on fibroblast cells, the main target. The results showed that none of them are toxic in the range of tested concentrations. Maximum cell growth was observed at 20 μg/ml. This concentration was chosen for further experiments. Not only vitamin C-loaded HSA nanoparticles did not show any toxicity in the evaluated dosage, but also, they could increase mouse fibroblast cell growth.

In addition, we also sought to investigate miR-133 expression changes in response to nanoparticles. Studies have shown that miR-133 can control collagen synthesis well through the TGF-β pathway (Duan et al., 2015). In the previous research, we showed the relationship between miR-155 and TGF-β as well (Shojania et al., 2019). According to our findings in these reports, there was an exciting point in the relationship between miR-133, miR-155, and wound healing. By reducing collagen synthesis, both of them showed an inhibitory role. So, treatment with nanoparticles containing vitamin C can remove this inhibition and accelerate wound healing. The effect of miR-133 through TGF-β-dependent depression of collagen synthesis has been well described, especially during liver fibrosis (Roderburg et al., 2013). The inhibitory role of the miR-133 molecule on collagen synthesis is defined in the present study, and nanoparticle treatment could significantly reduce the expression of miR-133 and increase col I, col III molecules simultaneously.

Drug control of wound healing mechanisms is of great importance. Any irregularity in this process leads to chronic conditions and/or prolongation of treatment. What has been done in this study can be a good candidate for inducing collagen expression by fibroblasts at the wound site. In addition, we did similar experiments in the previous study (Shojania et al., 2019), and parallel with this study, miR-133, in coordination with miR-155, showed precisely the pattern toward faster healing of the wound.

References

Clore, J. N., I. K. Cohen and R. F. Diegelmann (1979) Quantitation of collagen types I and III during wound healing in rat skin. Proceedings of the Society for Experimental Biology and Medicine 161(3): 337-340.

Duan, L. J., J. Qi, X. J. Kong, T. Huang, X. Q. Qian, D. Xu, J. H. Liang and J. Kang (2015) MiR-133 modulates TGF-β1-induced bladder smooth muscle cell hypertrophic and fibrotic response: implication for a role of microRNA in bladder wall remodeling caused by bladder outlet obstruction. Cellular signalling 27(2): 215-227.

Frantz, C., K. M. Stewart and V. M. Weaver (2010) The extracellular matrix at a glance. Journal of cell science 123(24): 4195-4200.

Kirsner, R. S. and W. H. Eaglstein (1993) The wound healing process. Dermatologic clinics 11(4): 629-640.

Klinge, U., Z. Si, H. Zheng, V. Schumpelick, R. Bhardwaj and B. Klosterhalfen (2000) Abnormal collagen I to III distribution in the skin of patients

with incisional hernia. European surgical research 32(1): 43-48.

Lanman, T. H. and T. H. Ingalls (1937) Vitamin C deficiency and wound healing: an experimental and clinical study. Annals of surgery 105(4): 616.

Rezaie, F., M. Momeni-Moghaddam and H. Naderi-Meshkin (2019) Regeneration and repair of skin wounds: various strategies for treatment. The international journal of lower extremity wounds 18(3): 247-261.

Roderburg, C., M. Luedde, D. V. Cardenas, M. Vucur, T. Mollnow, H. W. Zimmermann, and et al. (2013) miR-133a mediates TGF-β-dependent derepression of collagen synthesis in hepatic stellate cells during liver fibrosis. Journal of hepatology 58(4): 736-742.

Sanjari, T., T. Hajjar and M. Momeni-Moghaddam (2015) The role of mesenchymal stem cells in skin wound healing. Journal of Cell and Molecular Research 7(2): 70-75.

Saxena, S. K., R. Nyodu, S. Kumar and V. K. Maurya (2020). Current advances in nanotechnology and medicine. NanoBioMedicine, Springer: 3-16.

Shojania, H. R., M. Momeni-Moghaddam, S.-e. Hossini, M. Armin and J. Omrani Bidi (2019). MicroRNA 155 Downregulation by Vitamin C–Loaded Human Serum Albumin Nanoparticles During Cutaneous Wound Healing in Mice. The international journal of lower extremity wounds 18(2): 143-152.

Teymoori, A., M. Teimoori and M. Momeni-Moghaddam (2017) Non-coding RNAs Could Be New Tools for Cancer Treatment. Journal of Cell and Molecular Research 9(1): 44-53.

Xie, J., H. Bian, S. Qi, Y. Xu, J. Tang, T. Li and X. Liu (2008) Effects of basic fibroblast growth factor on the expression of extracellular matrix and matrix metalloproteinase-1 in wound healing. Clinical and Experimental Dermatology: Continuing professional development (CPD) 33(2): 176-182.

Scientific Reviewers

MANUSCRIPT PREPARATION

Manuscripts should be prepared in accordance with the uniform requirements for Manuscript's Submission to **"Journal of Cell and Molecular Research".**

Language: Papers should be in English (either British or American spelling). The past tense should be used throughout the results description, and the present tense in referring to previously established and generally accepted results. Authors who are unsure of correct English usage should have their manuscript checked by somebody who is proficient in the language; manuscripts that are deficient in this respect may be returned to the author for revision before scientific review.

Typing: Manuscripts must be typewritten in a font size of at least 12 points, double-spaced (including References, Tables and Figure legends) with wide margins (2.5 cm from all sides) on one side of the paper. The beginning of each new paragraph must be clearly indicated by indentation. All pages should be numbered consecutively at the bottom starting with the title page.

Length: The length of research articles should be restricted to ten printed pages. Short communication should not exceed five pages of manuscript, including references, figures and tables. Letters should be 400-500 words having 7-10 references, one figure or table if necessary. Commentaries and news should also be 800-1000 words having 7-10 references and one figure or table if necessary.

Types of Manuscript: JCMR is accepting original research paper, short communication reports, invited reviews, letters to editor, biographies of scientific reviewers, commentaries and news.

Statement of Human and Animal Rights: Author's should declare regulatory statement regarding the experiments using animals, human cells/tissues that all in vivo experiments have been performed according to the guidelines (explained by WHO, international animal rights federations or your respective institute) to use animals in their research work.

Conflict of Interest Statement: Authors or corresponding author should declare statement of conflict of interest at the last of manuscript.

Manuscript Evaluation Time: All submitted manuscripts will be evaluated and reviewed according to following evaluation schedule. Pre-Editorial Evaluation: All submitted manuscripts, right after their submission to JCMR will be evaluation by Editors for being according to the journal scope and format. This evaluation can take 2-7 days of submission. Reviewer's Evaluation: Selected manuscripts after pre-editorial evaluation will be sent to minimum two blind reviewers assigned by Editor-in-Chief. This process may take 21-27 days. Post Editorial Evaluation: After receiving reviewer's comments, editors evaluate the manuscripts considering the comments and decide their first decision. This process takes 3-5 days and then authors are informed regarding the editorial decision.

GENERAL ARRANGEMENT OF PAPERS

Title: In the first page, papers should be headed by a concise and informative title. The title should be followed by the authors' full first names, middle initials and last names and by names and addresses of laboratories where the work was carried out. Identify the affiliations of all authors and their institutions, departments or organization by use of Arabic numbers (1, 2, 3, etc.).

Footnotes: The name and full postal address, telephone, fax and E-mail number of corresponding author should be provided in a footnote.

Abbreviations: The Journal publishes a standard abbreviation list at the front of every issue. These standard abbreviations do not need to be spelled out within paper. However, non-standard and undefined abbreviations used five or more times should be listed in the footnote. Abbreviations should be defined where first mentioned in the text. Do not use abbreviations in the title or in the Abstract. However, they can be used in Figures and Tables with explanation in the Figure legend or in a footnote to the Table.

Abstract: In second page, abstract should follow the title (no authors' name) in structured format of not more than 250 words and must be able to stand independently and should state the Background, Methods, Results and Conclusion. Write the abstract in third person. References should not be cited and abbreviations should be avoided.

Keywords: A list of three to five keywords for indexing should be included at bottom of the abstract. Introduction should contain a description of the problem under investigation and a brief survey of the existing literature on the subject.

Materials and Methods: Sufficient details must be provided to allow the work to be repeated. Correct chemical names should be given and strains of organisms should be specified. Suppliers of materials need only be mentioned if this may affect the results. Use System International (SI) units and symbols.

Results: This section should describe concisely the rationale of the investigation and its outcomes. Data should not be repeated in both a Table and a Figure. Tables and Figures should be selected to illustrate specific points. Do not tabulate or illustrate points that can be adequately and concisely described in the text.

Discussion: This should not simply recapitulate the Results. It should relate results to previous work and interpret them. Combined Results and Discussion sections are encouraged when appropriate.

Acknowledgments: This optional part should include a statement thanking those who assisted substantially with work relevant to the study. Grant support should be included in this section.

References: References should be numbered and written in alphabetical order. Only published, "in press" papers, and books may be cited in the reference list (see the examples below). References to work "in press" must be accompanied by a copy of acceptance letter from the journal. References should not be given to personal communications, unpublished data, manuscripts in preparation, letters, company publications, patents pending, and URLs for websites. Abstracts of papers presented at meetings are not permissible. These references should appear as parenthetical expressions in the text, e.g. (unpublished data). Few example of referencing patterns are given as follows:

Examples of text references:

Cite a source written by one author: (Kikuchi, 2014)

Cite a source written by two authors: (Rinn and Chang, 2012)

Cite a source written by three or more authors: (Mead et al., 2015)

Examples of end references:

>>> Kikuchi K. (2014) Advances in understanding the mechanism of zebrafish heart regeneration. Stem Cell Research 13:542-555.

>>> Irfan-Maqsood M. (2013) Stem Cells of Epidermis: A Critical Introduction. Journal of Cell and Molecular Research 5:1, 1-2.

>>> Rinn J. L. and Chang H. Y. (2012) Genome regulation by long noncoding RNAs. Annual Review of Biochemistry 81:1-9.

>>> Bongso A., Lee E. H. and Brenner S. (2005) Stem cells from bench to bedside. World Scientific Publishing Co. Singapore, 38-55 pp.

(6 authors:) Mead B., Berry M., Logan A., Scott R. A., Leadbeater W. and Scheven B. A. (2015) Stem cell treatment of degenerative eye disease. Stem Cell Research 14:243-257.

Note: When citing more than six authors, give the name of the first author and abbreviate the others to et al.

(more than 6 authors:) Vaculik C., Schuster C., Bauer W., Iram N., Pfisterer K., Kramer G., et al. (2012) Human dermis harbors distinct mesenchymal stromal cell subsets. Journal of Investigative Dermatology 132:563-574.

Note: All the reference should be in EndNote format (JCMR EndNote Style is available on JCMR's web site, Author's Guideline)

Tables and Figures: Tables and Figures should be numbered (1, 2, 3, etc.) as they appear in the text. Figures should preferably be the size intended for publication. Tables and Figures should be carefully marked. Legends should be typed single-spaced separately from the figures. Photographs must be originals of high quality. Photocopies are not acceptable. Those wishing to submit color photographs should contact the Editor regarding charges.

JCMR Open Access Policy: Journal of Cell and Molecular Research follows the terms outlined by the Creative Common's Attribution-Only license (CC-BY) to be the standard terms for Open Access. Creative Commons License.

Note: All manuscripts submitted to JCMR are tracked by using "iThenticate" and "Plagiarism Tracker X" for possible plagiarism before acceptance.

Table of Contents

Journal of Cell and Molecular Research

Volume 13, Number 1, Summer, 2021